# CHEMICAL CHARACTERIZATION OF SOURCE-SPECIFIC ATMOSPHERIC ORGANIC AEROSOL VIA MASS SPECTROMETRY

Tianqu Cui

A dissertation submitted to the faculty at the University of North Carolina at Chapel Hill in partial fulfillment of the requirements for the degree of Doctor of Philosophy in the Department of Environmental Sciences and Engineering in the Gillings School of Global Public Health.

Chapel Hill
2019

Approved by:

Jason D. Surratt

Avram Gold

Barbara J. Turpin

Wanda M. Bodnar

Melita Keywood

## ABSTRACT

Tianqu Cui: Chemical Characterization of Source-Specific Atmospheric Organic Aerosol via Mass Spectrometry
(Under the direction of Jason D. Surratt)

Atmospheric fine aerosol ($PM_{2.5}$) is important to Earth's biogeochemical cycles and climate, and adversely impacts air quality and human health. Specifically, organic aerosol (OA) substantially contributes to $PM_{2.5}$ mass but remains poorly characterized due to the diversity and complexity of its sources, formation mechanisms, and chemical composition. A suite of state-of-the-art mass spectrometry (MS) methods were deployed and optimized to analyze distinct sets of source-specific OA samples collected from field studies and laboratory experiments in order to chemically characterize OA constituents at the molecular level.

First, over 200 archived marine aerosol samples collected from Cape Grim, Tasmania, Australia under remote background conditions from 1991-2015, were analyzed using ultra-performance liquid chromatography interfaced to a high-resolution quadrupole time-of-flight mass spectrometer equipped with an electrospray ionization source (UPLC/ESI-HR-QTOFMS) and gas chromatography interfaced to a quadrupole mass spectrometer equipped with electron ionization source (GC/EI-MS). Several ng $m^{-3}$ of biogenic (e.g., isoprene- and monoterpene-derived) secondary organic aerosol (SOA) tracers were quantified from 29 summer and winter seasons. Biogenic SOA tracers were enhanced during summer seasons and had moderate-to-strong correlations with marine bioactivity indicators such as methanesulfonic acid and chlorophyll-*a*.

In addition, UPLC/ESI-HR-QTOFMS coupled with inline diode array detection (DAD) were utilized to assess light-absorbing brown carbon (BrC) OA from over 100 systematically-performed laboratory-simulated primary and aged wildfire emissions during the 2016 Fire Influence on Regional and Global Environments Experiment (FIREX) at the US Forest Service Fire Science Lab in Missoula, Montana. 37 solvent-extractable BrC constituents were characterized in terms of their composition, contributions to $PM_{2.5}$ mass, emission factors, light absorbance, and evolution due to photochemical aging.

Furthermore, we developed and optimized a versatile hydrophilic interaction liquid chromatography (HILIC)/ESI-HR-QTOFMS method that can efficiently resolve and measure the major isoprene epoxydiols (IEPOX)-derived and several other water-soluble SOA constituents with enhanced resolution of separation, sensitivity of detection, and accuracy of measurements.

These findings provide detailed chemical composition of the atmospheric OA constituents that originate from varying sources, and thus, can serve as inputs for future studies on atmospheric analytical chemistry, earth science modeling, environmental management, and health effects of $PM_{2.5}$.

To my beloved parents.

## ACKNOWLEDGEMENTS

This dissertation would not have been achieved without many people who played important roles in my academic and personal life. First and foremost, I sincerely appreciate my advisor, Prof. Jason D. Surratt, for his generous and continuous support throughout my entire master and doctoral studies. I would not become who I am without his mentoring. I am also grateful for his kindness, trust, and patience, as well as the research and job opportunities he offered to me.

I would like to express my gratitude to Prof. Avram Gold, Prof. Barbara J. Turpin, Prof. Wanda M. Bodnar, and Dr. Melita Keywood for serving on my committee and providing valuable research opportunities and guidance. I would also like to acknowledge Prof. Richard M. Kamens and Prof. Kenneth G. Sexton for their mentoring and services as my committee members from 2015-2017.

I acknowledge the past and current Surratt group members, especially Prof. Ying-Hsuan Lin, Prof. Haofei Zhang, Prof. Zhenfa Zhang, Dr. Sri Hapsari Budisulistiorini, and Dr. Matthieu Riva for their tremendous help during my first a few years, and Yuzhi Chen, Dr. Yue Zhang, Hilary Green, Zhexi Zeng, and Erickson dos Santos, etc. for closely working with me on my research. I appreciate all the colleagues and friends I met at ESE and during collaboration for their support and friendship in lab and my daily life.

## TABLE OF CONTENTS

## LIST OF TABLES

## LIST OF FIGURES

## LIST OF SYMBOLS AND ABBREVIATIONS

AAE : Ångström absorption exponent

AC : air conditioning

ACN : acetonitrile

ACSM : aerosol chemical speciation monitor

AMS : aerosol mass spectrometer

APCI : atmospheric pressure chemical ionization

APPI : atmospheric pressure photoionization ionization

BBOA : biomass burning aerosol

BC : black carbon

BrC : brown carbon

BSOA : biogenic secondary aerosol

BSTFA : N,O-bis (trimethylsilyl) trifluoroacetamide

BVOC : biogenic volatile organic compounds

CCN : cloud condensation nuclei

Chl-*a* : chlorophyll-*a*

CIMS : chemical ionization mass spectrometer

CN : condensation nuclei

CSIRO : Commonwealth Scientific and Industrial Research Organization (Australia)

CSU : Colorado State University (United States)

DAD : diode array detector

DBE : double bond equivalent

DMA : differential mobility analyzer

DMS : dimethyl sulfide

DTAA : diaterpenylic acid acetate

EC : elemental carbon

EF : emission factor

EI : electron impact

ENSO : El Niño–Southern Oscillation

ESI : electrospray ionization

FIGAERO : filter inlet for gases and aerosol

FIREX : Fire Influence on Regional and Global Environments Experiment

FSL : fire science lab (Missoula, Montana, United States)

GC : gas chromatography

HILIC : hydrophilic interaction liquid chromatography

$^{1}$H NMR : proton nuclear magnetic resonance

HONO : nitrous acid

HP : Hewlett-Packard

HR : high resolution (mass spectrometry)

IB : ion balance

IEPOX : isoprene epoxydiol

iSOA : isoprene-derived secondary organic aerosol

LC : liquid chromatography

LOD : limit of detection

LOQ : limit of quantification

m/z : mass-to-charge ratio

MACR : methacrolein

MBTCA : 3-methyl-1,2,3-butane tricarboxylic acid

MCE : modified combustion efficiency

MeTHF : methyltetrahydrofuran

(2-) MG : (2-) methylglyceric acid

MODIS : moderate resolution imaging spectroradiometer

MPAN : methacryloylperoxynitrate

MS : mass spectrometry (or mass spectrometer)

$MS^n$ : tandem mass spectrometry

MSA : methanesulfonic acid

mSOA : monoterpene-derived secondary organic aerosol

MW : molecular weight

NAC : nitrogen-containing aromatic compound

NASA : National Aeronautics and Space Administration (United States)

NO : nitric oxide

NOAA : National Oceanic and Atmospheric Administration (United States)

$NO_x$ : oxides of nitrogen

NPLC : normal phase liquid chromatography

NSF : National Science Foundation (United States)

OA : organic aerosol

OC : organic carbon

•OH (or OH) : hydroxyl radical

OM : organic matter

PAH : polycyclic aromatic hydrocarbon

PDA : photodiode array

PILS : particle-into-liquid sampler

PM : particulate matter

$PM_1$ : particulate matter with aerodynamic diameter $\leq 1$ μm

$PM_{2.5}$ : particulate matter with aerodynamic diameter $\leq 2.5$ μm

$PM_{10}$ : particulate matter with aerodynamic diameter ≤ 10 μm

POA : primary organic aerosol

pptv : part(s)-per-trillion by volume

PTFE : polytetrafluoroethylene

Q-TOFMS : quadrupole time-of-flight mass spectrometry

$R^2$ : coefficients of determination (in statistics)

RH : relative humidity

RPLC : reverse-phase liquid chromatography

RT : retention time

SEMS : scanning electrical mobility system

SOA : secondary organic aerosol

SOAS : Southern Oxidant and Aerosol Study (field campaign)

SV-TAG : semi-volatile thermal desorption aerosol gas chromatogram

TIC : total ion chromatograms

TMCS : trimethylchlorosilane

TOC : total organic carbon

UNC : University of North Carolina at Chapel Hill (United States)

UHPLC : ultra high performance liquid chromatography

UPLC : ultra performance liquid chromatography

VOC : volatile organic compounds

WMO : World Meteorological Organization

WSOC : water-soluble organic carbon

# CHAPTER 1: INTRODUCTION

## 1.1 Atmospheric Organic Aerosol

Atmospheric fine aerosol (i.e., $PM_{2.5}$, particulate matter with aerodynamic diameters ≤ 2.5 μm) are important to atmospheric chemistry and physics, the biosphere, climate, and public health.[1] They are known to alter global radiative forcing by scattering and absorbing solar radiation and adjusting cloud formation properties via acting as cloud condensation nuclei (CCN).[2,3] Based on epidemiological studies, $PM_{2.5}$ are closely associated with respiratory diseases and premature death.[4] Numerous epidemiological studies show that $PM_{2.5}$ is correlated with severe health effects, including enhanced mortality, cardiovascular, and respiratory diseases.[5–7]

Organic aerosol (OA) has been extensively studied in the past decades, even though its sources, composition and chemical transformations remain poorly understood.[8,9] Field studies conducted in urban and rural areas showed OA can contribute a substantial fraction of the submicron aerosol ($PM_1$) mass in the troposphere.[10,11] Inorganic aerosol constituents, such as sulfate and nitrate, are mostly anthropogenic in origin, especially over continental locations, whereas OA can be attributed to both anthropogenic and biogenic (natural) sources.[10] Moreover, OA consists of both primary organic aerosol (POA) that is directly emitted from its sources into the atmosphere, and secondary organic aerosol (SOA) that is formed from the chemical transformation of atmospheric organic compounds, such as oxidation or multiphase chemistry of volatile organic compounds (VOCs), into lower-volatility organic products.[12] Although contribution of POA to OA mass could be substantial in some cases, SOA typically accounts for

a large (sometimes dominant) fraction of total OA mass, based on several complementary measurements of ambient aerosol, including organic carbon (OC) mass fraction,[13] loadings of water-soluble OC (WSOC),[14] and level of oxidation measured by aerosol mass spectrometry (AMS).[15,16]

## 1.2 Source-Specific Atmospheric Aerosol Constituents

### *1.2.1 Terrestrial Biogenic SOA from Isoprene and Monoterpenes*

Gaseous precursors of SOA can be emitted from anthropogenic (e.g., industry, transportation, household) and biogenic (e.g., terrestrial and oceanic lives) sources.[17] Biogenic VOCs (BVOCs) are considered to be major contributors to the global SOA burden rather than those emitted from anthropogenic sources, with total biogenic secondary organic aerosol (BSOA) fluxes estimated to be 88 TgC $yr^{-1}$.[18] Both laboratory and field studies indicate that BVOCs, such as isoprene[19–22] and monoterpenes[23,24], including α-pinene and β-pinene, play a vital role in global and regional atmospheric SOA production.

Isoprene ($C_5H_8$) is the most abundant non-methane hydrocarbon emitted into Earth's atmosphere with emissions estimated up to 600 Tg $yr^{-1}$ and is derived largely from deciduous trees.[25] The atmospheric oxidation of isoprene plays an important role in both tropospheric ozone ($O_3$) and SOA formation in forested regions affected by anthropogenic activities.[26–33] Specifically, hydroxyl radical-initiated oxidation of isoprene during the daytime under low-nitric oxide (NO) conditions produces substantial amounts of isoprene epoxydiols (IEPOX) (~50% yield).[34,35] The acid-catalyzed multiphase chemistry (e.g., reactive uptake) of IEPOX onto existing sulfate particles produces SOA constituents including 2-methyltetrols,[28,29,36,37] $C_5$-alkene triols,[28,29,36,37] 3-methyltetrahydrofuran-3,4-diols (3-MeTHF-3,4-diols),[29] organosulfates,[29,37–39] and low-volatility oligomers (Figure 1.1).[29,37,40] Studies have also pointed out that the mixed effects of sulfate (e.g.,

aerosol acidity, nucleophile, surface area, and salting-in) play a critical role in forming atmospheric IEPOX-derived SOA.[26,30,38,41–43]

Monoterpenes ($C_{10}H_{16}$), such as α-pinene and β-pinene, are estimated to be the second-largest class of BVOCs emitted into the global atmosphere. These BVOCs are primarily emitted from coniferous trees as well as other types of vegetation (e.g., shrubs and fruits).[44] Once these compounds are emitted, monoterpenes like α-pinene are quickly oxidized by •OH or ozone ($O_3$) during the daytime, and by nitrate radical ($NO_3$) during the nighttime, resulting in a complex mixture of first-generation oxidation products consisting primarily of carbonyls, carboxylic acids, alcohols, and organic nitrates.[45–49] Due to the lower vapor pressure of monoterpene-derived oxidation products, they partition between the gas and particle phases, resulting in the formation of SOA.[8,12,50–52] First-generation oxidation products of α-pinene may undergo further processing in the gas and aerosol phases, such as oxidation,[53,54] sulfation,[39,55] and oligomerization,[56–58] resulting in the formation of less volatile, high-molecular weight compounds. For example, pinonic acid is a semi-volatile organic and a significant fraction of pinonic acid is present in the gas phase at 283 K.[59] Through further reactions with •OH, gas-phase pinonic acid is oxidized to its second-generation oxidation product 3-methyl-1,2,3-butane tricarboxylic acid (MBTCA),[53,59] which has low vapor pressure and rapidly partitions into the aerosol phase, while other first and later generation compounds, such as pinic, terpenylic acid and/or diaterpenylic acid acetate, are believed to undergo oligomerization to form dimers,[60] which are effectively captured in the particle phase because of their reduced vapor pressures.

### *1.2.2 Marine-Originated Isoprene and Monoterpene-Derived SOA*

The background aerosol in the boundary layer over the remote oceans is quite different from continental atmospheric aerosols, in terms of the origin, particle number concentrations, and

organic mass fractions.[61] Atmospheric aerosol particles derived from marine sources can also play a significant role in the global climate system through direct and indirect effects.[62] In recent decades, sources and chemical composition of marine aerosol particles have been examined.[63–65] For example, in the late 1980s, it was hypothesized that dimethylsulfide (DMS)-derived sulfate contributed to the majority of the CCN in remote marine boundary layer.[63] However, recent studies have provided evidence that sea salt (inorganic) and organic constituents of marine aerosols are the likely major sources of CCN, whereas the contribution of DMS might be more limited than previously thought.[66,67] Quinn and Bates proposed mechanisms for the sources and production of CCN in the remote marine boundary layer, where DMS contributes to the marine boundary layer CCN population via a series of tropospheric atmospheric oxidation processes, whereas sea salt and organics are emitted as a result of wind-driven bubble bursting.[68] While primary aerosol is emitted directly from wind-driven bubble bursting on the ocean surface,[69] marine secondary aerosol originate largely from the atmospheric oxidation of BVOCs,[18,70] including phytoplankton-emitted DMS[63] and the well-established terrestrial BSOA precursors mentioned in the previous section, such as isoprene and monoterpenes.[44,71,72] While current debate focuses on the magnitude and spatial distribution of global fluxes of isoprene and monoterpenes as well as their contribution to submicron marine aerosol mass,[73,74] the origins, chemical composition and formation mechanisms of marine SOA derived from these precursors remain less well characterized than those over the continents.

Specifically, marine biota have been uncovered as an oceanic source of isoprene and monoterpene emissions,[71,72] with their production rates determined from a variety of marine phytoplankton, heterotrophic bacteria, and seaweeds,[75,76] and varied with plankton species, chlorophyll concentration, and environmental parameters such as solar radiation, temperature, and

nutrients.[73,77] Atmospheric mixing ratios of isoprene and monoterpenes over the oceans were measured up to several hundred parts-per-trillion by volume (pptv), and likely contributing to SOA formation derived from marine emissions.[72,78,79]. For example, high concentrations of isoprene-derived SOA and monoterpene-derived SOA tracers, up to 36 and 20 ng $m^{-3}$, respectively, have been measured from marine samples collected from the Arctic to Antarctic regions.[80] Modelling estimates based on marine chlorophyll-*a* extrapolate the global oceanic fluxes of isoprene to be below-1 to 12 TgC $year^{-1}$ and of α-pinene to be below-0.2 to 30 TgC $year^{-1}$.[81,82] In addition to the living biogenic sources, other potential aerosol sources such as dissolved organic matter released from bubble-bursting processes and photosensitized reactions of less-volatile phytoplankton-derived organics present in the sea surface microlayer were revealed.[83,84]

### *1.2.3 Biomass-Burning and Light-Absorptive Aerosol*

As a large source of atmospheric carbonaceous OA,[85–87] biomass burning-derived OA (BBOA) from wildfires contains thousands of gaseous and particulate constituents that can significantly influence atmospheric chemistry, cloud formation, climate, and human health.[88–90] Individual and categorized organic emissions from wildfires have been previously identified and quantified.[91–102] However, previous measurements did not always provide quantitative chemical composition data of the light-absorbing constituents (referred to as brown carbon, BrC) from biomass burning emissions, and thus, the specificity, light-absorption properties, and reactivity of wildfire emissions remain unclear, impeding accurate predictions of the impacts of wildfires on the environment. The light-absorbing components (i.e., chromophores) in BrC aerosol are expected to possess a high degree of unsaturation or conjugation,[86,103,104] but are rarely quantified along with other BBOA constituents or used as BrC tracers in the atmosphere.[105–107] In some circumstances, the overall light-absorbing properties of OA are dominated by a few chemical

classes of strong chromophores at trace levels,[108–110] such as polycyclic aromatic hydrocarbons (PAHs),[111,112] nitrogen (N)-containing aromatic compounds (NACs) and their derivatives.[105,106,109,110,113,114] The complex mixture of gas- and particle-phase biomass burning emissions, including BrC constituents, can undergo atmospheric oxidation and multiphase chemistry. Numerous studies indicate that optical and chemical properties of BrC may substantially evolve as BBOA ages in the atmosphere,[115–120] or may be affected by other factors such as solar irradiation[121,122] and relative humidity (RH).[123,124] However, due to the complex atmospheric perturbations and the uncontrolled nature of wildfires, characterization of BrC aerosol constituents from biomass burning emissions needs to be systematically assessed in the laboratory where variables can be constrained to minimize uncertainties from burn to burn.

### 1.3 Mass Spectrometric Techniques for Atmospheric Aerosol Measurements

Improvement to the basic knowledge of atmospheric aerosol heavily relies on better assessment and characterization of their detailed chemical composition and speciation in varied conditions and phases, which calls for the development and applications of advanced mass spectrometry (MS) based analytical techniques for aerosol measurements with online and offline analysis for both gaseous and condensed phases.[125,126] In the past several decades, MS techniques have been widely utilized for aerosol characterization, as it has been demonstrated to be a suitable and unmatched tool for both qualitative and quantitative analysis, unraveling the complexity of OA and providing molecular information on the aerosol composition and transformations. This has been done over a broad range of chemical species in OA with high sensitivity and robustness, especially when interfaced to gas or liquid chromatography for prior separation of the complex mixture.[127,128] Specifically, mass spectrometric characterization of atmospheric aerosol can be classified into offline (e.g., gas chromatography/mass spectrometry (GC/MS) and liquid

chromatography/mass spectrometry (LC/MS)) and online (e.g., AMS) techniques.[18] Offline techniques, which require OA time-integrated collection and extraction steps, offer molecular characterization of SOA tracers that are important in identifying their gaseous precursors and chemical formation processes. GC/MS, one of the most widely used offline techniques, requires an additional derivatization step that is necessary for detecting highly oxidized and polar compounds that largely comprise SOA. GC/MS with prior derivatization has been used to identify oxidized SOA compounds from various precursors.[22,24,28,129–131] LC/MS interfaced with electrospray ionization (ESI) or atmospheric pressure chemical ionization (APCI) is powerful in characterizing large polar organic compounds without the need for prior derivatization. This technique has been applied in characterizing SOA from chamber studies,[28,29,132] including sulfated- and nitrated-organics[38,55,133,134] as well as carboxylic acids and dimer esters.[135] In addition, molecular characterization of light-absorbing OA components (BrC) has been substantially advanced in recent years by coupling a light-absorption detector (i.e. photodiode array (PDA) detector, or diode array detector (DAD)) to LC/ESI-MS.[106,136] This method allows chemical characterization of BrC aerosol constituents to be precisely identified with their wavelength-dependent chromophores from a majority of non-absorbing OA constituents.

**1.4 Deficiencies of Current Analytical Techniques on Atmospheric Aerosol Characterization**

Offline techniques are limited temporally and spatially, causing our characterization of formation kinetics and critical intermediates to remain less effective.[18] These offline analytical techniques are also susceptible to both positive and negative artifacts due to evaporation, adsorption, and chemical reactions during the collection and analysis procedures.[137,138] For example, many of the IEPOX-derived SOA $C_5$ tracers mentioned above, including the 2-methyltetrols, $C_5$-alkene triols, and 3-MeTHF-3,4-diols, have generally been characterized in past

studies by gas chromatography interfaced to electron ionization mass spectrometry (GC/EI-MS) with prior trimethylsilylation,[28,29,36–38,129] and have been widely used to investigate SOA formation mechanisms, derive kinetic parameters, and evaluate model performance of IEPOX-derived SOA.[29,36,139,140] However, volatility and composition analysis by a filter inlet for gases and aerosol coupled to a chemical ionization mass spectrometer (FIGAERO-CIMS) equipped with iodide reagent ion chemistry demonstrated that IEPOX-derived SOA has lower volatility than predicted from the concentrations of commonly reported IEPOX SOA $C_5$ tracers; in particular the 2-methyltetrols, $C_5$-alkene triols and 3-MeTHF-3,4-diols. As a result, thermal decomposition of accretion products (oligomers) or other low-volatility organics, such as organosulfates, may contribute significantly to tracers previously measured by GC/EI-MS.[141] A second set of studies using FIGAERO-CIMS or semi-volatile thermal desorption aerosol gas chromatogram (SV-TAG) instrumentation with online derivatization reached similar conclusions on the potential impacts of thermal decomposition on OA composition measured.[142–145] As another example, different protocols based on ultra-performance liquid chromatography interfaced to high-resolution tandem mass spectrometry with electrospray ionization (UPLC/ESI-HR-$MS^n$), have been used to characterize organosulfates and oligomers. However, separation of polar, water-soluble components is conventionally attempted with reverse-phase liquid chromatography (RPLC) columns.[28,29,38,146] RPLC columns do not resolve such compounds well because of either extremely short retention times (RTs), poor peak shapes, or ion suppression effects due to co-eluting inorganic aerosol constituents, leading to potential complications in identifying and quantifying target compounds. The IEPOX-derived polyols are hydrophilic compounds owing to their hydroxyl functional groups, and the organosulfates are ionic polar compounds.[141,146] Hence, an alternative approach for the IEPOX-derived SOA characterization that could accomplish

simultaneous analysis of polar and water-soluble components while avoiding the drawbacks associated with current analytical methods would be highly desirable.

**1.5 Objectives of Dissertation**

Specific research questions outlined below are addressed in the Chapters 2-4 of this dissertation, with associated tables and figures attached at the end of each chapter:

*1. What are the sources and chemical composition of atmospheric OA over the remote oceans? How does BVOC-derived SOA (e.g., from isoprene and monoterpene) contribute to marine OA? Does it change over time?*

Chapter 2 presents the concentrations of a number of isoprene- and monoterpene-derived SOA tracers, measured from over 200 archived ocean-originated particulate samples collected from 1991-2015 at Cape Grim, Australia, analyzed using a suite of chromatographic and mass spectrometric techniques such as UPLC/ESI-HR-QTOFMS and GC/EI-MS. Consistent seasonal variations and moderate-to-strong correlations with marine bioactivity indicators such as methanesulfonic acid and chlorophyll-*a* were observed., suggesting that marine biota can provide sources of biogenic SOA in remote marine atmospheres.

*2. What are the deficiencies of the mass spectrometric techniques for characterizing atmospheric OA? How can we improve those analytical techniques especially those used in the previous chapter?*

These questions are addressed in Chapter 3, where we developed and optimized a versatile HILIC (as a complimentary/orthogonal chromatographic method to RPLC)/ESI-HR-QTOFMS method

that can efficiently resolve and measure the major IEPOX-derived and several other water-soluble SOA constituents with enhanced separation, sensitivity, and accuracy.

*3. What are the chemical compositions, emission rates, and differences of light-absorbing OA (BrC) constituents from primary and photochemically-aged wildfire emissions? How do they vary with different fuels burned?*

These questions are addressed in Chapter 4, where we used UPLC/ESI-HR-QTOFMS coupled with a UV-vis detector to characterize BrC OA from over 100 systematically-performed laboratory-simulated primary and aged wildfire emissions during the 2016 Fire Influence on Regional and Global Environments Experiment (FIREX) at the US Forest Service Fire Science Lab in Missoula, Montana. A large number of solvent-extractable BrC constituents (i.e., 37 in total) were characterized at the molecular level in terms of their compositions, contributions to $PM_{2.5}$ mass, emission factors, light absorbance, and their changes that occurred due to photochemical aging.

The last chapter (Chapter 5) presents conclusions based on the findings from the Chapters 2-4. Future work is also discussed in the last chapter. Supporting information associated with Chapter 2, 3, and 4 are enclosed in the Appendix A, B, and C, respectively.

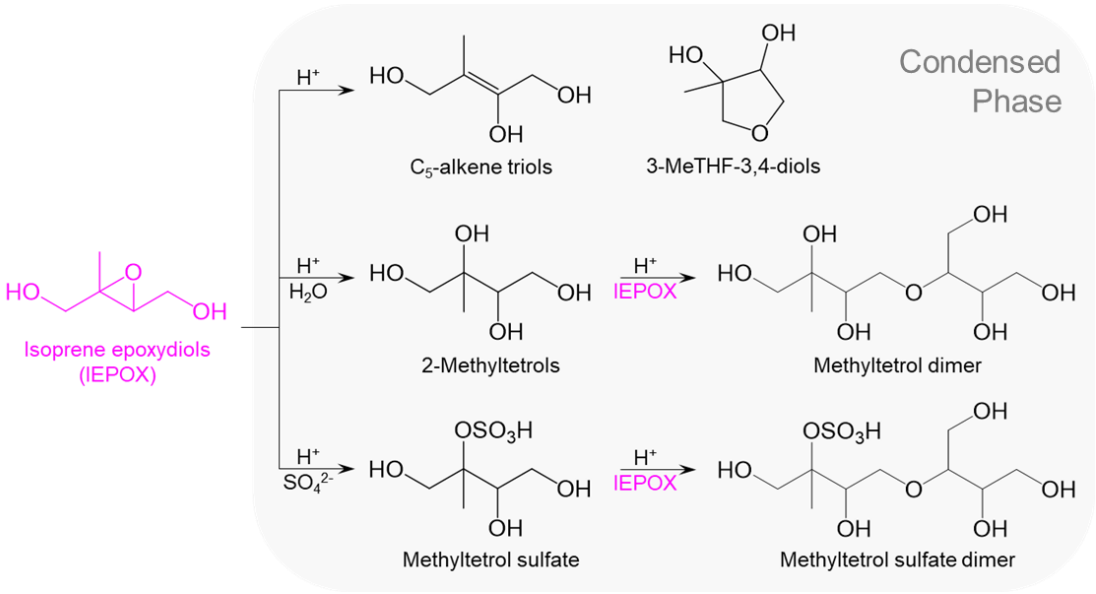


**Figure 1.1.** Simplified formation pathway of IEPOX-derived SOA tracers.

# CHAPTER 2: CHEMICAL CHARACTERIZATION OF ISOPRENE- AND MONOTERPENE-DERIVED SECONDARY ORGANIC AEROSOL TRACERS IN REMOTE MARINE AEROSOLS OVER A QUARTER CENTURY[1]

## 2.1 Overview

Isoprene and monoterpenes are ubiquitous precursors of biogenic secondary organic aerosol (SOA) over continental regions; however, their contributions to organic aerosol (OA) mass and chemical processes in remote marine atmospheres remain uncertain. Determining exact sources of organics in marine aerosol is needed in order to more accurately assess aerosol climate effects in remote locations through coupled atmospheric chemistry-climate simulations. Over 200 archived ocean-originated particulate samples collected from 1991-2015 at Cape Grim, Australia, were analyzed using a suite of chromatographic and mass spectrometric techniques. To our knowledge, this is one of the longest-running continual archives of marine aerosol samples collected under remote background conditions. Up to 6.75 and 1.11 ng $m^{-3}$ of isoprene- and monoterpene-derived SOA, respectively, were quantified using authentic standards. Although there was no clear temporal trend over the decades, consistent seasonal variations were observed with higher biogenic SOA in summer, which was moderately-to-strongly correlated ($r = 0.61$-$0.85$) with marine bioactivity indicators such as methanesulfonic acid and chlorophyll-*a*. These correlations indicate that marine biota likely emit biogenic SOA precursors that are able to

[1] This chapter has just been accepted for publication as a "Just Accepted Manuscript" in American Chemical Society Earth and Space Chemistry. "Chemical Characterization of Isoprene- and Monoterpene-Derived Secondary Organic Aerosol (SOA) Tracers in Remote Marine Aerosols over A Quarter Century" by Tianqu Cui, Hilary Green, Paul W. Selleck, Zhenfa Zhang, Rachel O'Brien, Avram Gold, Melita Keywood, Jesse H. Kroll, and Jason D. Surratt, *ACS Earth Space Chem.*, **doi:**10.1021/acsearthspacechem.9b00061. Copyright (2019) American Chemical Society.

contribute to remote background OA levels. Based on historical observations of OA mass estimated in the marine baseline samples, these biogenic SOA tracers contributed up to 0.71% (0.26±0.24% on average) of the total OA mass fraction. Our data suggest that larger sources of OA exist in remote marine atmospheres, such as primary OA produced from bubble-bursting processes or SOA precursors derived from photosensitized reactions of dissolved organic matter present in the sea surface microlayer.

**2.2 Introduction**

Atmospheric aerosol particles derived from marine sources can play a role in the global climate system through direct and indirect effects.[62] In recent decades, sources and chemical constituents of marine aerosol particles have been examined.[63–65] While primary aerosol is emitted directly from wind-driven bubble bursting on the ocean surface,[69] marine secondary aerosol particles originate largely from the atmospheric oxidation of biogenic volatile organic compounds (BVOCs),[18,70] including phytoplankton-emitted dimethylsulfide (DMS)[63] and well-established secondary organic aerosol (SOA) precursors such as isoprene and monoterpenes.[44,71,72] While current debate focuses on the magnitude and spatial distribution of global fluxes of isoprene and monoterpenes as well as their contribution to submicron marine aerosol mass,[73,74] the origins, chemical composition and formation mechanisms of marine SOA derived from these precursors remain poorly characterized.

Since marine biota were unveiled as a source of isoprene and monoterpene emissions,[71,72] their production rates have been determined from a variety of marine phytoplankton, heterotrophic bacteria, and seaweeds,[75,76] with production rates varying with plankton species, chlorophyll concentration, and environmental parameters (e.g., temperature, solar radiation, and nutrient abundance).[73,77] Oceanic studies report atmospheric mixing ratios of isoprene and monoterpenes

up to several hundred parts-per-trillion by volume (pptv), likely resulting in SOA derived from marine biological emissions.[72,78,79] Specifically, significant levels of isoprene-derived SOA (iSOA) and monoterpene-derived SOA (mSOA) tracers, up to 36 and 20 ng $m^{-3}$, respectively, have been measured from marine samples collected from the Arctic to Antarctic regions.[80] Modelling estimates based on marine chlorophyll-*a* extrapolate the global oceanic fluxes of isoprene to be < 1 to 12 TgC $year^{-1}$ and of α-pinene to be < 0.2 to 30 TgC $year^{-1}$ (from the "bottom-up" to "top-down" approaches).[81,82] In addition to biogenic sources, recent studies revealed potential aerosol sources involving dissolved organic matter from bubble-bursting processes and photosensitized reactions of non-volatile plankton-derived organics present in the sea surface microlayer, possibly resulting in subsequent SOA formation.[83,84]

Spatial distributions of oceanic emissions of isoprene and monoterpenes as well as their SOA tracers have been examined in a large number of field studies around the globe.[80,147] However, few field studies have been able to assess temporal trends of SOA quantity and composition.[148,149] Moreover, most field measurements have been performed at coastal locations and higher concentrations of SOA were observed than in central or remote oceans. The difference is likely due to higher levels of phytoplankton in coastal waters or continental outflows and coastal vessel emissions.[80,150] Therefore, continental and anthropogenic sources should be eliminated to determine the precise contribution of the remote marine-derived BVOCs to the formation of SOA.

In this study we analyzed over 200 marine-derived aerosol samples collected at Cape Grim, Australia, from austral summer and winter seasons during 1991-2015. To our knowledge, this is one of the longest-running filter sample archives of marine-derived aerosol monitored under clean background conditions, where continental outflows were intentionally excluded. Known iSOA and mSOA tracers were measured at the molecular level in filter extracts by ultra-performance liquid

chromatography interfaced to a high-resolution quadrupole time-of-flight mass spectrometer equipped with an electrospray ionization source (UPLC/ESI-HR-QTOFMS) and gas chromatography interfaced to a quadrupole mass spectrometer equipped with electron ionization source (GC/EI-MS).[60,130,134,151–153] Our study aimed to obtain the quantities and temporal trends of iSOA and mSOA from remote marine aerosol samples to gain insights into their sources and contributions over the oceans. In addition, correlations of marine bioactivity indicators, including methanesulfonic acid (MSA), oxalic acid, and chlorophyll-*a*, with iSOA and mSOA tracers were assessed to further establish marine sources.[63,154,155]

## 2.3 Experimental Section

### *2.3.1 Field Aerosol Collection under Baseline Conditions at Cape Grim, Australia*

The Cape Grim Baseline Air Pollution Station is located at the top of a 94-m cliff on the western side of the northwest tip of Tasmania, Australia (40°40'56" S, 144°41'18" E), as shown in Figure A1 (Appendix A). This station is surrounded by a rocky reef and nearby grassland. The station is a global monitoring station in the World Meteorological Organization (WMO)'s Global Atmospheric Watch Program, and has been operating since 1976.[156]

Week-long aerosol filter samples were collected from 1991-2015 using high-volume filter samplers (customized instrument in 1991-2002; and High-Volume sampler, Ecotech 3000 in 2003-2015) equipped with size-selective inlets, resulting in a particle size cut of coarse particulate matter ($PM_{10}$, aerosol with aerodynamic diameters of $\leq$ 10 μm) during 2003-2015 and $PM_{11\text{-}12}$ (aerosol with aerodynamic diameters of $\leq$ 11-12 μm) during 1990-2003. The sampling flow rate was 54 $m^3$ $h^{-1}$, regulated by pressure transducers over the 1990-2003 sampling period, and 67.8 $m^3$ $h^{-1}$, regulated by mass flow controllers over the 2003-2015 sampling period. The flow rates were audited and calibrated with a calibration orifice plate every 3 months, and the size-selective inlet

was cleaned and re-greased monthly. Samplers were equipped with Pallflex Emfab filters (PALL Life Sciences), 25 cm × 20 cm, constructed of pure borosilicate glass microfibers reinforced with woven glass cloth and bonded with polytetrafluoroethylene (PTFE). Monthly field blanks were taken by running the high-volume filter sampler for a few minutes.

To insure exclusive collection of ocean-originated aerosols, the high-volume filter samplers were operated only during periods with on-shore air flow that originated from the open ocean. From 1990-2003, the "Baseline Event Switch 2" was employed for particulate sample collection: wind direction between 190° and 280° (Figure A1), the condensation nucleus (CN) concentration < 600 particles $cm^{-3}$. Monthly operation with "Baseline Event Switch 3" commenced in 2003: wind direction between 190° and 280°; CN concentration threshold determined by the 90-percentile of CN hourly medians over 5 previous years at the 50-m level, further constrained by a radon concentration < 100 mBq $m^{-3}$ (an ideal indicator for continental emissions), interpolated using cubic splines to give daily values. Air mass origin maps, back trajectory data and angular radon distributions support the origin of air masses arriving at the station largely from the baseline sector. See Appendix A for details regarding sample collection, baseline criteria, and collocated data in annual or biennial Cape Grim Baseline Reports since 1976.

Exposed filters were stored at 3 °C at Cape Grim until they were transported to Commonwealth Scientific and Industrial Research Organization (CSIRO) laboratories at Aspendale, Victoria, where they underwent gravimetric mass determination and IC analysis for soluble ion concentrations, usually within two months of sample collection. Then the remaining non-extracted filters were stored at 3 °C until shipped to the University of North Carolina at Chapel Hill (UNC) in 2016 to be stored at -20 °C until extracted for the subsequent GC/EI-MS and UPLC/ESI-HR-QTOFMS analyses.

### *2.3.2 Filter Extractions*

#### *2.3.2.1 Strategy of Filter Extractions*

A total of 211 field samples and 26 field blank filters were selected from 14 summer seasons (mid-December – mid-February) and 15 winter seasons (mid-June – mid-August) during the 1991-2015 sampling period for chemical analysis of known iSOA and mSOA tracers. Each season was represented by compositing 5-9 week-long filters collected during the season, resulting in average seasonal concentrations being determined for each SOA tracer. An aliquot of each filter (12.5 cm × 20 cm) was individually extracted and combined by season in order to ensure sufficient mass for GC/EI-MS and UPLC/ESI-HR-QTOFMS analysis. This protocol provided sufficient time resolution of each biogenic SOA tracer over the entire sampling period in a cost-effective manner.

#### *2.3.2.2 Filter Extraction Procedures*

Filters were extracted with 20 mL of high-purity methanol (LC-MS CHROMASOLV-grade, Sigma-Aldrich) followed by sonication for 45 min. The methanol extracts were then blown dry under a gentle $N_2$ stream at room temperature (21-22 ℃). Dried seasonal extracts were reconstituted in 3 mL of methanol, split into three equal aliquots, blown dry and then reconstituted using solvents that were appropriate for the specific analytical technique applied to the chemical characterization as described in subsequent sections. Immediately prior to analysis, reconstituted seasonal extracts were filtered through a PTFE syringe filter (Agilent, 0.2-μm pore size) to remove undissolved sea salt particles, insoluble particles or filter fibers.

### *2.3.3 Aerosol-Phase Chemical Characterization*

#### *2.3.3.1 Instrumentation*

Chemical characterization of the iSOA and mSOA constituents were performed on a GC/EI-MS (Hewlett Packard 5890 Series II Gas Chromatograph interfaced to an HP 5971A Series Mass Selective Detector) and a UPLC/ESI-HR-Q-TOFMS (Agilent 6520 Series) operated in the negative ion mode. Operating details of both GC/EI-MS and UPLC/ESI-HR-QTOFMS have been described elsewhere and are briefly described below.[157]

#### *2.3.3.2 GC/EI-MS for Determination of iSOA*

For analysis by GC/EI-MS, the GC column (Econo-CapTM-ECTM-5, 30 m × 0.25 mm × 0.25 μm) was heated up to 310 ℃ and the ionization source operated at 70 eV; the full temperature elution program for the GC/EI-MS has been described previously by Surratt et al.[158] One aliquot of the dried seasonal extract was derivatized by addition of 200 μL BSTFA (N,O-bis (trimethylsilyl) trifluoroacetamide) + trimethylchlorosilane, 99:1 (v/v), Supleco) and 100 μL pyridine (98% anhydrous, Sigma-Aldrich,) followed by heating for 1 h at 70 ℃. Analysis was performed within 24 h following trimethylsilylation. iSOA standards were synthesized in-house by published procedures: 2-methylglyceric acid (2-MG), 2-methyltetrols (2-methylthreitol and 2-methylerythritol) and *cis*- and *trans*-3-methyltetrahydrofuran-3,4-diols (3-MeTHF-3,4-diols).[159,160] In addition, high-purity commercially available chemicals (all from Sigma-Aldrich, >99%), including levoglucosan and ketopinic acid, were used as authentic or surrogate external standards for identification and quantification.

#### *2.3.3.3 UPLC/ESI-HR-QTOFMS for Determination of mSOA*

For UPLC/ESI-HR-QTOFMS analysis, an aliquot of dried seasonal extract was reconstituted with 300 μL of 50:50 (v/v) methanol (LC-MS CHROMASOLV-grade, Sigma-

Aldrich) and high-purity deionized water (Milli-Q, 18.2 MΩ). 5 μL aliquots were injected onto a reverse-phase UPLC column (Waters ACQUITY UPLC HSS T3 column, 2.1× 100 mm, 1.8 μm particle size) eluted at a flow rate of 0.3 mL $min^{-1}$ with a mobile phase of methanol containing 0.1% acetic acid (LC-MS CHROMASOLV-grade, Sigma-Aldrich) and water containing 0.1% acetic acid (LC-MS CHROMASOLV-grade, Sigma-Aldrich). The gradient elution program used to separate these mSOA components has been previously described by Kristensen et al.[135]

A number of carboxylic acids and organosulfates (OSs) derived from monoterpenes and/or isoprene were examined and quantified by the UPLC/ESI-HR-QTOFMS operated in negative ion mode using authentic or surrogate standards. BVOC-derived OSs that were closely examined included glycolic acid sulfate ($C_2H_3O_6S^-$), lactic acid sulfate ($C_3H_6O_6S^-$), 2-MG OS ($C_4H_7O_7S^-$), 2-methyl-3-buten-2-ol (MBO)-derived OS ($C_5H_{11}O_6S^-$), 2-methyltetrol sulfates ($C_5H_{11}O_7S^-$) and a monoterpene-derived OS ($C_{10}H_{17}O_5S^-$);[134,161–163] however, no OSs were detected in any of the composited seasonal samples. Based on similarity of structures, terebic acid (Tokyo Chemical Industry, 98%) was used to quantify terebic and terpenylic acids, both of which are known mSOA constituents.[60,152] In addition, authentic pinic acid (Sigma-Aldrich, 99%) was used to quantify pinic acid, whereas authentic 3-methyl-1,2,3-butanetricarboxylic acid (MBTCA, Toronto Research Chemicals, 98%) was used to quantify MBTCA, but used as a surrogate standard to quantify diaterpenylic acid acetate (DTAA). Pinic acid, MBTCA, and DTAA are also known as mSOA tracers.[130,152,153,164]

*2.3.3.4 IC for Water-soluble Particle-Phase Constituents*

A 6.25-$cm^2$ section of each high-volume filter sample was cut and extracted to measure major water-soluble constituents, such as MSA and oxalic acid, by ion chromatography (IC,

Dionex ICS-3000), performed at the CSIRO laboratories within two months after collection (see Appendix A for details).

*2.3.3.5 Quality Control and Corrections*

Six-point calibration curves were constructed for each standard over the concentration range 0.25-50 µg $mL^{-1}$ for GC/EI-MS and 0.01-50 µg $mL^{-1}$ for UPLC/ESI-HR-QTOFMS. SOA tracers quantified from the field samples were not detected from any laboratory or field blanks. The extraction efficiency for all compound was >94%, confirmed by a second extraction and analysis of selected filters. The recovery rates of spiked standards were 85±15% for GC/EI-MS and 65±20 % for the UPLC/ESI-HR-QTOFMS. The results reported in this study have not been corrected for recovery. Carryover of SOA constituents quantified by GC/EI-MS and UPLC/ESI-HR-QTOFMS was found to be negligible by analyzing solvent blanks between injections of seasonal samples from Cape Grim. The analytical precision determined by quintuplicate injections of select samples and standards was 1.8±0.2% for GC/EI-MS and 3.6±1.2 % for UPLC/ESI-HR-QTOFMS.

Possible changes in the chemical composition of archived filter samples was also assessed during this study. Twenty-four selected filter samples covering 1990-2011 were reanalyzed using IC in 2016 in order to identify changes in inorganic or organic constituents. The following average increases from time of collection to 2016 were observed: $Na^+$, 4±20%; $Mg^{2+}$, 6±24%; $SO_4^{2-}$, 11±18%; oxalate, 18±40%; MSA, 1±29%. Different fractions of a set of filters (n=6) were analyzed by UPLC/ESI-HR-QTOFMS in 2011 and again in 2014. No change was observed over the three years of storage under dark conditions at -20ºC; however, this cannot fully rule out that some degradation of the iSOA and mSOA tracers did not occur during the years of storage at Cape Grim. It is worth noting here that the presence of iSOA tracers, such as 2-MG and the 2-

methyltetrols, was recently reported in ice core samples, representing several hundred years of atmospheric aerosol deposition.[148,149] Results of the analysis were interpreted under the assumption that the iSOA tracers were stable over time. Recent work has shown that iSOA is low-volatility in nature.[165] Further, as will be discussed in subsequent sections, the quantities of the iSOA and mSOA tracers are in good agreement with recent marine aerosol composition studies.

## 2.4 Results and Discussion

### *2.4.1 Isoprene-Derived SOA (iSOA) Tracers*

Figure 2.1, Table 2.1 and Table A1 show iSOA tracers, 2-MG, 2-methylerythritol, and 2-methylthreitol, were identified in aerosol samples collected from 27 of the 29 seasons (14 summers and 15 winters) during 1991-2015. Other well-established iSOA tracers, including the $C_5$-alkene triols (*cis*- and *trans*-2-methyl-1,3,4-trihydroxy-1-butane as well as 3-methyl-2,3,4-trihydroxy-1-butene),[166] *cis*- and *trans*-3-MeTHF-3,4-diols,[157] and the 2-methyltetrol sulfate esters,[134] were not detected in any of the samples, in contrast to continental aerosols such as those from the southeastern U.S.[160,167,168] The total mass of the three identified iSOA tracers ranged from 0.05 to 6.75 ng $m^{-3}$, with a mean of 1.70±1.66 ng $m^{-3}$. The summed iSOA tracer concentrations were 1-3 orders of magnitude lower than those typically observed in continental locations influenced by high isoprene emissions from deciduous trees and large amounts of acidic sulfate aerosol that promote iSOA formation.[151,157,160,169–174] The summed iSOA concentrations are comparable to results from previous studies of concentrations over the southern Pacific and Indian Oceans from September to March,[80] and over oceans at low latitudes in the Northern Hemisphere from October to March,[147] and approximately one order of magnitude higher than in the Canadian High Arctic from February to June.[175]

Among the three measured iSOA tracers, the 2-methyltetrols were the most abundant iSOA constituents, with 2-methylerythritol being more abundant than 2-methylthreitol (Table 2.1, Figure 2.1). The ratio of 2-methylerythritol to 2-methylthreitol was approximately 5:2, similar to previous oceanic observations.[80] 2-MG contributed only a small mass fraction (12% on average) to the total mass of the iSOA tracers measured during this study. Assuming that the organic aerosol (OA) mass measured in the 2002-2003 samples is representative of other years during 1991-2015, Table A2 shows a ratio of total identified iSOA tracers to the total $PM_{10}$ OA mass averaged to 0.40 % (up to 0.65%) in summer and 0.07% in winter (see Appendix A for OA estimation). The mass fractions are much lower than at continental sites, especially in the summertime southeastern U.S. where isoprene emissions combine with anthropogenic-derived acidic sulfate aerosol to yield large quantities of these SOA constituents (e.g., ~ 9% of total OA mass at Look Rock, Tennessee).[160]

A distinct seasonal variation was observed over the 1991-2015 sampling period (Figure 2.2), in which the summed mass concentration of iSOA tracers was higher in the austral summers than in the austral winters of the same year, with the sole exception being 1997 winter. The 1991-2015 mean of total iSOA was 2.84±1.66 ng $m^{-3}$ in summer compared to 0.64±0.66 ng $m^{-3}$ in winter. In the 13 years for which both summer and winter samples are available, winter concentrations accounted for only 20±17% of the total annual iSOA mass with the exception of four years (1994, 1997, 1999 and 2014), when winter concentrations contributed relatively larger fractions (32%, 61%, 41%, 29%, respectively). Such seasonal variations of iSOA tracers have also been observed at a number of terrestrial and marine sampling sites, but have typically been limited to a single year of sampling.[169,171,173,174,176]

No distinct temporal trend over the 1991-2015 sampling period was observed for iSOA tracers (p-value of slope = 0.89) and the mass fractions of the three iSOA tracers remained fairly

constant (Figure 2.2 and Table A1). The highest concentrations of the summed iSOA tracers (6.75 ng $m^{-3}$) occurred in summer of 1998, possibly a result of the 1997-1998 El Niño–Southern Oscillation (ENSO, La Niña phenomenon) that caused a flow of warm water to the equatorial western Pacific Ocean and eastern coast of Australia and consequent phytoplankton blooms.[177] However, total iSOA concentrations did not correlate with the Oceanic Niño Index (ONI) during the 1991-2015 sampling period. This was not surprising since the La Niña as well as the El Niño phenomena influences primarily the equatorial Pacific region, while the Cape Grim site is located below the -40° latitude. We are unable to conclude from our dataset how strongly (and by what mechanism) the 1997-1998 ENSO event enhanced iSOA levels.

iSOA tracers typically observed over the continents were not identified in our marine $PM_{10}$ samples. For instance, the three isomeric $C_5$-alkene triols were not detected concurrently with the 2-methyltetrols observed by GC/EI-MS at Cape Grim. This finding is consistent with previous oceanic measurements of average levels of $C_5$-alkene triols summed over a worldwide ocean cruise, reporting the $C_5$-alkene triols to be less abundant than the 2-methyltetrols and 2-MG.[80] The apparent absence of $C_5$-alkene triols in the GC/EI-MS analysis of Cape Grim sample extracts suggests that their concentrations were at or below the detection limits of our GC/EI-MS technique. In this regard, it is important to note recent work that has demonstrated 2-methyltetrol sulfates (if present) decompose during GC/EI-MS analysis to yield the $C_5$-alkene triols,[178] indicating that $C_5$-alkene triols reported by the GC/EI-MS analytical protocol may be artifacts of the analytical procedure. Given this suggestion, the absence of $C_5$-alkene triols in the Cape Grim samples analyzed by GC/EI-MS are in accord with the fact that the isomeric 2-methyltetrol sulfate esters were not detected by UPLC/ESI-HR-QTOFMS, a sensitive and definitive protocol for detection of organosulfates. Consistent with our findings, we note that during an austral summer, Claeys et

al. did not detect the $C_5$-alkene triol or 2-methyltetrol markers at Amsterdam Island, a pristine marine environment in the southern Indian Ocean.[179] Our inability to detect $C_5$-alkene triols, 2-methyltetrol sulfate esters and 2-MG sulfate at Cape Grim over a lengthy period of sampling might be explained by: (1) insufficient ambient concentrations due to the low isoprene emission/flux as well as low yield relative to 2-MG and 2-methyltetrols; (2) oceanic formation pathways of 2-MG and 2-methyltetrol sulfates differing from those over continental locations,[160,180] and (3) degradation (hydrolysis of isoprene-derived organosulfates[181]) over long-term storage. Since formation of $C_5$-alkene triols has been associated with acidic sulfate aerosol,[157,158] our lack of detection may also suggest that the remote marine aerosol collected at Cape Grim is not as acidic as continental aerosol.[32,160]

Laboratory studies have demonstrated that 2-MG and 2-methyltetrols are formed through different chemical pathways from the hydroxyl radical-initiated oxidation and/or ozonolysis of isoprene. Specifically, 2-methyltetrols are the major products of isoprene photochemical oxidation by OH under conditions of low nitrogen oxide concentrations (low-$NO_x$ conditions) via the isoprene epoxydiol (IEPOX) pathway.[182] Over continental areas, acid-catalyzed multiphase reaction of IEPOX on acidic sulfate aerosol yields these iSOA tracers. Over oceanic regions, 2-methyltetrols may form through IEPOX hydrolysis in non-acidic aqueous inorganic aerosol or through cloud processing.[183,184] Chamber studies by Kleindienst et al. and Riva et al. have shown that isoprene ozonolysis can also yield these iSOA tracers;[185,186] however, average seasonal $O_3$ concentrations at Cape Grim ranged from ~ 35 ppb in winter to ~ 15 ppb in summer (Figure A2) and did not correlate with the seasonal trend of iSOA, likely ruling out ozonolysis as a source of these iSOA marker compounds. 2-MG is formed predominantly by OH-initiated oxidation of isoprene under high-$NO_x$ conditions via a pathway through methacrolein (MACR) and

methacryloylperoxynitrate (MPAN).[158,187] In remote oceans the mixing ratios of $NO_x$ are typically below 10 pptv within the marine boundary layer,[188] and 2-MG, if present, must occur through alternative chemical pathways. For example, Kleindienst et al. demonstrated that both 2-MG and 2-methyletrols could form in the absence of both $NO_x$ and acidic sulfate aerosol when isoprene was photochemically oxidized during smog chamber studies; however, the exact mechanisms of their formations under these conditions remain unclear.[189] All in all, under low-$NO_x$ conditions, OH-initiated oxidation of isoprene could lead to the 2-methyltetrols and 2-MG, the iSOA markers we detected, and might explain the absence of their corresponding organosulfates (i.e., 2-methytetrol and 2-MG sulfates) in remote marine aerosol.

### *2.4.2 Monoterpene-Derived SOA (mSOA) Tracers*

Five mSOA tracers (terebic acid, terpenylic acid, DTAA, MBTCA, and pinic acid) are summarized in Tables 2.1 and A1 and in Figure 2.1. The mSOA tracers were identified in almost all of the 29 seasons. The sum of the five mSOA tracers ranged from 0.03 to 1.11 ng $m^{-3}$, with an average of 0.33±0.30 ng $m^{-3}$. This is approximately one-fifth of the quantified iSOA tracers, probably due to less significant marine sources of monoterpenes compared to isoprene in this region.[73]

The mSOA tracer concentrations were up to three orders of magnitude lower than those measured at many continental sites,[169–171,190] but comparable to the oceanic concentrations over the Southern Ocean and seas adjacent to the Australian continent ranging from latitudes of 30-60°S,[80] and over oceans at low latitudes in the Northern Hemisphere.[147] Unlike iSOA tracers, the measured concentrations of mSOA tracers were much lower than those in the Canadian High Arctic,[175] which is probably influenced by the continental emissions of monoterpenes from boreal forests.

In addition to the five reported mSOA tracers, corresponding ions of additional mSOA tracers, such as 3-hydroxyglutaric, 3-hydroxy-4,4-dimethylglutaric and 2-hydroxy-4-isopropyladipic acids,[190] were detected but not quantified because of the lack of authentic standards (and lack of appropriate surrogates). Other known mSOA tracers such as hydroxyterpenylic acid,[191] α-pinene-derived organosufates,[134] and dimer esters such as pinyl-diaterebyl ester (molecular weight (MW) 344), pinyl-diaterpenyl eseter (MW 358), pinonyl-pinyl ester (MW 368),[60,135,192–194] were also targeted for analysis but were below the detection limit of the UPLC/ESI-HR-QTOFMS.

Similar to the iSOA tracers, an obvious seasonal variation was observed throughout the quarter century period of filter collection (Figure 2.2), with higher concentrations of mSOA tracers in austral summers than in winters. The seasonal mean concentration of the total mSOA tracers was 0.53±0.21 ng $m^{-3}$ in summer and 0.15±0.09 ng $m^{-3}$ in winter. In the 13 years with both summer and winter samples available, winter concentrations accounted for only one fifth (22±7%) of the summed mSOA mass. Moreover, the individual and summed iSOA concentration measured by the GC/EI-MS and mSOA measured by the UPLC/ESI-HR-QTOFMS agreed well with each other over the decades (Tables 2.2 and 2.3), but neither correlated with levoglucosan (Table 2.2). Although levoglucosan, a well-known biomass burning tracer, was not correlated with either iSOA or mSOA, long-range transport of continental-derived levoglucosan could contribute from time-to-time to the remote marine OA collected at Cape Grim (See Baseline Report information in Appendix A).

No distinct general trend for the measured mSOA tracers was observed during the entire sampling period (p-value = 0.29). As in the case of iSOA tracers, the highest concentration of total

mSOA tracers (1.00 ng $m^{-3}$) occurred in summer of 1998, which may indicate the same source or event leading to phytoplankton blooms and the enhanced formation of mSOA and iSOA tracers.

In contrast to the iSOA tracers, the relative fractions of the five mSOA tracers did not remain constant over time. Of the five reported mSOA tracers, DTAA was the most abundant species, followed by terpenylic acid, terebic acid, MBTCA, pinic acid. These five mSOA tracers have also been reported by UPLC/ESI-HR-QTOFMS as the most abundant mSOA tracers in laboratory-generated α-pinene SOA.[135,192] Consistency between the field observations and the laboratory studies above, including the relative abundance of the tracers above and absence of dimer esters, suggests that these mSOA tracers were primarily produced from OH-initiated oxidation over ozonolysis of α-pinene.

### *2.4.3 Correlation of iSOA and mSOA with Particle-Phase Bioactivity Indicators*

Phytoplankton chemically fix carbon and release metabolites into sea water and the atmosphere, including dimethylsulfide (DMS), isoprene, and monoterpenes.[63,71,72,195] DMS is oxidized to MSA and isoprene to oxalic acid (through glyoxal, methylglyoxal, and pyruvic acid).[63,196–198] Studies suggest that aqueous-phase oxidation of marine biota-derived unsaturated fatty acids and phenolic compounds also contribute to the presence of oxalic acid in marine aerosol.[179,199,200] Hence, MSA and oxalic acid are considered to be bioactivity tracers for phytoplankton.[63,65,154,196] Since isoprene and monoterpenes are co-emitted with DMS by many phytoplankton species,[76] the iSOA and mSOA tracers might be anticipated to correlate with MSA and oxalic acid in the particulate phase.[201] Table 2.3 and Figure A3, show the correlation of summed iSOA tracers (∑iSOA) with summed mSOA tracers (∑mSOA) and MSA over 29 seasons from 1991-2015 and with oxalic acid over 21 season from 1996-2015. ∑iSOA is moderately

correlated with ∑mSOA (r = 0.74), MSA (r = 0.61) and oxalic acid (r = 0.62), while ∑mSOA is somewhat more strongly correlated with MSA (r = 0.75) and oxalic acid (r = 0.81).

The seasonal variations of ∑iSOA and ∑mSOA were described in Figure 2.2 and tracers MSA, oxalic acid, and chlorophyll-*a* in Figure 2.2. Overall, Figure 2.2 shows a consistent pattern of seasonal variations (with the exception of ∑iSOA during 1997-1998). The most pronounced pattern is displayed by MSA with all winter concentrations < 10 ng $m^{-3}$ and all summer concentrations >60 ng $m^{-3}$. The seasonal pattern of oxalic acid was less pronounced than MSA, possibly due to more sources of oxalic acid as just described. However, the correlations of oxalic acid and MSA with ∑iSOA were almost the same as those with ∑mSOA. Such moderate correlations highlight the likely role of phytoplankton as a marine source of the BVOCs (isoprene and monoterpenes), indicating that iSOA and mSOA might be formed through the similar atmospheric processes to that of other marine biogenic aerosol components (i.e., MSA and oxalic acid) originating from phytoplankton. It is noted here that the sodium ion ($Na^+$) concentration measured from the Cape Grim aerosol samples had no significant correlation with either the iSOA or mSOA tracers (r = -0.30 and -0.29, respectively, and with p-values > 0.05). The lack of significant correlation with $Na^+$ aerosol mass concentration further suggests that the measured iSOA and mSOA tracers are secondary rather than primary in nature.

### *2.4.4 Correlation of iSOA and mSOA with Chlorophyll-a*

As another proxy for phytoplankton activity, integrated chlorophyll-*a* content was obtained over 13 seasons from 2004-2015, corresponding to the same period of filter collection, averaged for the region within 30-60°S and 90-150°E (Figure 2.2). This region was selected based on back trajectory studies (Appendix A) for suitable timescales (~ 3.8 days) of SOA formation and transport. The chlorophyll-*a* content, measured daily over the entire planet by the Moderate

Resolution Imaging Spectroradiometer (MODIS) instrument aboard NASA's Terra and Aqua satellites, was retrieved from a NASA Earth Observations' online resource with high resolution (0.1° latitude × 0.1° longitude, monthly or 8-day). The trend of satellite-measured chlorophyll-*a* concentrations (seasonal average = 0.126±0.011 mg $m^{-3}$) closely matched local measurements from 2003-2006 in seawater samples collected offshore at Couta Rocks, approximately 50 km south of Cape Grim (Figure A4).

Chlorophyll-*a* concentrations exhibited seasonal variation, ranging between 0.075-0.180 mg $m^{-3}$ (Figure 2.2), with higher levels in summer than winter, consistent with the ∑iSOA and ∑mSOA during the same period and in accord with expectation based on activity of phytoplankton as a source. This source assignment is supported by a moderate-to-strong correlation with ∑iSOA ($r = 0.74$) and ∑mSOA ($r = 0.85$) (Table 2.3 and Figure A3) and is consistent with the role of phytoplankton emissions as a source of marine isoprene and monoterpenes. As has been suggested for MSA, low concentrations of iSOA and mSOA over remote marine locations may contribute to cloud condensation nuclei (CCN).[202] More work is warranted to investigate to what extent marine iSOA and mSOA can serve as CCN; however, laboratory studies by Engelhart et al. demonstrated that pure SOA derived from the OH-initiated oxidation of isoprene in the absence of sulfate aerosol had similar CCN activation kinetics to pure ammonium sulfate aerosol.[203] Furthermore, a recent study over the mid-western U.S. reported isoprene-derived organosulfates, which are also known iSOA tracers, in cloud water samples.[204] Taken together, these prior laboratory and field measurements of iSOA indicate that iSOA may contribute (in part) to CCN activity of aerosol.

**2.5 Conclusions**

Since the marine aerosol samples chemically characterized in this study originated over the open ocean, where terrestrial emissions were largely absent, our results provide important

quantitative background levels of marine biogenic SOA over a 25-year period (i.e., 1991-2015). Spatial distributions of marine iSOA and mSOA tracers were previously observed at higher concentrations over the coastal/tropical regions than the open oceans.[147] In the southern mid latitudes (30°S-60°S), where Cape Grim is located, iSOA and mSOA were one to two orders of magnitude lower than those in the other oceanic regions.[80] Our observations indicate that there are marine sources of isoprene and monoterpenes derived from phytoplankton activity leading to biogenic SOA formation over the open oceans. Although isoprene, monoterpenes, and chlorophyll-*a* were not as abundant at Cape Grim as other coastal and oceanic sites,[73] oxidation of isoprene and monoterpenes yields measurable seasonal and temporal trends of iSOA and mSOA. iSOA and mSOA do not contribute substantial mass to the total OA mass (0.26±0.24%, up to 0.71%) measured at this site, possibly because $PM_{10}$ samples were collected instead of submicron particles to which iSOA and mSOA mainly contribute.[205] Notably, recent Arctic measurements have also shown that SOA in that remote marine atmosphere does not have chemical characteristics that are typical of continental SOA (i.e., the OA is secondary but arising from a different set of precursors than isoprene and monoterpenes);[206] specifically, it was shown that SOA is required to form in order to fit the aerosol size distributions measured during the Arctic summer even though the mean isoprene and monoterpene mixing ratios were 1.5 and 5 pptv, respectively.[205,207] The latter supports our findings that secondary OA sources other than isoprene and monoterpenes exist in the remote marine atmosphere.

It is noted that the summed mass concentrations of oxalic acid and MSA were ~ 28 times higher than the summed concentrations of iSOA and mSOA. Additionally, the sum of iSOA, mSOA, oxalic acid, and MSA mass concentrations contributed up to 19.0% of the total OA mass (Table A2), which is consistent with Claeys et al. at Amsterdam Island during summertime.[179]

Consequently, more work is needed to chemically characterize other OA constituents (e.g., saccharides and fatty acids) that additionally contribute to marine aerosol in order to reveal their sources. In particular, more information is required to fully understand the OA constituents associated with phytoplankton blooms in order to more clearly identify the processes that generate OA such as bubble bursting processes and SOA precursors likely derived from the sea surface microlayer.[207] Preliminary findings obtained from the UPLC/ESI-HR-QTOFMS method operated in both negative and positive ion modes revealed the presence of nitrogen (N)-containing organic species (Table A3), as indicated by the accurate measured mass. The tentatively identified N-containing species (as well as CHO and CHOS compounds) may also contribute to the uncharacterized OA mass that remains in this study; however, we did not include these preliminary findings of the N-containing, CHO, and CHOS compounds because we did not have appropriate standards to fully identify their structures as well as accurately quantify their mass concentrations. As a result, characterization of these compounds is beyond the scope of the present study. Our results provide observations and motivation for future laboratory, field, and modelling studies to assess the potential of the marine sources leading to biogenic SOA and OA formation over the open oceans.

**2.6 Acknowledgement**

This work was funded by the National Oceanic and Atmospheric Administration (NOAA) Climate Program Office's AC4 Program, award number NA13OAR4310064. Continued support for the Cape Grim Program from the Australian Bureau of Meteorology and CSIRO and the personal effort of numerous Cape Grim support staff maintaining equipment and collecting samples over the program lifetime is gratefully acknowledged. Ian Galbally and Suzie Molloy from CSIRO are thanked for providing the monthly ozone data from Cape Grim, Nada Derek from

CSIRO is thanked for assistance with graphics. Steven Sai Hang Ho, Judith Chow from Desert Research Institute and Bim Graham are thanked for the collection and analysis of total OA mass measured in the Cape Grim 2002-2003 samples.

**Table 2.1**. Summary of isoprene-derived SOA (iSOA) and monoterpene-derived SOA (mSOA) tracers (ng $m^{-3}$) measured by GC/EI-MS and UPLC/DAD-ESI-HR-QTOFMS, respectively, in aerosol samples collected from austral winter and summer seasons from 1991-2015.

| | n[a] | mean | median | min. | max. | S.D.[b] |
|---|---|---|---|---|---|---|
| **iSOA tracers** | | | | | | |
| 2-methylglyceric acid | 28 | 0.20 | 0.17 | bdl[c] | 0.72 | 0.16 |
| 2-methylthreitol | 28 | 0.44 | 0.27 | bdl | 1.81 | 0.44 |
| 2-methylerythritol | 29 | 1.07 | 0.86 | 0.05 | 4.21 | 1.05 |
| *subtotal* | | *1.70* | *1.30* | *0.05* | *6.75* | *1.66* |
| **mSOA tracers** | | | | | | |
| terebic acid | 29 | 0.08 | 0.04 | 0.007 | 0.32 | 0.08 |
| terpenylic acid | 29 | 0.08 | 0.07 | 0.007 | 0.23 | 0.07 |
| pinic acid | 29 | 0.02 | 0.01 | 0.003 | 0.05 | 0.01 |
| MBTCA[d] | 23 | 0.03 | 0.03 | bdl | 0.15 | 0.04 |
| DTAA[e] | 29 | 0.11 | 0.08 | 0.008 | 0.36 | 0.10 |
| *subtotal* | | *0.33* | *0.23* | *0.026* | *1.11* | *0.30* |

[a] n is number of seasons detected (out of total 29 seasons).
[b] S.D. is one standard deviation.
[c] bdl indicates below detection limit.
[d] MBTCA is 3-methyl-1,2,3-butanetricarboxylic acid.
[e] DTAA is diaterpenylic acid acetate.

**Table 2.2**. Pearson correlation coefficients (r) of concentrations (ng $m^{-3}$) of individual iSOA, levoglucosan, and mSOA tracers measured by GC/EI-MS or UPLC/ESI-HR-QTOFMS from aerosol samples collected from 29 austral summer and winter seasons from 1991-2015.

| Correlations (r) | iSOA Tracers | | | mSOA Tracers | | | | | Other |
|---|---|---|---|---|---|---|---|---|---|
| | 2-MG | 2-Methyl threitol | 2-Methyl erythritol | Terebic acid | Terpeny-lic acid | Pinic acid | MBTCA | DTAA | Levoglu-cosan |
| 2-MG[a] | 1.00 | 0.80 | 0.81 | 0.80 | 0.82 | 0.43 | 0.69 | 0.48 | 0.21 |
| 2-Methylthreitol | | 1.00 | 1.00 | 0.76 | 0.58 | 0.16 | 0.73 | 0.47 | 0.07 |
| 2-Methylerythritol | | | 1.00 | 0.78 | 0.60 | 0.17 | 0.75 | 0.47 | 0.06 |
| Terebic acid | | | | 1.00 | 0.72 | 0.34 | 0.60 | 0.67 | -0.06 |
| Terpenylic acid | | | | | 1.00 | 0.56 | 0.55 | 0.64 | 0.10 |
| Pinic acid | | | | | | 1.00 | -0.05 | 0.42 | -0.02 |
| MBTCA[b] | | | | | | | 1.00 | 0.50 | 0.28 |
| DTAA[c] | | | | | | | | 1.00 | 0.13 |
| Levoglucosan | | | | | | | | | 1.00 |

[a] 2-MG stands for 2-methylglyceric acid.
[b] MBTCA is 3-methyl-1,2,3-butanetricarboxylic acid.
[c] DTAA is diaterpenylic acid acetate.

**Table 2.3**. Pearson correlation coefficients (r) of concentrations of summed iSOA tracers (∑iSOA), summed mSOA tracers (∑mSOA), oxalic acid, methanesulfonic acid (MSA), and Chlorophyll-*a* (Chl-*a*) determined by GC/EI-MS, UPLC/DAD-ESI-HR-QTOFMS, IC, or satellite, respectively, from austral summer and winter seasons from 1991-2015.

| **Correlations** (r) | ∑iSOA | ∑mSOA | Oxalic | MSA | Chl-*a* |
|---|---|---|---|---|---|
| ∑iSOA | 1.00 | 0.74 | 0.62 | 0.61 | 0.74 |
| ∑mSOA | | 1.00 | 0.81 | 0.75 | 0.85 |
| Oxalic acid | | | 1.00 | 0.69 | 0.56 |
| MSA | | | | 1.00 | 0.83 |
| Chlorophyll-*a* | | | | | 1.00 |

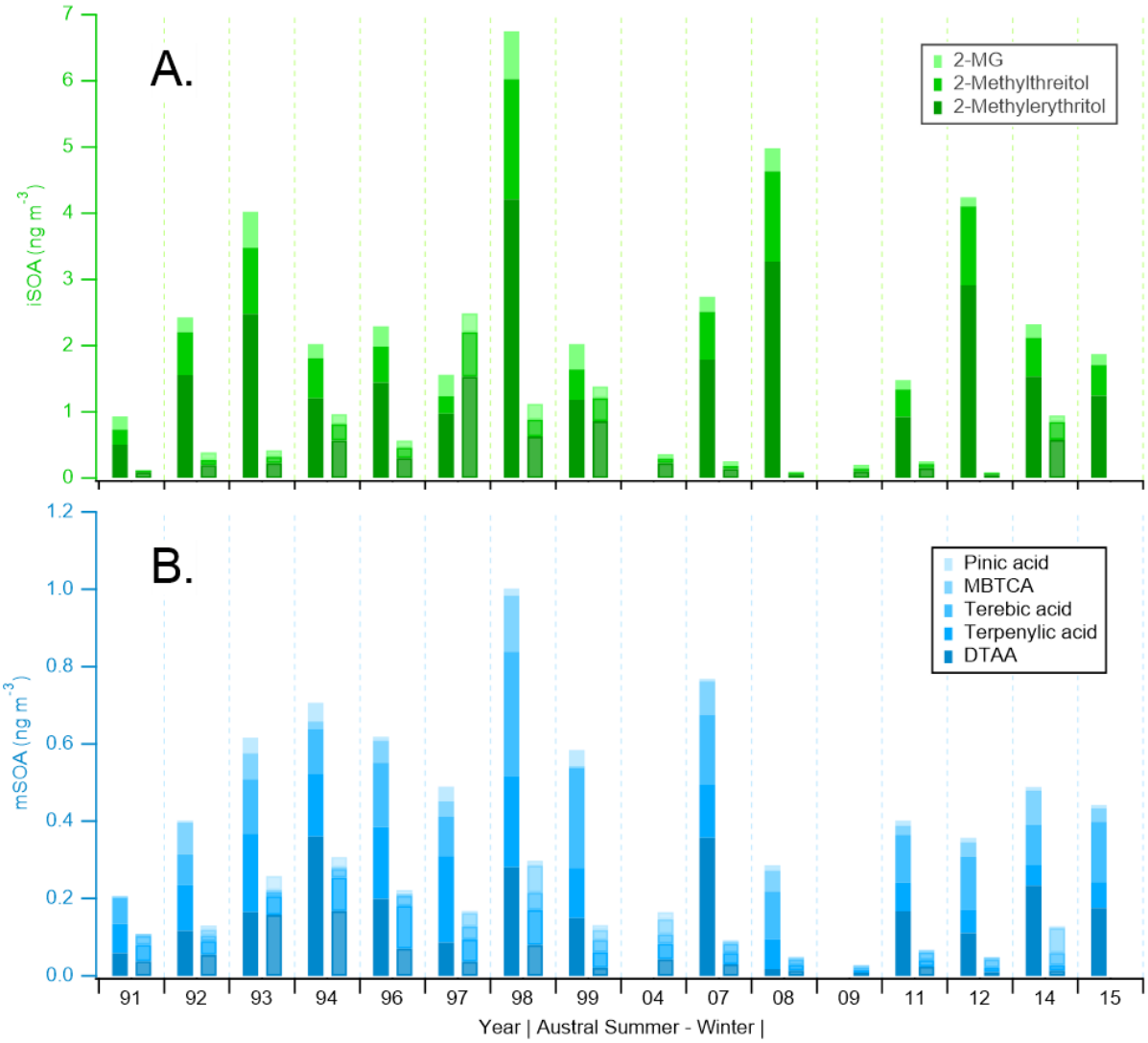


**Figure 2.1. (A.)** Three isoprene-derived SOA tracers (iSOA, in ng $m^{-3}$) measured by GC/EI-MS; **(B.)** five monoterpene-derived SOA tracers (mSOA, in ng $m^{-3}$) measured by UPLC/ESI-HR-QTOFMS in the 29 selected seasons from 1991-2015. The stacked bars on the right side within each year, if available, represent the austral winters (mid-Jun. – mid-Aug.) of that year, and are displayed in a slightly lighter color.

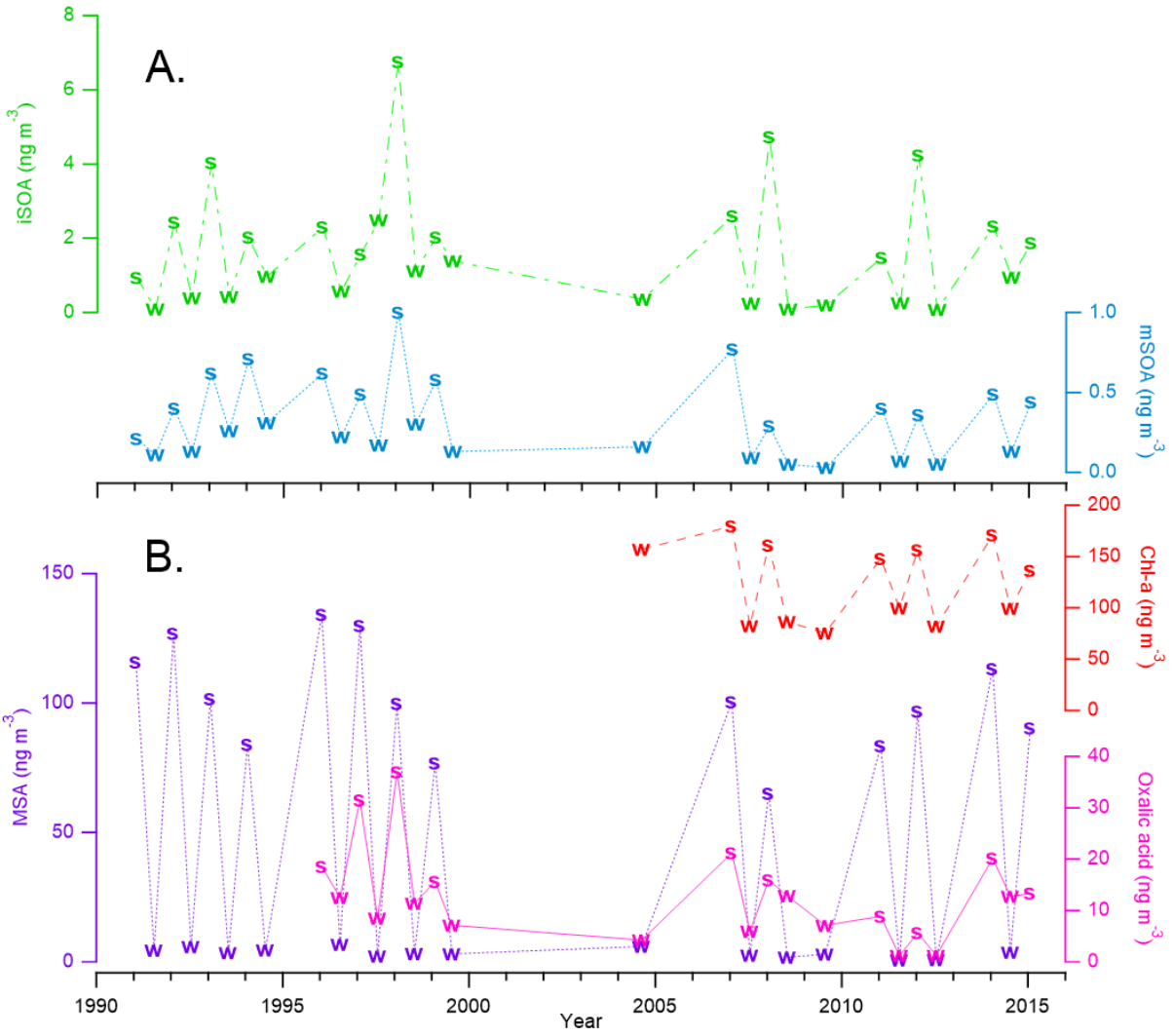


**Figure 2.2.** Seasonal and temporal trends of: **(A.)** summed isoprene-derived SOA (iSOA) and monoterpene-derived SOA (mSOA) tracers; and **(B.)** methanesulfonic acid (MSA), oxalic acid, and chlorophyll-*a* (Chl-*a*) in the 29 selected seasons from 1991-2015.

# CHAPTER 3: DEVELOPMENT OF A HYDROPHILIC INTERACTION LIQUID CHROMATOGRAPHY METHOD FOR THE CHEMICAL CHARACTERIZATION OF ISOPRENE EPOXYDIOL-DERIVED SECONDARY ORGANIC AEROSOL[2]

## 3.1 Overview

Acid-catalyzed multiphase chemistry of isoprene epoxydiols (IEPOX) on sulfate aerosol produces substantial amounts of water-soluble secondary organic aerosol (SOA) constituents, including 2-methyltetrols, methyltetrol sulfates, and oligomers thereof in atmospheric fine particulate matter ($PM_{2.5}$). These constituents have commonly been measured by gas chromatography interfaced to electron ionization mass spectrometry (GC/EI-MS) with prior derivatization or by reverse-phase liquid chromatography interfaced to electrospray ionization high-resolution mass spectrometry (RPLC/ESI-HR-MS). However, both techniques have limitations in explicitly resolving and quantifying polar SOA constituents due either to thermal degradation or poor separation. With authentic 2-methyltetrol and methyltetrol sulfate standards synthesized in-house, we developed a hydrophilic interaction liquid chromatography (HILIC)/ESI-HR-quadrupole time-of-flight mass spectrometry (QTOFMS) protocol that can chromatographically resolve and accurately measure the major IEPOX-derived SOA constituents in both laboratory-generated SOA and atmospheric $PM_{2.5}$. 2-Methyltetrols were simultaneously

[2] This chapter is reproduced by permission from "Development of a Hydrophilic Interaction Liquid Chromatography (HILIC) Method for the Chemical Characterization of Water-Soluble Isoprene Epoxydiol (IEPOX)-Derived Secondary Organic Aerosol" by Cui, T.; Zeng, Z.; dos Santos, E. O.; Zhang, Z.; Chen, Y.; Zhang, Y.; Rose, C. A.; Budisulistiorini, S. H.; Collins, L. B.; Bodnar, W. M.; de Souza, R. A. F.; Martin, S. T.; Machado, C. M. D.; Turpin, B. J.; Gold, A.; Ault, A. P. and J. D. Surratt, *Environ. Sci. Process. Impacts*, 2018, *20* (11), 1524–1536. Copyright (2018) Royal Society of Chemistry.

resolved along with 4-6 diastereomers of methyltetrol sulfate, allowing efficient quantification of both major classes of SOA constituents by a single non-thermal analytical method. The sum of 2-methyltetrols and methyltetrol sulfates accounted for approximately 92%, 62%, and 21% of the laboratory-generated β-IEPOX aerosol mass, laboratory-generated δ-IEPOX aerosol mass, and organic aerosol mass in the southeastern U.S., respectively, where the mass concentration of methyltetrol sulfates were 171-271% the mass concentration of methyltetrol. Mass concentrations of methyltetrol sulfates were 0.39 and 2.33 μg $m^{-3}$ in a $PM_{2.5}$ sample collected from central Amazonia and the southeastern U.S., respectively. The improved resolution clearly reveals isomeric patterns specific to methyltetrol sulfates from acid-catalyzed multiphase chemistry of β- and δ-IEPOX. We also demonstrate that conventional GC/EI-MS analyses overestimate 2-methyltetrols by up to 188%, resulting (in part) from the thermal degradation of methyltetrol sulfates. Lastly, $C_5$-alkene triols and 3-methyltetrahydrofuran-3,4-diols are found to be largely GC/EI-MS artifacts formed from thermal degradation of 2-methyltetrol sulfates and 3-methyletrol sulfates, respectively, and are not detected with HILIC/ESI-HR-QTOFMS.

**3.2 Introduction**

Atmospheric fine particulate matter ($PM_{2.5}$, aerosol particles with aerodynamic diameters ≤ 2.5 μm) adversely affects air quality. High concentrations of $PM_{2.5}$ can lead to degradation of outdoor visibility[208] and adversely affect human health through cardiovascular and respiratory diseases.[209] Moreover, atmospheric $PM_{2.5}$ plays a critical role in climate change through both direct and indirect mechanisms.[210] Organic aerosol (OA) constituents are recognized to contribute a substantial fraction of $PM_{2.5}$ mass from urban to remote regions around the world.[211] OA is further characterized into primary organic aerosol (POA) and secondary organic aerosol (SOA). POA is directly emitted in the particle phase from sources, such as sea spray, wildfires, automobiles and

cooking, while SOA is formed from the atmospheric oxidation of volatile organic compounds (VOCs) emitted by both anthropogenic and natural sources. Specifically, low volatility oxidation products from VOCs either nucleate or condense onto existing particles and undergo multiphase chemistry to form SOA, which is estimated to contribute 70-90% of OA mass found within $PM_{2.5}$.[212]

Isoprene is the most abundant non-methane hydrocarbon emitted into Earth's atmosphere and is derived largely from deciduous trees.[25] The atmospheric oxidation of isoprene plays an important role in both tropospheric ozone ($O_3$) and SOA formation in forested regions affected by anthropogenic activities.[26–33] The hydroxyl radical-initiated oxidation of isoprene during the daytime under low-nitric oxide (NO) conditions produces substantial amounts of isoprene epoxydiols (IEPOX) (~50% yield).[34,35] The acid-catalyzed multiphase chemistry (reactive uptake) of IEPOX onto anthropogenic sulfate particles has been shown to produce SOA constituents including 2-methyltetrols,[28,29,36,37] $C_5$-alkene triols,[28,29,36,37] 3-methyltetrahydrofuran-3,4-diols (3-MeTHF-3,4-diols),[29] organosulfates,[29,37–39] and oligomers.[29,37,40] Studies have also pointed out that the mixed effects of sulfate (e.g., aerosol acidity, nucleophile, surface area, and salting-in) play a critical role in forming atmospheric IEPOX-derived SOA.[30,38,41–43]

Protocols for chemical characterization of IEPOX-derived SOA $C_5$ tracers, including the 2-methyltetrols, $C_5$-alkene triols, and 3-MeTHF-3,4-diols, have generally employed gas chromatography interfaced to electron ionization mass spectrometry (GC/EI-MS) with prior trimethylsilylation.[28,29,36–38,129] These tracer species have been widely used to investigate SOA formation mechanisms, derive kinetic parameters, and evaluate model performance of IEPOX-derived SOA.[29,36,139,140] However, volatility and composition analysis by a Filter Inlet for Gases and Aerosol coupled to a Chemical Ionization Mass Spectrometer (FIGAERO-CIMS) equipped

with iodide reagent ion chemistry demonstrated that IEPOX-derived SOA has lower volatility than predicted from the concentrations of commonly reported IEPOX SOA $C_5$ tracers, in particular the 2-methyltetrols, $C_5$-alkene triols and 3-MeTHF-3,4-diols, and therefore thermal decomposition of accretion products (oligomers) or other low volatility organics such as organosulfates may contribute significantly to tracers.[141] A second set of studies using FIGAERO-CIMS or semi-volatile thermal desorption aerosol gas chromatogram (SV-TAG) instrumentation with online derivatization reached similar conclusions on the impact of thermal decomposition.[142–145] Different protocols, based on ultra-performance liquid chromatography interfaced to high-resolution tandem mass spectrometry with electrospray ionization (UPLC/ESI-HR-$MS^n$), have been used to characterize organosulfates and oligomers. However, separation of polar, water-soluble components is conventionally attempted with reverse-phase liquid chromatography (RPLC) columns.[28,29,38,146] RPLC columns do not resolve such compounds well because of either extremely short retention times (RTs), poor peak shapes, or ion suppression effects due to co-eluting inorganic aerosol constituents, leading to potential complications in identifying and quantifying target compounds. The IEPOX-derived polyols are hydrophilic compounds owing to their hydroxyl functional groups, and the organosulfates are ionic polar compounds.[141,146] Hence, an alternative approach for the IEPOX-derived SOA characterization that could accomplish simultaneous analysis of polar and water-soluble components while avoiding the drawbacks associated with current analytical methods would be highly desirable.

Hydrophilic interaction liquid chromatography (HILIC) is as an alternative LC method to RPLC to separate hydrophilic (i.e., water-soluble) compounds, including peptides and nucleic acids[213] and has recently been reported to separate water-soluble organosulfates with excellent resolution.[214–216] The HILIC solid phase can be silica gel with a decreased surface concentration

of silanol groups, or silica chemically bonded to polar groups, such as amino, amide, cyano, carbamate, diol, polyol, or zwitterionic sulfobetaine groups.[217] A HILIC column separates analytes by forming a water-rich layer, which is partially immobilized around the hydrophilic ligands on the stationary phase. Analytes can undergo partitioning between the bulk organic eluents and the water-rich layer to separate based on different levels of retention.[218] Although retention order on HILIC columns is similar to that on normal phase liquid chromatography (NPLC) columns, HILIC utilizes more polar mobile phases (e.g., acetonitrile (ACN) and Milli-Q water) than the NPLC so that the HILIC method is compatible for interfacing with ESI-MS sources.[219] ESI is a soft ionization detection method not involving sample heating or derivatization and is appropriate for detection of polar $C_5$ tracers, and oligomers as well as water-soluble organosulfates. Based on the demonstrated success of HILIC in the chemical characterization of organosulfates from synthesized standards and field samples,[214–216] we undertook development of a HILIC/ESI-HR-quadrupole time-of-flight mass spectrometry (HILIC/ESI-HR-QTOFMS) method for the simultaneous separation, characterization, and quantitation of water-soluble IEPOX-derived SOA constituents from laboratory-generated β-IEPOX and δ-IEPOX SOA as well as $PM_{2.5}$ collected from the southeastern U.S. at Look Rock, Tennessee (TN), during the Southern Oxidant and Aerosol Study (SOAS) in 2013 and central Amazonia at Manaus, Brazil in 2016. The HILIC/ESI-HR-QTOFMS protocol developed here can resolve IEPOX-derived 2-methyltetrols, methyltetrol sulfates and oligomers thereof, allowing unambiguous identification and quantification. Current atmospheric models explicitly simulate SOA from the acid-catalyzed multiphase chemistry of IEPOX (i.e., the formation of 2-methyltetrols and methyltetrol sulfates),[140,220–222] and the accurate quantification of the 2-methyltetrols and the derived organosulfates will increase confidence in evaluation of model predictions, which will in turn lead to improved modeling. Improvement in

quantification of organosulfates will additionally provide much needed data for establishing carbon and sulfur mass closure (or mass balance) in IEPOX-derived SOA measured or predicted during future lab and field studies.

## 3.3 Experimental Section

### *3.3.1 Synthesized Chemicals*

#### *3.3.1.1 Trans-β- and δ-IEPOX*

Racemic *trans*-β-IEPOX (trans-2-methyl-2,3-epoxybutane-1,4-diol) and δ-IEPOX (3-methyl-3,4-epoxy-1,2-butanediol) were synthesized in-house according to published methods.[223,224]

#### *3.3.1.2 IEPOX-Derived SOA Standards: 2-methyltetrols, 2-methyltetrol sulfates, and 3-methyltetrol sulfates*

Diastereomeric mixtures of racemic 2-methyltetrols (racemic 2-methylerythritol and 2-methylthreitol, MW = 136 g $mol^{-1}$) were synthesized by acid hydrolysis of δ-IEPOX according to the procedure described in Bondy et al.[223] A diastereomeric mixture of racemic 2-methyltetrol sulfates ((2*R*,3*S*)/((2*S*,3*R*)- and (2*S*,3*S*)/(2*R*,3*R*)-1,3,4-trihydroxy-2-methylbutan-2-yl sulfates, MW = 216 g $mol^{-1}$; Table 1) was synthesized from 2-methyltetrol. Briefly, the primary and secondary hydroxyl groups of 2-methyltetrol were protected by acetylation with acetic anhydride. The acetylated product was purified by column chromatography on $SiO_2$, eluted with ethyl acetate and then sulfated by a published procedure.[225] The protecting acetyl groups were then removed by treatment with ammonia to afford the expected diastereomeric 2-methyltetrol sulfates. The purity of the 2-methyltetrol sulfates was determined by proton nuclear magnetic resonance ($^1$H NMR) spectroscopy analysis to be > 99 % (Figure B1, in Appendix B). The diastereomeric 3-methyltetrol sulfate racemates ((2*R*,3*S*)/((2*S*,3*R*)- and (2*S*,3*S*)/(2*R*,3*R*)-2,3,4-trihydroxy-3-methylbutyl sulfates;

MW = 216 g $mol^{-1}$; Table 1) were prepared from δ-IEPOX by a procedure described in Bondy et al.[223] Briefly, to an ice-cold solution of δ-IEPOX in ACN, $Bu_4NHSO_4$ and a small amount of potassium bisulfate were added and the reaction allowed to warm to room temperature and stirred overnight. The resulting mixture of sulfate esters was purified on a Dowex 50W x 4-100 ion exchange column. The final product contained 95.5% 3-methyltetrol sulfates by $^1H$ NMR analysis.

### *3.3.2 HILIC/ESI-HR-QTOFMS Method*

An Agilent 6520 Series Accurate Mass Q-TOFMS instrument interfaced to an Agilent 1200 Series UHPLC system, equipped with an ESI source operated in the negative (-) ion mode, was used to chemically characterize IEPOX-derived SOA standards, as well as lab and field samples. Optimum ESI conditions were: 3500 V capillary voltage, 130 V fragmentor voltage, 65 V skimmer voltage, 300 ºC gas temperature, 10 L $min^{-1}$ drying gas flow rate, 35 psig nebulizer, 25 psig reference nebulizer. ESI-QTOFMS mass spectra were recorded from mass-to-charge ratio (*m/z*) 60 to 1000. HILIC separations were carried out using a Waters ACQUITY UPLC BEH Amide column (2.1×100 mm, 1.7 µm particle size, Waters) at 35 ºC. The mobile phases consisted of eluent (A) 0.1% ammonium acetate in water, and eluent (B) 0.1% ammonium acetate in a 95:5 (v/v/) ACN (HPLC Grade, 99.9%, Fisher Scientific)/Milli-Q water. Both eluents were adjusted to a pH of ~9.0 with $NH_4OH$.[215] The gradient elution program was eluent A, 0% for 4 min, increasing to 15% from 4 to 20 min, constant at 15% between 4 and 24 min, decreasing to 0% from 24 to 25 min, and constant at 0% from 25 to 30 min. The flow rate and sample injection volume were 0.3 mL $min^{-1}$ and 5 µL, respectively. Data were acquired and analyzed by Mass Hunter Version B.06.00 Build 6.0.633.0 software (Agilent Technologies). At the beginning of each analysis period, the mass spectrometer was calibrated using a commercially available ESI-L low-mass concentration tuning mixture (Agilent Technologies) in a 95:5 (v/v) ACN/Milli-Q water.

Instrument mass axis calibration was conducted in the low-mass range (*m/z* 50-1700). Seven masses were used for calibration: *m/z* 68.9958, 112.9856, 301.9981, 601.9790, 1033.9881, 1333.9689, and 1633.9498. The adduct of hexakis (1H,1H,3H-tetrafluoropropoxy) phosphazene + acetate (*m/z* 980.0164), purine (*m/z* 119.0363), and leucine enkephalin (*m/z* 554.2620) were continuously infused for real-time mass axis correction. The mass resolution of the ESI-HR-QTOFMS was approximately 8,000-12,300 from *m/z* 113-1600.

For comparison purposes, RPLC separations (Waters ACQUITY UPLC HSS T3 $C_{18}$ column, 2.1×100 mm, 1.8 μm particle size) were also conducted on selected samples that were analyzed by HILIC, where pure methanol (99.9%, Fisher Chemical) was used as the mobile phase (B) and standards and samples were prepared in 50:50 Milli-Q water/methanol. The detailed operating procedures for RPLC separations have been described elsewhere.[226] In addition, GC/EI-MS analysis with prior derivatization was performed following the procedures described previously.[29,37] In brief, a diluted aliquot of each filter extract was dried and trimethylsilylated by reaction with 200 μL of BSTFA + TMCS (*N*,*O*-bis (trimethylsilyl) trifluoroacetamide + trimethylchlorosilane, 99:1, Supelco) and 100 μL of pyridine (anhydrous, 99.8%, Sigma-Aldrich). The reaction mixture was heated at 70 ℃ for 1 h and analyzed on a Hewlett-Packard (HP) 5890 Series II gas chromatograph coupled to a HP 5971A mass selective detector with an Econo-Cap-EC-5 capillary column (30 m × 0.25 mm i.d., 0.25 μm film thickness) within 24 h. The 65-min temperature program of the GC initiated at 60 ℃ for 1 min, and then rose with a temperature ramp of 3 ℃ $min^{-1}$ to 200 ℃ and isothermally held for 2 min, followed by another temperature ramp of 20 ℃ $min^{-1}$ to 310 ℃ and isothermally held for 10 min. The temperatures of both the GC inlet and detector were at 250 ℃.

### *3.3.3 Laboratory-Generated SOA from β- and δ-IEPOX*

SOA from acid-catalyzed reactive uptake of *trans*-β-IEPOX or δ-IEPOX was generated in the 10-$m^3$ indoor environmental smog chamber at the University of North Carolina as described previously.[29,42] Briefly, experiments were carried out under dark and wet conditions (50-55%, RH) at 295±1 K. Prior to each experiment, the chamber was flushed continuously with clean air for ~24 hours corresponding to a minimum of seven chamber volumes until the particle mass concentration was < 0.01 μg $m^{-3}$ to ensure that there were no pre-existing aerosol particles. Chamber flushing also reduced VOC concentrations below the detection limit (~75 ppt for IEPOX) of an iodide-adduct high-resolution time-of-flight chemical ionization mass spectrometer (HR-TOF-CIMS). Operating details of the HR-TOF-CIMS have been previously described.[42] Temperature and RH in the chamber were continuously monitored using a dew point meter (Omega Engineering Inc., Norwalk, CT). Acidic $(NH_4)_2SO_4$ seed aerosol was injected into the pre-humidified chamber using a custom-built atomizer with an aqueous solution of 0.06 M $(NH_4)_2SO_4$ and 0.06 M $H_2SO_4$ until the desired total aerosol volume concentration (~75 $\mu m^3$ $cm^{-3}$) was achieved. After seed injection, the chamber was left static for at least 30 min to ensure that the seed aerosol was stable and uniformly mixed. Then, 30 mg of *trans*-β- or δ-IEPOX was injected into the chamber at 2 L $min^{-1}$ for 10 min and then 4 L $min^{-1}$ for 50 min by passing high-purity nitrogen gas through a heated manifold (60 °C) containing an ethyl acetate solution of one of the IEPOX isomers described in section 2.1.1.

On completion of IEPOX injection, a filter sample was collected for the subsequent offline analysis using HILIC (or RPLC)/ESI-HR-QTOFMS. Aerosols were collected onto a 47 mm Teflon filter (0.2 μm, Pall Scientific) in a stainless-steel filter holder for 30 min at a flow rate of 13.2 L $min^{-1}$. The filter sample along with a blank filter taken from the same batch on the day of the

experiment were stored in a 20 mL scintillation vial at -20 ℃ prior to extraction and analysis. In addition to the filter sampling, SOA generated from the reactive uptake of IEPOX was collected using a particle-into-liquid sampler (PILS, Model 4001, Brechtel Manufacturing Inc., Hayward, CA - BMI) system at the end of each experiment. The aerosols were sampled through an organic vapor denuder (Sunset Laboratory Inc.) and a 2.5-μm size-cut pre-impactor at a flow rate of ~12.5 L $min^{-1}$. The sample air flow was then mixed adiabatically with a steam flow heated at 98.5-100 ℃ in the PILS condensation chamber to produce high supersaturation of water vapor that grow particles to collectable sizes for collection onto a quartz impactor plate by inertial impaction. Impacted droplets were transferred by a wash-flow at ~0.55 mL $min^{-1}$ through a debubbler and the resulting bubble-free sample liquid was delivered through a tubing with an inline filter into 2-mL poly vials held on an auto-collector (BMI) with a rotating carousel. Air sampling rate and wash-flow rate were examined and recorded before and after each experiment. Milli-Q water used in the wash-flow was spiked with 25 μM lithium bromide (LiBr, Sigma-Aldrich, 99.5%) as an internal standard to correct for dilution caused by condensation of water vapor during droplet collection. The dilution factor was typically from 1.1-1.2. The PILS vials were promptly stored under dark conditions at 2 ºC upon collection until analysis. Chamber aerosol number distributions, which were subsequently converted to total aerosol surface area and volume concentrations, were monitored by a scanning electrical mobility system (SEMS v5.0, BMI) containing a differential mobility analyzer (DMA, BMI) coupled to a mixing condensation particle counter (MCPC, Model 1710, BMI), in order to estimate the total aerosol mass. Summary of the experimental conditions can be found in Table S1.

### *3.3.4 Field Sample Collection of $PM_{2.5}$*

*3.3.4.1 Look Rock, Tennessee, Southeastern U.S.*

Quartz filter samples of $PM_{2.5}$ were collected at a field site (Look Rock, TN, USA) during the Southern Oxidant and Aerosol Study (SOAS) campaign in summer 2013 by a previously described procedure.[31] The filters were stored in the dark in a -20 ℃ walk-in freezer until chemical analysis. The sample selected for re-analysis was collected for three hours (16:00-19:00 local time) when one of the highest isoprene-derived SOA concentrations was measured during the campaign.[31,32]

*3.3.4.2 Manaus, Brazil, Central Amazonia*

$PM_{2.5}$ samples were collected from November 28 - December 1 (transition of dry-to-wet season), 2016 on pre-baked Tissuquartz Filters (Whatman, 20 cm × 25 cm) using a high-volume $PM_{2.5}$ sampler (ENERGÉTICA with $PM_{2.5}$ Size Selective Inlet) located in the School of Technology of the Amazonas State University in Manaus, Brazil, near a major road. The high-volume $PM_{2.5}$ sampler was located 6 m above the ground and was equipped with a cyclone operated at 1.13 $m^3$ $min^{-1}$. Sampler was flow calibrated and the filter holder was cleaned with the filter extraction solvent (95:5 ACN/Milli-Q water for HILIC or methanol for RPLC) each day before sampling to ensure no carryover between samples. All filters were pre-baked for 12 h at 550 ℃ and all samples were collected for 24 h. $PM_{2.5}$ mass was determined by weighing filters before and after sampling (at 21±2 ℃, under < 50% RH). Filters were stored at -18 ºC in the dark until analysis. Similar to the sample selected from Look Rock, one sample (i.e., November 30, 2016) selected for re-analysis had the highest loading of $PM_{2.5}$ and IEPOX-derived SOA tracers (e.g. 2-methyltetrols and $C_5$-alkene triols) measured by GC/EI-MS among all samples.

### *3.3.5 Sample Preparation for Offline Analyses*

#### *3.3.5.1 2-Methyltetrol and Methyltetrol Sulfate Standards*

The 2-methyltetrol, 2-methyltetrol sulfate and 3-methyltetrol sulfate standards were stored at -20 ℃ until use. The standards were dissolved in a 2 mg $mL^{-1}$ Milli-Q water solution, and then serially diluted immediately with 95:5 (v/v) ACN/Milli-Q water to 50, 10, 1, 0.25, 0.1, 0.025, and 0.01 μg $mL^{-1}$ standards. The diluted standards were kept at 4 ℃ and analyzed within 24 h of preparation with the laboratory and field samples described below.

#### *3.3.5.2 Laboratory-Generated IEPOX SOA Samples*

Blank and sample filters of SOA generated from *trans*-β-IEPOX and δ-IEPOX were immersed in 22 mL of methanol and first extracted for 23 min by ultra-sonication, the water bath replaced with cool water, and then extracted again for 22 min. This was done to ensure the water bath inside the sonicator did not get too warm (from 25-30 ℃, measured by a thermometer). The extracts were filtered through polypropylene membrane syringe filters and the solvent was evaporated under a gentle stream of nitrogen gas. Half of the dried methanol extracts were reconstituted with 150 μL of 95:5 (v/v) ACN/Milli-Q water and then diluted by a factor of 100 or 50, respectively for the β-IEPOX- and δ-IEPOX-derived SOA samples, in order to prepare the methyltetrol sulfates in the linear range of the calibration curves. The concentrations of the methyltetrol sulfates in the 150 μL reconstituted solutions were not saturated and calculated later to be 360-410 μg $mL^{-1}$, which were much lower than the solubility of the methyltetrol sulfates that were determined to be at least 2500 μg $mL^{-1}$; specifically, maximum solubility was determined by dissolving 25 mg of the methyltetrol sulfate standards in 10 mL of 95:5 (v/v) ACN/Milli-Q water. The aqueous PILS samples collected for the laboratory-generated IEPOX SOA near the end of the experiment were diluted by a factor of 20 using ACN in order to prepare them in 95:5 (v/v)

ACN/Milli-Q water, and promptly analyzed using the HILIC/ESI-HR-QTOFMS method without any further pretreatment.

*3.3.5.3 Field Samples*

A 37-mm-diameter punch from the quartz filter from Look Rock along with a lab blank filter were extracted as described above. Half of the Look Rock $PM_{2.5}$ extract was reconstituted with 150 µL of 95:5 (v/v) ACN/Milli-Q water and then diluted by a factor of 20.

Similarly, a 47-mm diameter punch from the selected quartz filter from Manaus, Brazil, as well as a lab blank filter, was extracted as described above. The residues were reconstituted in 1 mL methanol and a 0.3 mL aliquot was dried and reconstituted in 150 µL of 95:5 (v/v) ACN/Milli-Q water, and then diluted by a factor of 30 for analysis by HILIC/ESI-HR-QTOFMS.

## 3.4 Results and Discussion

### *3.4.1 Separation of Standards: 2-Methyltetrols, 2- and 3-Methyltetrol Sulfates*

The synthesized standards of 2-methyltetrols, 2- and 3-methyltetrol sulfates (Section 2.1.2) were analyzed by both RPLC and HILIC columns coupled to the ESI-HR-QTOFMS. As shown in the extracted ion chromatograms (EICs at *m/z* 215.023 ± 0.01) in Figure 3.1, both 2- and 3-methyltetrol sulfate standards co-elute from the RPLC column as one peak at 1.5 min (Figure 3.1, a1-a2). By contrast, the HILIC protocol resolved the 2-methyltetrol sulfate diastereomers at RTs of 4.2 and 5.2 min. (Figure 3.1-b1 and B2). The unambiguous synthetic route allows assignment of the diastereomers as the tertiary sulfates. Two additional trace peaks at RTs of 2.1 and 2.6 min are also resolved and assigned to the secondary methyltetrol sulfate diastereomers ((2*R*,3*S*)/(2*S*,3*R*)- and (2*S*,3*S*)/(2*R*,3*R*)-1,3,4-trihydroxy-3-methylbutan-2-yl sulfates) present as a trace impurity (< 1%). The standard derived from hydrolysis of δ-IEPOX shows the predominant peaks at 8.0 and 8.3 min, assigned as the expected primary sulfate diastereomers (95.5%) (Figure

3.2-a1 and B2). A small quantity of the diastereomers at RTs of 2.1 and 2.6 min assigned to the secondary sulfates (~1.2 %) is resolved, and the tertiary sulfates at 4.2 and 5.2 min are also present in a small amount (~6.7%) (Figure 3.1-b2 and B2). These results are in line with the resolution of diastereomers of methyltetrol sulfates observed in ambient aerosol by Hettiyadura et al. using similar HILIC techniques; however, structural assignments in this past study were tentative and not based on unambiguous synthetic routes.[215,216] The secondary sulfate diastereomers in the HILIC trace of the standard derived by hydrolysis of δ-IEPOX are reasonably explained by a small yield of the less favored secondary hydrolysis product. The presence of 2-methyltetrol sulfates (tertiary sulfates) is surprising and will be discussed in more detail below in relation to the analysis of δ-IEPOX-derived SOA.

Comparison of the total ion chromatograms (TICs) acquired by RPLC and HILIC from an IEPOX-derived SOA in Figure B3, along with Figure 3.1, unequivocally demonstrates the superiority of HILIC for resolving the multiple diastereomeric components of SOA, especially organosulfates derived from IEPOX.

Figure 3.2-a1 shows that the deprotonated 2-methyltetrol diastereomers (racemic 2-methylerythritol and 2-methylthreitol) eluted at an identical RT of 4.0 min using the HILIC column. By contrast, GC/EI-MS analysis with prior derivatization is able to separate the 2-methyletrol diastereomers.[28,29,37] However, HILIC protocol is able to resolve diastereomers of 2- and 3-methyltetrol sulfates not resolvable by either GC/EI-MS or RPLC. Importantly, the 2-methyltetrols were simultaneously detected and resolved along with the methyltetrol sulfates. To our knowledge, this HILIC/ESI-HR-QTOFMS method presents the first time that the major IEPOX-derived SOA constituents, confirmed by authentic 2-methyletrols, 2- and 3-methyltetrol

sulfates, have been chromatographically resolved and characterized by a single mass spectrometric technique operated with one column and ionization mode.

The linear dynamic range for the 2-methyltetrols was 0.01-25 μg $mL^{-1}$ with a limit of detection (LOD) of 7.74 μg $L^{-1}$ and a limit of quantification (LOQ) of 25.8 μg $L^{-1}$ (Table 1). The linear dynamic range of 2-methyltetrol sulfates was 0.01-10 μg $mL^{-1}$, with an LOD of 1.72 μg $L^{-1}$ and an LOQ of 5.75 μg $L^{-1}$. The linear dynamic range of 3-methyltetrol sulfates was 0.01-25 μg $mL^{-1}$, with an LOD of 3.83 μg $L^{-1}$ and an LOQ of 12.8 μg $L^{-1}$. Coefficients of determination ($R^2$) values of the calibration curves ranged from 0.9994-1.0000. The linear dynamic ranges of the organosulfates in this study are broader than those reported by Hettiyadura et al., which ranged from 0.025-0.5 μg $mL^{-1}$.[215] The high $R^2$ and low LOQ values suggest the high performance of HILIC method is the most effective procedure for quantification of organosulfates in IEPOX-derived SOA.

### *3.4.2 Identification of 2-Methyltetrols and Methyltetrol Sulfates in Laboratory-Generated SOA and Ambient $PM_{2.5}$ Samples*

Authentic 2-methyltetrol, 2- and 3-methyltetrol sulfate standards were used to identify and quantify the corresponding SOA tracers. Figure 3.2 (a1-a5) compares the EICs at *m/z* 135.066, which correspond to the deprotonated 2-methyltetrols resolved on the HILIC column, from the 10 μg $mL^{-1}$ standards of authentic 2-methyltetrols, aerosol filter extracts of laboratory-generated SOA derived from *trans*-β-IEPOX and δ-IPEOX, $PM_{2.5}$ samples from the Look Rock field site during 2013 SOAS campaign and from Manaus, Brazil in November 2016. The chromatographic peak at 4.0 min corresponding to the 2-methyltetrols were observed in all samples as the predominant peak, which demonstrates that HILIC/ESI-HR-QTOFMS can unequivocally identify the 2-methyltetrols in laboratory and ambient $PM_{2.5}$ samples.

Figure 3.2 (b1-b5) compares the EICs at *m/z* 215.023 of 10 μg $mL^{-1}$ standards of authentic 2- and 3-methyltetrol sulfates, filter samples of laboratory-generated SOA derived from *trans*-β-IEPOX and δ-IEPOX, $PM_{2.5}$ samples collected from Look Rock during the 2013 SOAS campaign and from Manaus, Brazil in November 2016, respectively. The predominant primary sulfate diastereomers at RTs of 8.0 and 8.3 min in the 10 μg $mL^{-1}$ 3-methyltetrol sulfate standard (Figure 3.2-b1, solid line) are present as abundant components of the laboratory-generated δ-IEPOX SOA (Figure 3.2-b3) and as expected, were absent from the 10 μg $mL^{-1}$ standard of the 2-methyltetrol sulfate (Figure 3.2-b1, dashed line), and the laboratory-generated *trans*-β-IEPOX SOA (Figure 3.2-b2), confirming their origin as the acid-catalyzed multiphase chemistry of δ-IEPOX. In addition, the diastereomeric peaks at RTs of 4.2 and 5.2 min were unexpectedly present in Figure 3.2-b3 as major SOA products from δ-IEPOX. This diastereomeric pair can be unequivocally assigned as the tertiary sulfates, which cannot be generated from δ-IEPOX without isomerization. Hence the trace in Figure 3.2-b3 indicates importance of isomerization on reactive uptake of δ-IEPOX.[29] Furthermore, Figure 3.2-b2 shows only a single significant product eluting at 5.2 min, indicating the presence of a single pair of enantiomer products. This peak is therefore indicative of *trans*-β-IEPOX as the source, but surprisingly requires that substitution at the tertiary carbon proceeds either with complete retention or complete inversion of optical configuration. Since the expected $S_N1$ substitution mechanism generally results in epimerization of asymmetric centers (i.e. diastereomeric products would be expected), the substitution is either extremely rapid or involves an $S_N2$ mechanism. Such observations will be helpful in studies to determine the origin and formation pathway of ambient methyltetrol sulfates. Full scan mass spectra of selected chromatographic peaks at *m/z* 215.023 in Figure 3.2 are shown in Figure B4.

The 2- and 3-methyltetrol sulfates derived from β- and/or δ-IEPOX were present in ambient $PM_{2.5}$ SOA collected at the Look Rock and Manaus field sites (Figure 3.2, b4-b5). The two diastereomers arising uniquely from δ-IEPOX (8.0, 8.3 min), and predominant in the 3-methyltetrol sulfate standard, were barely detected in the ambient aerosol samples. This observation supports (*cis*- or *trans*-) β-IEPOX as the predominant ambient IEPOX isomer, accounting for 97% of total ambient IEPOX,[35] which corroborates results based on ESI-ion mobility spectrometry (IMS)-HR-TOFMS as reported by Krechmer et al.[227] for the $PM_{2.5}$ collected from the Look Rock site during the 2013 SOAS campaign. Hence, the methyltetrol sulfate diastereomers at 2.1, 2.6, 4.2, 5.2 min support β-IEPOX isomers as the major contributor to the $PM_{2.5}$ collected at both of the Look Rock and Manaus field sites, which demonstrates the advantage of HILIC/ESI-HR-QTOFMS in differentiation of isomers and apportionment of reaction pathways.[29,31,37]

### *3.4.3 Quantification of 2-Methyltetrols and Methyltetrol Sulfates in Laboratory-Generated SOA and Ambient $PM_{2.5}$ Samples*

Concentrations of the 2-methyltetrols and methyltetrol sulfates in the laboratory-generated SOA collected by PILS and ambient $PM_{2.5}$ filters were quantified by HILIC/ESI-HR-QTOFMS and are summarized in Table 2. For the 2- and 3-methyltetrol sulfates, integrated areas of the 4-6 chromatographic peaks were summed to derive an overall response. As a result, the response factor (defined as the ratio of peak area to concentration) of the 2-methyltetrol sulfate standard was ~50% greater than that of the 3-methyltetrol sulfate standard. PILS sampling was chosen for better mass closures and to avoid uncertainties due to filter sampling artifacts and additional pretreatment procedures. Methyltetrol sulfates were quantified by an authentic 2-methyltetrol sulfate standard since the two major chromatographic peaks (RTs at 4.2 and 5.2 min) were consistently

predominant in the standard and the $PM_{2.5}$ samples, except that authentic 3-methyltetrol sulfate was used as a standard to quantify methyltetrol sulfate in laboratory-generated SOA from δ-IEPOX. The percentage of 2-methyltetrols and methyltetrol sulfates in total aerosol mass is also shown in Table 2, calculated by dividing the mass concentration of each compound by the total aerosol mass obtained from SEMS-MCPC, assuming a particle density of 1.42 g $cm^{-3}$ for β-IEPOX SOA or 1.55 g $cm^{-3}$ for δ-IEPOX SOA (see Appendix B for details). The analytical uncertainty in the quantification was determined to be up to ~14.1% (Appendix B). As shown in Table 3.2, the concentration of the 2-methyltetrols in laboratory-generated *trans*-β-IEPOX-derived SOA was 63.98 μg $m^{-3}$ (33.9% of total particle mass) and the concentration of methyltetrol sulfates was 109.67 μg $m^{-3}$ (58.2% of total particle mass). In the laboratory-generated SOA from δ-IEPOX, the concentration of the 2-methyltetrols 29.49 μg $m^{-3}$ (19.6% of total aerosol mass) and methyltetrol sulfates was 62.98 μg $m^{-3}$ (41.9% of total aerosol mass). Together, the two IEPOX-derived SOA tracers contributed 92.1±13.0% of the total aerosol mass from β-IEPOX and 61.5±8.7% of the total aerosol mass from δ-IEPOX (Table 2). The methyltetrol sulfates account for approximately twice the 2-methyltetrol mass. The mass fractions of methyltetrol sulfates indicate conversion of a significant amount of inorganic sulfate seed aerosol to organosulfates, supported by measurements using ion chromatography for the PILS samples (Figure B5).

In addition to the monomeric methyltetrol sulfates (*m/z* 215.023), Figure 3.3 shows that the HILIC column resolves multiple isomeric methyltetrol sulfate dimers (*m/z* 333.086) in laboratory SOA generated from β- and δ-IEPOX, suggesting oligomeric products as a likely source of the unaccounted for aerosol mass. RPLC did not resolve isomers of either species, since all water-soluble species co-eluted at ~2 min (Figure B3).[29,37] Additionally, small intensities of 2-

methyltetrol dimers ($C_{10}H_{21}O_7^-$, *m/z* = 253.129) were detected in ambient samples from Look Rock and Manaus field sites. These dimers were not quantified due to the lack of authentic standards.

In the Look Rock $PM_{2.5}$ sample with the highest IEPOX-derived SOA concentration observed during the 2013 SOAS campaign,[31] the mass concentration of the 2-methyltetrol was measured by HILIC/ESI-HR-QTOFMS to be 0.86 μg $m^{-3}$, accounting for 5.6% of the total OA mass, or 7.5% of the total organic carbon (OC) mass. The total OA mass concentration averaged during the sampling period was determined to be 15.30 μg $m^{-3}$ using an Aerodyne Aerosol Chemical Speciation Monitor (ACSM),[31] and the total OC mass concentration from the same sample was measured to be 5.04 μgC $m^{-3}$ using a Sunset laboratory OC-elemental carbon (EC) aerosol analyzer. Methyltetrol sulfates, quantified using the 2-methyltetrol sulfate standard, were determined to be 2.33 μg $m^{-3}$, accounting for 15.3% of the total OA (or 12.9% of the total OC) mass, and significantly higher than 1.14 μg $m^{-3}$ measured by RPLC/ESI-HR-QTOFMS.[12] This discrepancy suggests that the RPLC/ESI-HR-QTOFMS method likely underestimates the methyltetrol sulfate concentrations, possibly resulting from insufficient dilution of Look Rock sample extracts (leading to concentrations beyond the linear range of the method), or appropriate isomeric standards, or caused by ion suppression due to co-elution with other water-soluble organic or inorganic aerosol components. The sum of the 2-methyltetrols and methyltetrol sulfates quantified by the new method accounted for 20.9±2.9% of the total OA mass in the Look Rock sample during the 2013 SOAS campaign when high intensity of isoprene and anthropogenic emissions (acidic sulfate aerosol) were observed, making IEPOX-derived SOA the single largest contributor to the characterized OA constituents.[31]

For the Manaus sample, the HILIC/ESI-HR-QTOMS analysis measured 0.14 and 0.39 μg $m^{-3}$ for 2-methyltetrols and methyltetrol sulfates, respectively, accounting for 0.74% and 1.34% of

the total OC mass concentration (8.12 μgC $m^{-3}$ for this particular sample collected on November 30, 2016) measured by a Sunset laboratory OC-EC aerosol analyzer. In addition, elevated concentrations of levoglucosan (0.46 μg $m^{-3}$ by GC/EI-MS), EC (1.18 μgC $m^{-3}$ by a Sunset OC-EC aerosol analyzer), and $PM_{2.5}$ (46.1 μg $m^{-3}$) were observed on this particular day, and more generally during the November 28-30, 2016, sampling period due to the large influence of biomass burning. In fact, average levoglucosan, OC, EC, and $PM_{2.5}$ concentrations during this biomass burning intensive period were 0.41 μg $m^{-3}$, 8.0 μgC $m^{-3}$, 1.3 μgC $m^{-3}$, and 43.6 μg $m^{-3}$, respectively. The elevated biomass burning likely explains why the IEPOX-derived SOA tracers accounted for a lower % contribution to the total OC mass versus the southeastern U.S. sample (Table 2), which the latter had little influences of biomass burning.

### *3.4.4 Other Measurable Water-Soluble Organic Compounds in Ambient $PM_{2.5}$*

In addition to the targeted analysis for the 2-methyltetrols and methyltetrol sulfates, we were able to detect several other isoprene-derived organosulfates in the ambient $PM_{2.5}$ samples. Figure 3.4 shows the EICs of organosulfates with chemical formulas $C_4H_7O_7S^-$ (*m/z* 199, accurate mass = 198.9912), $C_5H_9O_7S^-$ (*m/z* 213, accurate mass = 213.0069), and $C_5H_7O_7S^-$ (*m/z* 211, accurate mass = 210.9912) detected in the $PM_{2.5}$ samples from Look Rock and Manaus. These species have also been reported from other field and laboratory studies, including EICs obtained from HILIC/ESI-MS.[39,214–216] The ion of *m/z* 199 was confirmed as the sulfate ester derived from another isoprene SOA tracer 2-methylglyceric acid in high-$NO_x$ conditions.[30,228] The structures of the *m/z* 211 and 213 were tentatively proposed with EICs consistent with previous observations.[39,214,216]

### *3.4.5 Discrepancy between HILIC/ESI-HR-QTOFMS and GC/EI-MS – Thermal Degradation of Organosulfates*

Table 3 lists the concentrations of 2-methyltetrols in samples of SOA from β-IEPOX, δ-IEPOX, Look Rock, and Manaus quantified in parallel by HILIC/ESI-HR-QTOFMS and GC/EI-MS with prior derivatization. The concentrations of 2-methyltetrols determined by GC/EI-MS were 204, 236, 160, and 288%, respectively, of that determined by HILIC/ESI-HR-QTOFMS. The discrepancies are consistent with suggestions that GC/EI-MS overestimates semi-volatile marker compounds because of thermal degradation of low volatile accretion products (e.g., oligomers or possibly organosulfates).[141] To investigate whether the overestimation in fact resulted from thermal degradation or trimethylsilylation of the analytes, calibration curves of 2-methyltetrol, 2- and 3-methyltetrol sulfates were generated by GC/EI-MS along with the four SOA samples. As shown in Figure 3.5/B6/B7 (b-c), the isoprene-derived SOA tracers commonly observed by GC/EI-MS, including $C_5$-alkene triols, 2-methyltetrols, and 3-MeTHF-3,4-diols, were detected in the pure 2- and 3-methyltetrol sulfate standards. Figure B6 (b-c) clearly illustrates the formation of 2-methyltetrols in the GC/EI-MS analysis of the 50 μg $mL^{-1}$ 2- and 3-methyltetrol sulfate standards. The GC/EI-MS EIC of *m/z* 219 for the 50 μg $mL^{-1}$ derivatized standard of authentic 2-methyltetrol diastereomer mixture is characterized by peaks at RTs of 34.0 and 34.8 min. Peaks with relative intensities of ~0.25 and ~5% at the same RTs characterize the EICs at *m/z* 219 of the pure 2- and 3-methyltetrol sulfate standards. The 2-methyltetrols from degradation of the organosulfates can partially explain the large discrepancy measured between the HILIC/ESI-HR-QTOFMS and GC/EI-MS methods. Other organosulfates and oligomers present in the aerosol samples may also contribute to the discrepancy. The $C_5$-alkene triol tracers for isoprene SOA, have been detected only by GC/EI-MS or SV-TAG methods.[28,29,36,143,229] Lopez-Hilfiker et al. have

reported that the high concentrations of $C_5$-alkene triols measured in $PM_{2.5}$ samples analyzed by these procedures, in which samples are treated at high-temperature, are not consistent with their estimated volatility, and suggest that these compounds are degradation products of IEPOX-derived organosulfates and oligomers.[141] Based on the semi-quantitative relationship established for the $C_5$-alkene triols produced from the 2-methyltetrol sulfate standards prepared (Appendix B), 30.0%, 42.8%, and 14.7% of the $C_5$-alkene triols measured by GC/EI-MS could be attributed to the potential thermal degradation of the 2-methyltetrol sulfates in the $PM_{2.5}$ samples from laboratory-generated β-IEPOX SOA, Look Rock, and Manaus, respectively (Table S2). Similarly, 11.1% of the 2-methyltetrols and approximately all 3-MeTHF-3,4-diols in laboratory-generated δ-IEPOX SOA may be products of the thermal degradation of the 3-methyltetrol sulfates (Table S3). As demonstrated above, thermal degradation of organosulfates as well as low volatile accretion aerosol products (i.e., oligomers) explains a substantial fraction of the isoprene-derived SOA tracers previously measured through analytical methods such as GC/EI-MS or SV-TAG in which samples are treated at high temperatures.[230] HILIC/ESI-HR-QTOFMS avoids such treatment and is therefore preferred for accurate quantification of IEPOX-derived SOA constituents.

### 3.5 Conclusions

The availability of authentic IEPOX-derived SOA standards was critical in developing the HILIC/ESI-HR-QTOFMS method described here. This protocol was used to evaluate IEPOX-derived SOA samples generated in laboratory studies or $PM_{2.5}$ samples collected from two isoprene-rich regions. The HILIC column can resolve the major water-soluble IEPOX-derived SOA constituents, including the 2-methyltetrols, methyltetrol sulfates and the corresponding dimers that are predicted to form in regional and global scale atmospheric chemistry models.[140,220–222,231–233] The major water-soluble IEPOX-derived SOA constituents can be quantified by one

method with improved accuracy. We have demonstrated the ability to distinguish between different diastereomers of β- and δ-IEPOX-derived methyltetrol sulfates, which allows the contribution of the IEPOX isomers to be apportioned with the availability of authentic sulfate standards. Analysis by the HILIC method avoids high-temperatures required by GC/EI-MS or SV-TAG methods which cause degradation of IEPOX-derived organosulfates and oligomers to 2-methyltetrols, $C_5$-alkene triols, and 3-MeTHF-3,4-diols with consequent distortion of actual product distributions.[141,232]

By taking advantage of authentic standards and the HILIC/ESI-HR-QTOFMS method, we have estimated the mass fractions of the 2-methyltetrols and the methyltetrol sulfates in laboratory and ambient SOA samples. In summary, these two types of SOA constituents, likely the two largest contributors, contributed 92.1±13.0%, 61.5±8.7% to total aerosol mass, and 20.9±2.9% to OA mass from the laboratory-generated β-IEPOX SOA, laboratory-generated δ-IEPOX SOA, and Look Rock $PM_{2.5}$, respectively. These two SOA constituents contributed ~2.1% to OC mass from Manaus $PM_{2.5}$ sample, which was likely lower owing to the fact that biomass burning was a large contributor to the OC mass during this sampling period whereas the Look Rock $PM_{2.5}$ sample had little influences of biomass burning. The methyltetrol sulfates are the largest single contributor to the IEPOX SOA mass, contributing ~2-3 times of the mass of the 2-methyltetrols. The predominant contributions of organosulfates (> 90% of the reactive uptake of β-IEPOX) reveal the significance of conversion of inorganic sulfate to organosulfate, implying the critical role of inorganic sulfate as a nucleophile, and emphasize the importance of the multiphase chemistry of IEPOX leading to SOA formation in the isoprene-rich regions. In addition, oligomers derived from the methyltetrol sulfates and the 2-methyltetrols may explain the missing fraction of the total aerosol mass.

Large abundances of methyltetrol sulfates in atmospheric $PM_{2.5}$ could explain previous observations of the low-volatility nature of IEPOX-derived SOA in ambient aerosol.[141] The HILIC/ESI-HR-QTOFMS procedure described here can resolve water-soluble organic constituents from isoprene photochemical products generated via non-IEPOX pathways. HILIC separation can be interfaced to current RPLC/ESI-HR-QTOFMS procedures to develop two dimensional LC/ESI-HR-QTOFMS, further enhancing resolution of hydrophilic organic compounds in $PM_{2.5}$.

### 3.6 Acknowledgement

This work was funded by the National Science Foundation (NSF) under Atmospheric and Geospace (AGS) Grant 1703535. This work was also support in part by the NSF under Chemistry (CHE) Grant 1404644, and CAPES Foundation by Brazil Ministry of Education, Brasilia, DF 70.040-020, Brazil. The UNC Biomarker Mass Spectrometry Facility, which contains the HILIC/ESI-HR-QTOFMS instrument, is supported by the National Institute for Environmental Health Sciences (NIEHS) Grant 5P20-ES10126.

**Table 3.1.** Properties of the 2-methyltetrol, 2-methyltetrol sulfate and 3-methyltetrol sulfate standards characterized by HILIC/ESI-HR-Q-TOFMS, including retention times (RTs), linear range (L. Range), coefficient of determination ($R^2$), limit of detection (LOD), limit of quantification (LOQ) of ten replicate injections. Note that structures are for one of two diastereomers for each standard and ions are shown for the methyltetrol sulfates.

| **Standard** | **Synthesized Structural Isomer** | **Structure** | **[M-H]$^-$** | ***m/z*** | **RT(s)** (min) | **L. Range** (μg mL$^{-1}$) | **$R^2$** | **LOD** (μg L$^{-1}$) | **LOQ** (μg L$^{-1}$) |
|---|---|---|---|---|---|---|---|---|---|
| 2-methyltetrols | 2-methyl erythritol and 2-methyl threitol | 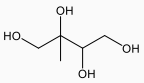 | $C_5H_{11}O_4^-$ | 135.066 | 4.0 | 0.01-25 | 0.9994 | 7.74 | 25.8 |
| 2-methyltetrol sulfates | 1,3,4-trihydroxy-2-methylbutan-2-yl sulfate | 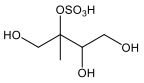 | $C_5H_{11}O_7S^-$ | 215.023 | 2.1, 2.6, 4.2, 5.2 | 0.01-10 | 0.9996 | 1.72 | 5.75 |
| 3-methyltetrol sulfates | 2,3,4-trihydroxy-3-methylbutyl sulfate | 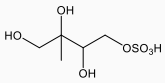 | $C_5H_{11}O_7S^-$ | 215.023 | 2.1, 2.6, 4.2, 5.2, 8.0, 8.3 | 0.01-25 | 1.0000 | 3.83 | 12.8 |

**Table 3.2.** Concentrations and mass fractions of 2-methyltetrols and methyltetrol sulfates measured from laboratory-generated SOA and ambient $PM_{2.5}$ samples by HILIC/ESI-HR-QTOFMS.

| | 2-Methyltetrols | | Methyltetrol sulfates | |
|---|---|---|---|---|
| | Mass Conc. ($\mu g\ m^{-3}$) [a] | % Total Mass [b] | Mass Conc. ($\mu g\ m^{-3}$) | % Total Mass |
| Laboratory β-IEPOX SOA | 63.98 | 33.9 % | 109.67 | 58.2 % |
| Laboratory δ-IEPOX SOA | 29.49 | 19.6 % | 62.98 | 41.9 % |
| Look Rock, TN, USA | 0.861 | 5.6 (7.5) % | 2.334 | 15.3 (12.9) % |
| Manaus, Brazil | 0.137 | (0.74) % | 0.390 | (1.34) % |

[a] The mass concentrations of 2-methyltetrols and methyltetrol sulfates were measured from the PILS samples for the laboratory-generated SOA, and from the filter samples for the Look Rock and Manaus samples;

[b] The total aerosol masswas used for the mass closure for the laboratory-generated SOA, while the organic aerosol (or organic carbon, shown in parentheses) mass was used for the mass closure for the Look Rock and Manaus samples. The total aerosol mass was determined using an SEMS-MCPC system for the laboratory-generated SOAs, assuming the particle density to be 1.42 or 1.55 g $cm^{-3}$ after reaction from β- or δ-IEPOX (Appendix B). The total organic aerosol mass for the Look Rock sample was measured by an ACSM. The OC mass for the Look Rock and Manaus samples was measured using EC/OC analyzers. The relative analytical uncertainty in the quantification was determined to be up to ~14.1% (Appendix B).

**Table 3.3**. Concentrations and discrepancies of 2-methyltetrols (μg $m^{-3}$) from laboratory-generated SOA and ambient $PM_{2.5}$ samples measured by HILIC/ESI-QTOFMS and GC/EI-MS.

| **2-Methyltetrols** (μg $m^{-3}$) | **HILIC/ESI-QTOFMS** | **GC/MS** | **Ratio** (GC/HILIC) |
|---|---|---|---|
| Laboratory β-IEPOX SOA | 69.05 | 140.86 | 204 % |
| Laboratory δ-IEPOX SOA | 51.91 | 122.56 | 236 % |
| Look Rock, TN, USA | 0.861 | 1.381 | 160 % |
| Manaus, Brazil | 0.137 | 0.394 | 288 % |

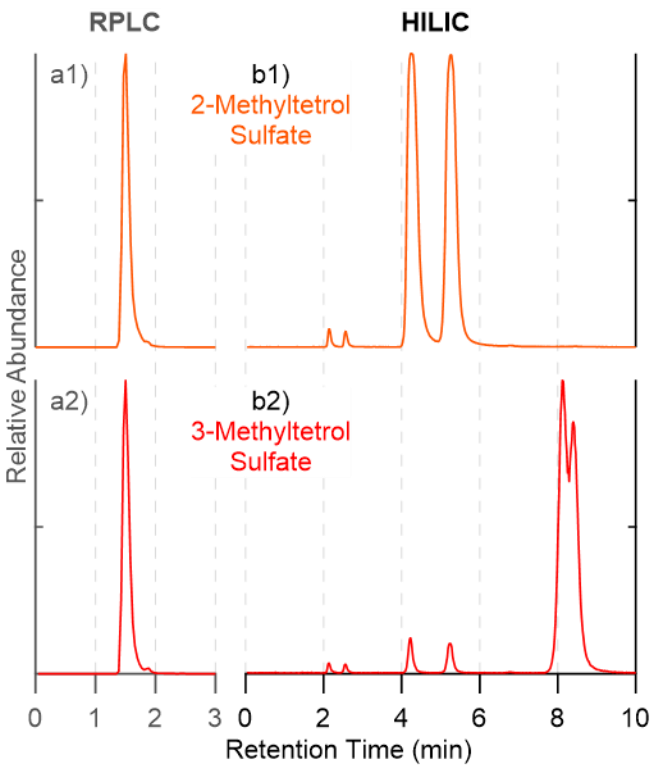


**Figure 3.1.** Extracted ion chromatograms (EICs) at *m/z* 215.023 corresponding to methyltetrol sulfates. Using **a)** RPLC $C_{18}$ column, and **b)** HILIC BEH amide column: standards of 1) 2-methyltetrol sulfates; 2) 3-methyltetrol sulfates. Standards were prepared at 10 µg $mL^{-1}$. No significant peaks were observed beyond the shown periods of retention time.

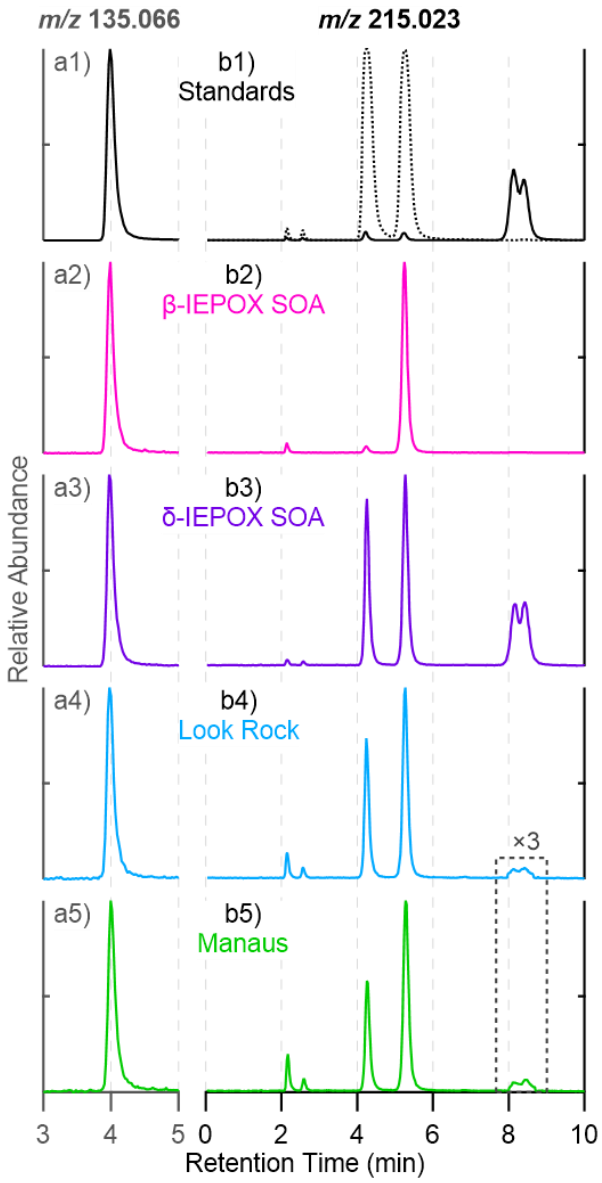


**Figure 3.2.** EICs obtained from HILIC for **a)** *m/z* 135.066 corresponding to 2-methyltetrols, **b)** *m/z* 215.023 corresponding to methyltetrol sulfates from: 1) 10 µg $mL^{-1}$ synthesized standard (b1: 2-methyltetrol sulfates (dashed line) and 3-methyltetrol sulfates (solid line)); 2) laboratory-generated β-IEPOX SOA; 3) laboratory-generated δ-IEPOX SOA; 4) $PM_{2.5}$ sample collected at Look Rock during 2013 SOAS campaign; 5) $PM_{2.5}$ sample collected at Manaus in Nov. 2016. The laboratory-generated β-IEPOX SOA, δ-IEPOX SOA, Look Rock, and Manaus samples were diluted by a factor of 200, 100, 40, and 100, respectively. No significant peaks were observed beyond the shown periods of retention time.

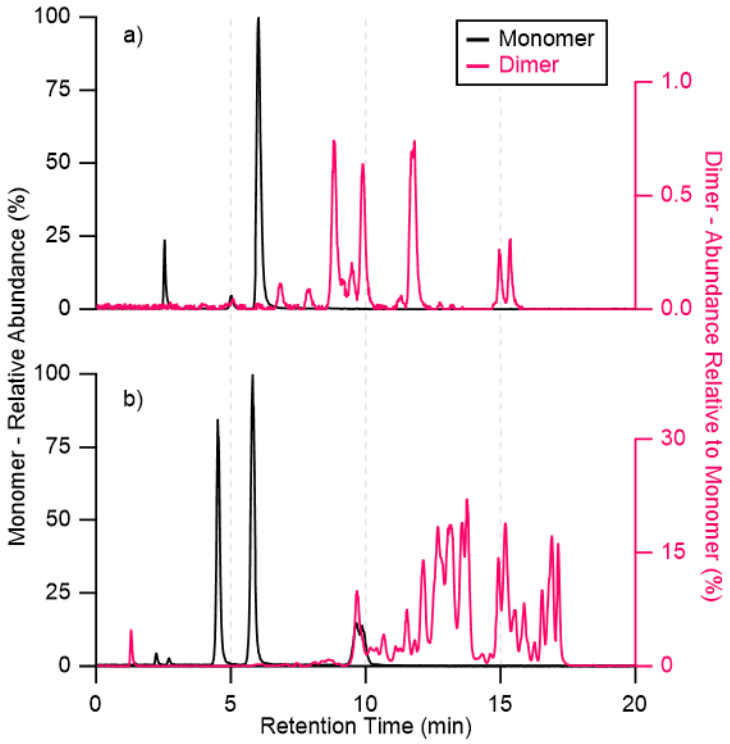


**Figure 3.3.** EICs of *m/z* 215.023 ($C_5H_{11}O_7S^-$) and 333.086 ($C_{10}H_{21}O_{10}S^-$) corresponding to methyltetrol sulfate monomers and dimers, respectively, from **a)** laboratory-generated β-IEPOX SOA diluted by a factor of 200; and **b)** laboratory-generated δ-IEPOX SOA. No significant peaks were observed beyond 20 min.

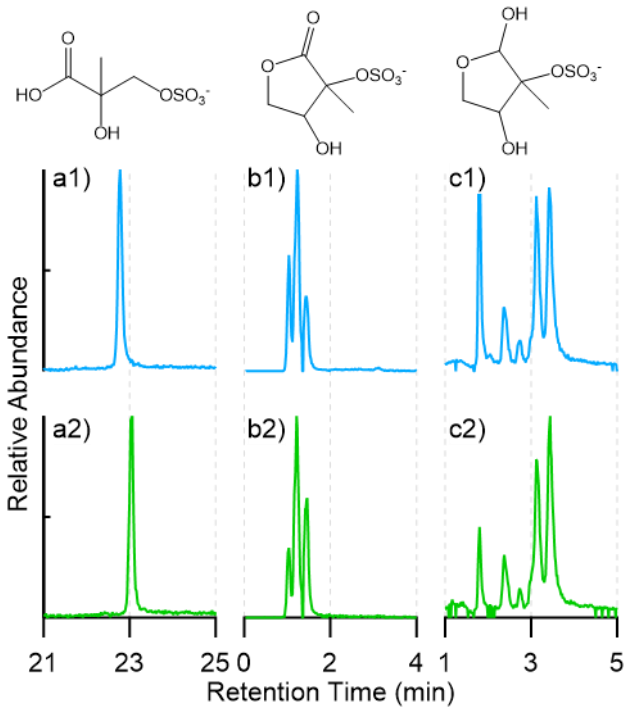


**Figure 3.4.** EICs of other water-soluble organosulfates with their proposed structures: **a)** *m/z* 199 corresponding to $C_4H_7O_7S^-$, **b)** *m/z* 211 corresponding to $C_5H_7O_7S^-$, and **c)** *m/z* 213 corresponding to $C_5H_9O_7S^-$ observed in $PM_{2.5}$ samples collected from 1) Look Rock during 2013 SOAS campaign; 2) Manaus in Nov. 2016. No significant peaks were observed beyond the shown periods of retention time.

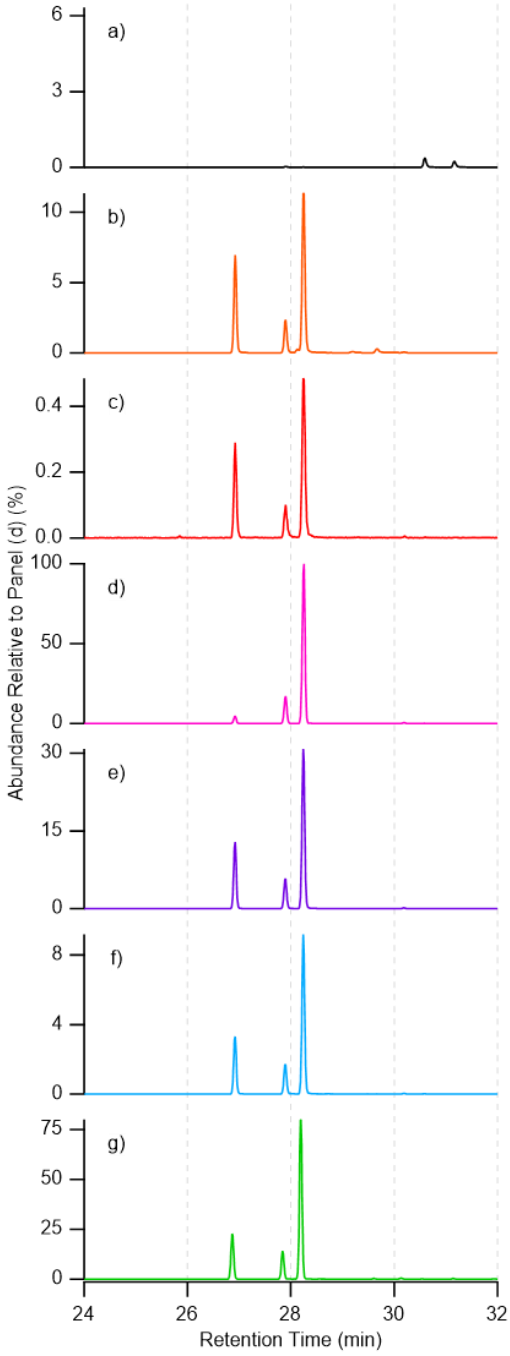


**Figure 3.5.** GC/EI-MS EICs of *m/z* 231 corresponding to $C_5$-alkene triols (RT = 26.9, 27.9, 28.3 min) from: **a)** 50 µg $mL^{-1}$ standard of 2-methyltetrol; **b)** 50 µg $mL^{-1}$ standard of 2-methyltetrol sulfate; **c)** 50 µg $mL^{-1}$ standard of 3-methyltetrol sulfate; **d)** laboratory-generated β-IEPOX SOA; **e)** laboratory-generated δ-IEPOX SOA; **f)** $PM_{2.5}$ sample at Look Rock during 2013 SOAS campaign; **g)** $PM_{2.5}$ sample at Manaus in Nov. 2016. Note that the y-axis scale was adjusted to the highest peak in each panel, with the labelled abundance in percentage relative to that in Panel (d).

# CHAPTER 4: CHEMICAL COMPOSITION OF BROWN CARBON AEROSOL FROM PRIMARY AND PHOTOCHEMICALLY-AGED LABORATORY-SIMULATED WESTERN US WILDFIRE EMISSIONS[3]

## 4.1 Overview

Light-absorbing brown carbon (BrC) aerosols from wildfires substantially impact air quality and climate. During the 2016 Fire Influence on Regional and Global Environments Experiment (FIREX), 107 laboratory-simulated wildfires were performed at the US Forest Service Fire Science Laboratory. Fuels combusted were from western US coniferous and chaparral ecosystems, such as Ponderosa pine, Douglas fir, and manzanita, including their canopy, litter, and rotten log components. BrC constituent identities and quantities from primary and photochemically-aged emissions were characterized at the molecular level by ultra-performance liquid chromatography coupled to both diode array UV detection and electrospray ionization high-resolution quadrupole time-of-flight mass spectrometry. Thirty-seven solvent-extractable BrC constituents, such as nitro-aromatics (e.g., methyl nitrocatechol) and guaiacol/styrene derivatives (e.g., vanillic acid/coniferyl aldehyde), were quantified from 20 selected experiments using authentic/surrogate standards, accounting for 3.3±1.9% on average (up to 9.1%) of $PM_{2.5}$ mass; these correlated ($R^2$ = 0.74) with Ångström absorption exponents. BrC emission factors were on average 1.71±3.23 (up to 13.68) g $kg^{-1}$ fuel burned. Notably, rotten logs produced the largest BrC aerosol mass fractions and emission factors. Photochemical aging of primary emissions

[3] This chapter is in preparation for submission to *Environmental Science & Technology*.

formed/enhanced a number of organic aerosol constituent levels; most were BrC species (i.e., nitro-aromatics). This study provides detailed emission factors and chemical composition of BrC to improve model predictions of changes in air quality and climate due to western US wildfire emissions.

## 4.2 Introduction

Light-absorbing carbonaceous constituents of atmospheric organic aerosol (OA), referred to as brown carbon (BrC), can efficiently absorb near-UV and visible radiation, potentially altering Earth's radiative forcing and global climate.[234–237] Although BrC has been recognized as a significant contributor to aerosol light absorption[237] and its composition and optical properties previously assessed,[104,235,236,238] quantitative predictions of the atmospheric impacts of BrC aerosol remain uncertain due to its chemical complexity and high reactivity.[104,238] The light-absorbing components (i.e., chromophores) in BrC aerosol are expected to possess a high degree of unsaturation or conjugation,[86,103,104] but are rarely quantified and used as OA tracers in the atmosphere.[105–107] In some circumstances, the overall light-absorbing properties of OA are dominated by a few chemical classes of strong chromophores at trace levels,[108–110] such as polycyclic aromatic hydrocarbons (PAHs),[111,112] nitrogen (N)-containing aromatic compounds (NACs) and their derivatives.[105,106,109,110,113,114]

The current challenge for chemical characterization of BrC aerosol constituents is to precisely identify their wavelength-dependent chromophores from a majority of non-absorbing OA constituents. This typically requires combining high-performance liquid chromatography (HPLC) for separation, spectrophotometry for detection of UV-vis light-absorption properties, and high-resolution mass spectrometry (HRMS) for chemical identification at the molecular level.[114] In a recent comprehensive study utilizing HPLC/HRMS equipped with both electrospray

ionization (ESI) and atmospheric pressure photoionization ionization (APPI) operated in the negative and positive ion modes, over 40% of light absorbance from biomass burning emissions was attributed to solvent-extractable BrC compounds with diverse molecular structures spanning a very broad range of molecular weights and polarities.[136]

As a large source of atmospheric carbonaceous OA (as well as BrC),[85–87] biomass burning-derived organic aerosol (BBOA) from wildfires contains thousands of gaseous and particulate constituents that can significantly influence atmospheric chemistry, cloud formation, climate, and human health.[88–90] Individual and categorized organic emissions from wildfires have been previously identified and quantified.[91–102] However, previous measurements did not always provide quantitative chemical composition data of BrC constituents from biomass burning emissions, and thus, the specificity, light-absorption properties, and reactivity of wildfire emissions remain unclear, impeding accurate predictions of the impacts of wildfires on the environment. The complex mixture of gas- and particle-phase biomass burning emissions, including BrC constituents, can undergo atmospheric oxidation and multiphase chemistry. Numerous studies indicate that optical and chemical properties of BrC may substantially evolve as BBOA ages in the atmosphere,[115–120] or affected by other factors such as solar irradiation[121,122] and relative humidity (RH).[123,124] However, due to the complex atmospheric perturbations and the uncontrolled nature of wildfires, characterization of BrC aerosol constituents from biomass burning emissions needs to be systematically assessed in the laboratory where variables can be controlled to minimize uncertainties from burn to burn.[239]

During the six-week 2016 Fire Influence on Regional and Global Environments Experiment (FIREX) (https://www.esrl.noaa.gov/csd/projects/firex/) campaign led by the National Oceanic and Atmospheric Administration (NOAA), over a hundred combustion experiments were

systematically performed in a large-scale indoor facility at the US Forest Service Fire Science Laboratory (FSL) in Missoula, Montana. Combusted fuels were characteristic of western US coniferous and chaparral ecosystems, including Ponderosa pine, Lodgepole pine, Douglas fir, Engelmann spruce, Subalpine fir, and chaparral (manzanita or chamise).[239] Specific components of the conifers and shrubs (e.g., canopy, rotten log, litter, duff, and mixtures of above to mimic their realistic complexes) were combusted under a variety of controlled conditions.

In this study, the identities, quantities, and evolution of BrC aerosol constituents were characterized from laboratory-simulated wildfire emissions. During the 2016 FIREX campaign, primary biomass burning emissions were collected onto Teflon filter samples and then extracted with methanol and analyzed by: (1) ultra-performance liquid chromatography coupled to both diode array detection and electrospray ionization high-resolution quadrupole time-of-flight mass spectrometry (UPLC/DAD-ESI-HR-QTOFMS); and (2) gas chromatography electron ionization mass spectrometry (GC/EI-MS) with prior derivatization through trimethylsilylation. Effects of photochemical aging on primary biomass burning emissions were investigated using the Colorado State University (CSU) 10-$m^3$ portable smog chamber in order to systematically assess changes in of BrC aerosol composition in the presence of UV irradiation and nitrous acid (HONO). HONO photolysis was used as a source of both hydroxyl radical and oxides of nitrogen ($NO_x$) in order to photochemically oxidize (or age) the primary biomass burning emissions. Our measurements provide quantitative chemical composition data and emission factors of BrC aerosol constituents at the molecular level from the laboratory-simulated primary and aged biomass burning emissions with varying fuel types and burn conditions. From this data, we also tentatively propose formation mechanisms of BrC aerosol constituents. These data will likely provide critical inputs needed for

future modeling studies that examine the impacts of biomass burning derived BrC aerosols on air quality, climate, and human health in the western U.S.

## 4.3 Experimental Section

### *4.3.1 Laboratory-Simulated Wildfire Emissions*

The laboratory-simulated wildfire emissions produced during the first phase of the multi-year FIREX campaign provided an opportunity to deploy a large suite of state-of-the-art instruments and analytical methods under burning conditions that aimed to mimic ambient burns. More detailed information about the FSL facility and operation has been described by Koss et al.,[97] Selimovic et al.,[239] and several other studies from FIREX 2016.[90,96,240,241] In brief, 107 controlled combustion experiments involving 39 fuels, including different fuel components, were systematically performed in the large (12.5 m × 12.5 m × 22 m-height, approximately 3500 $m^3$) FSL indoor combustion chamber. The fuels burned were collected to represent fire-prone western North America ecosystems, including Douglas fir (*Pseudotsuga menziesii*), Engelmann spruce (*Picea engelmanii*), Lodgepole pine (*Pinus contorta*), Ponderosa pine (*Pinus ponderosa*), Subalpine fir (*Abies lasiocarpa*), chaparral manzanita (*Arctostaphylos*) and chamise (*Adenostoma fasciculatum*). These fuel types were burned in replicate experiments, results from these burns are reported herein. Combustion of specific components of these fuels, such as canopy, litter, and duff, as well as mixtures of components to mimic the complexities of realistic ecosystems, were managed in many of the experiments.

Two configurations of combustion experiments were arranged at FSL for primary or diffused fire emissions. In the first configuration, fires were ignited and evolved underneath a 1.6-m diameter 21-m exhaust stack and fire emissions were elevated through the stack. This set of "Stack Burns" allowed access to composition and changes in direct (primary) emissions during

the course of a burn and typically lasted for 10-30 minutes. During the second configuration of experiments, the entire large combustion room was filled with fire emissions (diffused), referred to as "Room Burns." These burns lasted up to several hours and provided a relatively more compositionally-stable mixture that is more relevant to ambient wildfires. In addition, smog chamber experiments of primary biomass burning emissions from selected fuel types were conducted in the Colorado State University (CSU) portable smog chamber to determine how photochemical reactions may alter primary BBOA or secondary BrC aerosol components. Detailed instrumentation and operation of the two configurations are described in the following two subsections.

### *4.3.2 Primary Emissions from "Stack Burns"*

During the "Stack Burn" experiments, direct (primary) emissions traveled up through the 21-m stack at a constant flow rate (~3.3 m $s^{-1}$). A 20.3 cm diameter, ~20-m semi-rigid aluminum duct was attached as a sampling port into the stack on a sampling platform surrounding the round stack 17-m above the fuel bed. This was done in order to transfer the primary fire emissions to the FSL's wind tunnel room, where the particulate samples were collected for subsequent offline analysis. At the height of the platform, temperature and mixing ratios were consistent across the width of the round stack, confirming well-mixed emissions that can be monitored by a number of different sampling lines throughout the burn.[242] The flow rate through the aluminum duct, driven by a blower and verified by an anemometer, was roughly 20,000 L $min^{-1}$, resulting in a residence time of ~1.5 s in the aluminum duct. With this short residence time, minimal losses were expected within the transfer duct, allowing intercomparison between our measurements described herein with the large suite of collocated measurements.

Two parallel 37-mm Teflon filters (Pallflex air monitoring filters, Pall Corp.) were collected for primary $PM_{2.5}$ emissions from all the 75 "Stack Burns" (Figure C1, Appendix C). A 0.95-cm diameter copper tubing was chosen to connect the two filter holders to the aluminum duct and to match the flow velocity. The pressure difference between the aluminum duct and the sampling room was negligible (< 2 inches of water, or 500 Pa). The two home-made filter holders with a 2.5-µm size-cut inlet were operated at a sampling flow rate of 10 L $min^{-1}$, which was calibrated using a DryCal (Mesa Laboratories, Model Defender 520) gas-flow calibrator. With an inline pressure gauge (Magnehelic Inc.), a relationship between pressure and the sampling flow rate was established to monitor the decline of flow rate due to potential overloading of aerosol particles on filter membranes. At least one field filter blank was collected on each day (or every 5 "Stack Burns"). The filter samplers were turned on (or off) exactly when the FSL fire operators sent the signal for the ignition of the fuels (or extinguishment of the combustion). Upon collection, filter samples were weighed for the second time in the FSL's filter weighing room using a sensitive electronic balance to determine the mass of $PM_{2.5}$ collected ($m_{PM_{2.5}}$, Table 4.1) onto the filters, before immediately (within 5-60 min) storing them in 22-mL scintillation vials. These vials were stored at -20°C until shipped and chemically analyzed at UNC.

Twenty out of the 75 "Stack Burn" experiments were selected to represent the six most commonly burned fuels, including Ponderosa pine (PP), Lodgepole pine (LP), Douglas fir (DF), Engelmann spruce (EP), Subalpine fir (SF), and chaparral manzanita (M) or chamise (C). For each fuel, 3-4 burns with different components were selected (Table 4.1 and Figure C2 in Appendix C). Selection criteria considered different components of the trees (e.g., canopy, duff, litter, rotten log, or representative mixture); additionally, higher time-averaged $PM_{2.5}$ concentrations (> 800 µg $m^{-}$

$^3$), longer burn duration (> 10 min), larger burned fuel weight (> 250 g), and darker filter colors were preferred.

### *4.3.3 Photochemical Evolution of BrC during "Room Burns"*

The CSU smog chamber setup and instrumentation are shown in Figure C3 (Appendix C). The portable chamber was ~1.8 m × ~1.8 m × ~3.2 m when fully inflated, and can be collapsed down to ~2 $m^3$ to achieve a higher exchange rate per unit time when flushed. Four panels of UV lamps were mounted on the front and rear doors inside a wooden shelter of the chamber for irradiation. A portable air conditioning (AC) unit was attached to the outside of the chamber to control the temperature around the chamber when the UV lamps were on. A total organic carbon analyzer (TOC) was operated in real-time Turbo mode (time resolution = 4 s) and coupled to a particle-into-liquid sampler (PILS, Model 4001, Brechtel Inc., Hayward, CA). The PILS-TOC was used to monitor the real-time water-soluble organic carbon (WSOC) fraction in the particle phase. In addition, regular PILS samples were collected into 12-mL polypropylene vials simultaneously with an auto-sampler (Brechtel Inc.). Two organic vapor denuders with carbon strips were deployed upstream the PILS to ensure exclusive collection of particle-phase emissions. In addition, a 2.5-µm impactor was mounted prior to the PILS sample inlet to remove large (mostly soot) particles and the impactor plate was cleaned every a few days or as needed between burns. An iodide chemical ionization mass spectrometer (CIMS, Aerodyne Research Inc.) was deployed to monitor the gaseous components in real-time.[90]

A typical time profile of chamber operation and real-time monitoring are shown in Figure 4.2. Prior to and after each experiment, the chamber started with ~20% of its total volume (for a higher air exchange rate) and was flushed using clean air generated at the FSL facility. Chamber flushing was also conducted with the UV lamps turned on for better cleaning. Prior to the room

combustion used for chamber experiments, HONO, which was used as an OH precursor, was injected into the chamber by nebulizing a freshly prepared solution of 25mL of 1% $NaNO_2$ in 50mL of 10% $H_2SO_4$ in a glass bulb for 50-60 min at 2 L $min^{-1}$.[243] This typically resulted in 5-6 ppm $NO_x$ and (5-7)×$10^6$ molecules/$cm^3$ OH radicals in the fully inflated chamber, as measured by previous users of the CSU chamber at FIREX. After fuels were ignited, the high-concentration fire emission of gases and particles ($PM_{2.5}$ up to several thousands of µg/$m^3$) were allowed to mix in the large combustion room for 15-30 minutes and then introduced into the smog chamber through three parallel Dekati diluters (Model DI-1000) with a combined flow of approximately 190 L $min^{-1}$ for 50-60 min, diluted by a factor of 15 with clean air generated in the FSL facility. The first set of filters and PILS samples for the "fresh" smoke was collected during the smoke injection for 30 min to coordinate with expanding chamber volume starting from 20% of its total volume. After the smoke injection, the chamber was inflated to nearly 95% full and the injected contents were allowed to stabilize for 35-45 min to obtain the wall-loss rates of particles. The UV lamps and AC were turned on to initiate photooxidation of the primary fire emissions. Usually 45-60 min after UV irradiation, when the PILS-TOC signal of particulate WSOC stopped growing and stabilized, the second set of filters and PILS samples was collected for 60 min for the "photochemically-aged" emissions.

### *4.3.4 Offline Aerosol Characterization*

#### *4.3.4.1 UPLC/DAD-ESI-HR-QTOFMS*

An Agilent 6520 Series Accurate Mass Q-TOFMS instrument (Agilent Technologies, Santa Clara, CA) interfaced to an Agilent 1200 Series UPLC system, and equipped with an ESI source operated in both negative and positive ion modes,[40] was used to chemically characterize BrC constituents from filter samples collected from "Stack Burns" and smog chamber experiments

of "Room Burns" during the 2016 FIREX campaign. In brief, chromatographic separations were carried out using a Waters ACQUITY UPLC HSS T3 $C_{18}$ column (2.1×100 mm, 1.7 µm particle size, Waters Corporation, Milford, MA) at 45°C. The mobile phases consisted of eluent (A) 0.1% acetic acid in Milli-Q water, and eluent (B) 0.1% acetic acid in pure methanol (99.9%, Fisher Chemical) for negative ion mode analyses, or eluent (A) 0.1% ammonium acetate in Milli-Q water and eluent (B) 0.1% ammonium acetate in pure methanol for positive ion mode analyses. The gradient elution program was as follows: eluent (A) held at 100% from 0-2 min, decreased linearly to 10% from 2-10 min, held constant at 10% between 10-11 min, increased linearly to 100% from 11-15 min, and held constant at 100% during a 5-min post run column re-equilibration. The flow rate and sample injection volume were 0.3 mL $min^{-1}$ and 5 µL, respectively. A Diode Array UV Detector (DAD) between the UPLC system and the mass spectrometer was operated to measure absorbance of each sample from 200 to 800 nm (with a step of 2 nm). At the beginning of each analysis period, the mass axis of the Q-TOFMS was calibrated using a commercially available ESI-L low-mass tuning mixture (Agilent Technologies, Santa Clara, CA) containing seven masses ranging from 60-1700 Da. For real-time mass correction, a solution containing 3 reference mass components was continuously infused. The refence compounds employed for negative ion analysis were: acetate adduct ion of hexakis (1H,1H,3H-tetrafluoropropoxy) phosphazene at mass-to-charge ratio (*m/*z) 980.0164, deprotonated purine at *m/z* 119.0363, and leucine enkephalin at *m/z* 554.2620.,. These same compounds were used for real-time mass axis correction (calibration) during the positive ion mode analyses, using the corresponding m/z values for positively charged ions. The resultant mass resolution of the ESI-HR-QTOFMS over *m/z* 60-1700 ranged from 11,000 at the low mass end to 17,000 at the high mass end. Raw data were acquired and processed with MassHunter Software (Version B.06.00 Build 6.0.633.0, Agilent Technologies, Santa Clara, CA).

*4.3.4.2 GC/EI-MS*

GC/EI-MS analysis with prior derivatization was performed to measure several well-established biomass burning tracers, such as anhydrosugars, following detailed procedures previously described.[157,158] In brief, filter samples were analyzed within 24 h of derivatization with a Hewlett-Packard (HP) 5890 Series II gas chromatograph coupled to a HP 5971A mass selective detector, with an Econo-Cap-EC-5 capillary column (30 m × 0.25 mm i.d., 0.25 μm film thickness) and the electron ionization source operated at 70 eV. The 65-min temperature program of the GC initiated at 60 ℃ for 1 min, then increased by 3 ℃ $min^{-1}$ to 200 ℃ and isothermally held for 2 min, followed by another temperature ramp of 20 ℃ $min^{-1}$ to 310 ℃ and isothermally held for 10 min. The temperatures of both the GC inlet and detector were operated at 250 ℃.

*4.3.4.3 Sample Preparation, BrC Identification and Quantification.*

One of the two filters collected from each of the selected "Stack Burn" and smog chamber experiments was extracted individually with 20 mL methanol by 45 min sonication, blown dry under a gentle $N_2$ stream at room temperature (21-22℃), re-dissolved in 2.0 mL of methanol and divided into 3 aliquots of 0.5 mL, 0.5 mL, and 1.0 mL. The first 0.5 mL aliquot was dried completely and reconstituted with 150 μL of 50:50 (v/v) methanol/water solvent mixture for the subsequent UPLC/DAD-ESI-HR-QTOFMS analysis; the second 0.5 mL aliquot was dried completely and reconstituted with 100 μL of BSTFA + TMCS (N,O-bis (trimethylsilyl) trifluoroacetamide + trimethylchlorosilane, 99:1, Supelco) and 50 μL of pyridine (anhydrous, 99.8%, Sigma-Aldrich), and heated at 70°C for 90 min for trimethylsilylation prior to the GC/EI-MS analysis; the remaining 1.0 mL aliquot was stored at -20°C for future analyses. Immediately prior to analysis, each reconstituted extract was filtered through a PTFE syringe filter (Agilent, 0.2-μm pore size) to remove undissolved particles (e.g., soot components).

Chromatographically resolved BrC chromophores were measured by the DAD for light absorbance at 365 and 405 nm, and subsequently detected by ESI-HR-QTOFMS. The method of identifying solvent-extractable ESI-detectable organic compounds responsible for the observed light absorption is demonstrated in Figure C4 (Appendix C).[114,244] Briefly, this method includes peak detection aligned on UV-vis and ion chromatograms, background subtraction of mass spectra, formula assignment, and BrC identification assisted with accurate mass measurements (i.e., elemental composition determination of the parent BrC ions), tandem MS (MS/MS) generated fragment ions, grouping of isotopic peaks, constraints of elements ($C \leq 30$, $H \leq 60$, $O \leq 20$, $N \leq 10$, and $S \leq 2$), Nitrogen Rule, double bond equivalents (DBE) determinations, hydrophilicity (or water-solubility) indicated by retention times (RTs), and previously-reported BBOA composition. In addition to identifying the BrC chromophores observed with prominent light absorbance, a large number (over 50) of known BrC species was examined by searching for their exact *m/z* values in the mass spectral raw data.

To quantify BrC aerosol constituents identified by UPLC/DAD-ESI-HR-QTOFMS, 8 external (2-nitrophenol, 4-nitro-o-cresol, 4-nitro-1-naphthol, 4-methyl-5-nitrocatechol, vanillin, acetovanillone, sinapinic acid, and coniferyl aldehyde) and 2 internal (ketopinic acid and camphor-10-sulfonic acid) commercially-available authentic standards were prepared for 7-point calibration curves from 0.01-500 μg $mL^{-1}$ with detection limits below 0.01 or 0.1 μg $mL^{-1}$. More information about the authentic standards (e.g., manufacturer, purity, retention time, exact and measured *m/z* values, fragment ions, linear range as well as $R^2$ of calibration curves, and response factors) are listed in Table C1 (Appendix C). The recovery rate for ketopinic acid when using methanol as an extraction solvent (determined by UPLC/ESI-HR-QTOFMS) was 89.8±2.4% (average ± standard deviation) among the 20 selected samples. As a quality control/assurance check, two filter samples

with the largest $PM_{2.5}$ masses out of the 20 "Stack Burn" samples were re-extracted using 70:30 (v/v) acetonitrile/toluene solvent mixture. Most of the identified BrC species were not detected from this second extraction, suggesting that the first extraction with methanol was an acceptable extraction solvent. Only a few BrC aerosol constituents (e.g., vanillic acid, coniferyl aldehyde) were detected from the second extraction, but the abundance was lower than 1.5% of that from the first extraction, except for 2-nitrophenol whose extraction efficiency using methanol was roughly 55%.

For quantification by GC/EI-MS, levoglucosan and mannosan were used as external authentic standards, derivatized following the same protocol as for the samples, to prepare 7-point calibration curves from 0.25-500 μg $mL^{-1}$, while ketopinic acid was used as an internal standard (Table C1, Appendix C). The detection limit is below 1 and 2.5 μg $mL^{-1}$ for levoglucosan and mannosan, respectively. The GC/EI-MS recovery rate (derived from ketopinic acid) was 100.0±3.5%.

The quantified individual BrC and other OA constituents were eventually normalized to percentages of the $PM_{2.5}$ mass collected onto the filters ($f_{X/PM_{2.5}}$ as shown in Figure 4.1 in the results section), using the Equation (i) below:

$$\text{(i) } f_{X/PM_{2.5}} = \frac{r_X/RF_X \times V_s \times frac_X}{m_{PM_{2.5}}}$$

where $r_X$ is the peak area of OA constituent X directly integrated from UPLC/ESI-HR-QTOFMS or GC/EI-MS data; $RF_X$ is the response factor (peak area per μg $mL^{-3}$, with examples shown in Table C1) used for quantifying X, so the quotient "$r_X/RF_X$" calculates concentration of X in the liquid UPLC/ESI-HR-QTOFMS or GC/EI-MS sample (μg $mL^{-1}$); $V_s = 0.15$ mL is the reconstituted liquid sample volume; $frac_X = 0.25$ is the fraction of the filter extract analyzed by UPLC/ESI-HR-QTOFMS or GC/EI-MS; and $m_{PM_{2.5}}$ is the collected $PM_{2.5}$ mass (μg, Table 4.1).

*4.3.4.4 Modified Combustion Efficiency and Emission Factors*

Modified combustion efficiency (MCE) reflects the mix of two major combustion processes for open burning of biomass, which includes flaming and smoldering, and is defined as background-corrected values of $CO_2/(CO_2+CO)$.[91,245] An MCE value near 1.0 is an indication of nearly pure flaming, while a lower MCE (~0.8) is an indication of nearly pure smoldering.[91] An MCE value of 0.9 would indicate roughly equal duration of both. The fire-integrated MCE was obtained from Selimovic et al.[239] and is listed in Table 4.1 for the 20 selected "Stack Burns." The time-integrated emission factors (EFs) of individual and summed BrC and saccharide (anhydrosugar) OA tracers were calculated using the Equation (ii) as followed:

$$\text{(ii) } EF_X = \frac{f_{X/PM_{2.5}} \times c_{PM_{2.5}} \times Q_{stack} \times t_{burn}}{m_{fuel}}$$

where $EF_X$ is the time-integrated EF of the OA constituent X from a fire (g X per kg fuel burned), $f_{X/PM_{2.5}}$ is the fraction of X (%) normalized to percent collected $PM_{2.5}$ mass on filter, calculated using Equation (i); $c_{PM_{2.5}}$ is the time-integrated mass concentration of $PM_{2.5}$ (μg $m^{-3}$, Figure C2, Appendix C) in the sampling tubing over the entire filter collection period, calculated by collected $PM_{2.5}$ mass (μg, Table 4.1) divided by sampled air volume ($m^3$, at 10.0 L $min^{-1}$), and it is reasonable to assume the same mass concentration of X and $PM_{2.5}$ at the top of the stack due to minimal loss of particles as a result of short residence time (< 2 s); $Q_{stack}$ is the estimated constant volumetric air flow rate through the stack (~ 6.0 $m^3$ $s^{-1}$); $t_{burn}$ is the duration of burn (s), which equals to the exact duration of filter collection; and $m_{fuel}$ is the mass of dry fuel burned (kg).

*4.3.4.5 Comparison between "Fresh" and Photochemically-Aged Emissions.*

Non-targeted MS analyses were performed to compare the filter samples collected for the "fresh" and photochemically-aged emissions from the smog chamber experiments in order to reveal the potential production of secondary BBOA at the molecular level, especially for BrC. The

raw data files acquired from UPLC/ESI-HR-QTOFMS were first transformed into mzXML format by ProteoWizard (http://proteowizard.sourceforge.net/),[246] and then processed by the online metabolomics platform XCMS (https://xcmsonline.scripps.edu/).[247] Workflow parameters were adopted from a previous work with modifications.[248] In brief, the centWave algorithm was used for peak detection, with a peak width range from 5-60 seconds, and the mass error tolerance was set at 20 ppm. Peak alignment required an *m/z* width (mzwid) at 0.025, and a minimum fraction (minfrac) of the sample group at 0.6. Annotation and molecular formula assignment were achieved by XCMS and verified by MassHunter. The differences of detected ions between the "fresh" and photochemically-aged emissions (4 repeated injections of each) were evaluated by Welch t-test with a threshold p-value set at 0.01, a minimum ion intensity (peak height) set at 5000 and response (peak area) at 30000, and a minimum fold-change at 1.5 after correction for the collected air volume, since the sample for photochemically-aged emissions was collected for a longer time.

## 4.4 Results and Discussion

### *4.4.1 BrC and Other OA Constituents from Primary Emissions.*

Following the approaches described in the last section, 37 solvent-extractable particulate BrC constituents were tentatively identified from the 20 selected "Stack Burns" of primary emissions, as shown in Figure 4.1. These identified BrC compounds were categorized into five groups based on structure and functional groups, including 12 nitro-aromatics, 6 guaiacol-derivatives, and 6 styrene-derivatives. The DBE of the tentatively assigned formulas ranged from 4-11, which is reasonable for light-absorptive structures.[104] In addition to the 5 BrC species confirmed by comparative analysis with authentic standards of 4-methyl-5-nitrocatechol, 2-nitrophenol, vanillin, acetovanillone, and coniferyl aldehyde, 21 candidate formulas were

tentatively proposed based on MS/MS fragments (or functional groups), hydrophilicity (or water-solubility) as indicated by RTs, and the literature.

The identified BrC was individually quantified using authentic or surrogate standards and normalized to percentages of the $PM_{2.5}$ mass collected onto the filter. The surrogate standards were chosen to quantify BrC components in the same category, if available, and based on the similarity of functional groups and RTs. As a result, Figure 4.1 shows that the summed mass of the 37 BrC compounds (∑BrC) measured in this study accounted for 3.34±1.90% of the collected $PM_{2.5}$ mass averaged from the 20 selected primary emissions, with guaiacol- and styrene-derivatives being the top two most abundant groups. Notably, the rotten logs of Ponderosa pine and Douglas fir emitted the first- and second-most BrC as a fraction of $PM_{2.5}$ mass, 9.07% and 7.99%, respectively, while the other components of fuels produced 1.57-3.97% BrC by $PM_{2.5}$ mass. The results suggest larger differences among components of the tree (e.g., rotten log vs. others), as compared to the plant species (e.g., Douglas fir vs. Ponderosa pine), even though the relative contribution of 5 identified categories were consistent.

Light-absorption from the identified BrC constituents was assessed following the approach demonstrated in Figure C4 (Appendix C). For example, the largest peak in the UV-vis chromatogram from the rotten log of Douglas fir (DF-RL) in Figure C5 (Appendix C), was later confirmed to be coniferyl aldehyde using the authentic standard and accounted for 1.46% of the total $PM_{2.5}$ mass. However, it contributed to 20.5% of the total effective light absorbance measured at 365 nm, which reveals the strong efficiency from such a BrC chromophore in terms of light-absorbance per unit mass.

The correlation of the ∑BrC with the Ångström absorption exponent (AAE) is examined for selected “Stack Burns” (Figure C6, Appendix C). Larger AAE values are indicative of aerosol

absorption dominated by BrC constituents, and usually is related to smoldering conditions (i.e., low MCE) and high single-scattering albedos (SSA, the ratio of scattering to total extinction) values.[249] The AAE values before Burn #31 were obtained at two wavelengths (401 and 870 nm) by Selimovic et al.,[239] and after Burn #32 they were approximated with a power-law function (absorption = $C \times \lambda^{-AAE}$)[250] by Li et al.[240] It is noted that Li et al. did not approximate AAE values for burns after #32. The strong correlation ($R^2 = 0.74$) between ∑BrC and AAE suggests that the variation of the calculated AAE can be largely attributed to the BrC constituents identified by the UPLC/DAD-ESI-HR-QTOFMS method, despite that there might be uncharacterized BrC constituents due to insufficient solvent-extraction or ESI efficiency as well as differences in wavelengths used for detection or calculation between different researchers from this campaign.

In addition to the BrC measured by UPLC/DAD-ESI-HR-QTOFMS, levoglucosan and mannosan were identified as the first and second largest peaks on the GC/EI-MS total ion chromatograms (TICs, Figure C7 in Appendix C) of the 20 selected "Stack Burns." On average, these two BBOA tracers accounted for 9.5±1.3% and 2.2±0.4% (up to 27.2% and 7.5%) of the collected $PM_{2.5}$ mass, respectively, and 3.54 times (1.61-7.13) greater than the emitted ∑BrC. Their concentrations are closely comparable with those collocated measurements reported by Jen et al..[96] Based on RT, the third largest peak from the GC/EI-MS TICs was likely to be galactosan, another common BBOA tracer and isomer of levoglucosan and mannosan, but was not quantified due to lack of an authentic standard.

The emission factors (EFs) of the BrC and anhydrosugar BBOA constituents were calculated using the Equation (ii) and shown in Table 4.1 for the summed 37 measured BrC ($EF_{\sum BrC}$) and 2 measured sugar ($EF_{\sum sugar}$) compounds. The $EF_{\sum BrC}$ was 1.71±3.23 g $kg^{-1}$ averaged from the 20 "Stack Burns", with a maximum of 13.68 g $kg^{-1}$ from the DF-RL, while the $EF_{\sum Sugar}$

was 5.91±13.07 g $kg^{-1}$ on average, with a maximum of 59.47 g $kg^{-1}$ also from the DF-RL. Interestingly, this burn was calculated with the lowest MCE (0.7805) and the second-most collected $PM_{2.5}$ mass among the 20 "Stack Burns," suggesting the combustion was dominated by smoldering and thus associated with larger EFs for BBOA, including BrC constituents and anhydrosugars. The duff of Engelmann spruce was observed with second-largest $EF_{\sum BrC}$ and $EF_{\sum sugar}$, probably due the longest burn duration (48 min), the second-least MCE (0.8681), and the most collected $PM_{2.5}$ mass. The third-largest $EF_{\sum BrC}$ and $EF_{\sum sugar}$ occurred from the burning of the rotten log of Ponderosa pine, which is consistent with the observed heaviest emissions of BrC and sugars from rotten logs (Figure 4.1).

### *4.4.2 BrC from Photochemically-Aged Emissions*

The evolution of BrC and other OA constituents was investigated using the smog chamber experiments conducted for photochemical aging of the primary biomass burning emissions with presence of HONO as a source of OH radicals. For example, the particulate water-soluble organic carbon (WSOC) monitored in real-time by the PILS-TOC is shown in Figure 4.2 from the combustion of Longleaf pine, in which the most secondary WSOC formation was observed, and in Figure C8 (Appendix C) for another six experiments summarized in Table C2. Rapid secondary particulate formation of WSOC was observed immediately after UV irradiation commenced at ~1.65 h upon smoke injection. The rapid net growth of WSOC lasted until 2.2 h, followed by the second filter collection period starting at 2.3 h into the experiment and lasting for 1 h, which represented the photochemically-aged emission. The chemical compositions of the photochemically-aged aerosol were compared to the first set of filter samples collected for the "fresh" emissions.

The effective absorbance at 365 nm (calculation demonstrated in Figure C5 of Appendix C) increased by 65% from the "fresh" emissions to the photochemically-aged emissions, while an elevated signal was simultaneously observed in the TIC chromatogram from UPLC/ESI-HR-QTOFMS (Figure C9, Appendix C), indicating substantial formation of secondary BrC OA constituents through photochemistry during the smog chamber experiments. Non-targeted MS analysis revealed that a number of SOA species were formed (or enhanced by > 50%) through the photooxidation (irradiation) of certain primary emissions. As shown in Figure 4.3, 29 secondary BBOA were identified from the Longleaf pine emissions (Fire #97). Among them, as shown in Table C3, nitro-catechol ($C_6H_5NO_4$), trimethoxycinnamic acid ($C_{12}H_{14}O_5$), and methyl nitro-catechol and its isomers ($C_7H_7NO_4$) were identified with largest ion intensities. The assigned molecular formulas suggest that 17 of them were possibly nitro-aromatics with molecular weights ranging from 139-310 g $mol^{-1}$ and DBE from 5-10, including the three mentioned above, as well as nitrophenol ($C_6H_5NO_3$), methylnitrophenol ($C_7H_7NO_3$), nitrofuroic acid ($C_5H_3NO_5$), hydroxynitrobenzoic acid ($C_7H_5NO_5$), and dimethylnitrobenzenetriol ($C_8H_9NO_5$), which are reasonably to be light-absorptive structures. Consistent numbers of secondary BBOA constituents, as well as primary ones that were reduced or consumed, were identified from the additional six smog chamber experiments (Figure C10). These results indicate strong potential of nitro-aromatics as secondary BrC chromophores formed during photooxidation of primary emissions in the presence of NO (from HONO).

**4.5 Atmospheric Implications**

In this study, 37 solvent-extractable BrC constituents, such as nitro-aromatics (e.g., methyl nitrocatechol) and guaiacol/styrene derivatives (e.g., vanillic acid/coniferyl aldehyde), were identified from 20 primary laboratory-simulated wildfire emissions. Quantified using authentic

and surrogate standards, the ∑BrC accounted for 3.3±1.9% on average (up to 9.1%) of $PM_{2.5}$ mass. On average, the EFs of ∑BrC was calculated to be 1.71±3.23 (up to 13.68 g $kg^{-1}$). The detailed EFs of individual BrC constituents could be used by modelers to predict how the quantity of fuels burned in a wildfire yields light-absorbing BrC aerosols. Our BrC quantification suggests that the large variability in BrC emissions from the laboratory-simulated wildfires is much more influenced by the component of fuel (e.g., rotten log) burned than the differences between the plants of fuel. Additionally, the chemical composition and quantities of BrC constituents reported from the laboratory-simulated wildfire emissions can also serve as valuable inputs for future toxicological studies on their potential health effects, since burning of biomass fuels (e.g., wildfires) is one of the most important sources of gaseous and particulate air pollutants on global and regional scales, and many of its constituents, such as PAHs, have been subject to major concern in all environmental compartments due to their mutagenic and carcinogenic properties.[112,251] Thus, characterizing hazardous components of these environmental pollutants is required to protect public health, especially for the susceptible US and global populations under the influence of wildfires or other sources of intensive biomass burning emissions. In addition, photochemical aging of primary emissions formed/enhanced organic aerosol constituent levels; most were BrC species (i.e., nitro-aromatics). This study provides data needed to improve predictions of changes in air quality and climate due to western US wildfire emissions and subsequent atmospheric photochemical aging.

### 4.6 Acknowledgement

This work was supported by the National Oceanic and Atmospheric Administration (NOAA) Climate Program Office's AC4 program, award no. NA16OAR4310106. The UNC

Biomarker Mass Spectrometry Facility is funded, in part, by the National Institute of Environmental Health Sciences (grant no. P30ES010126).

**Table 4.1.** Information of the 20 selected combustion experiments from the 6 most commonly burned fuels during the 2016 FIREX campaign.

| Fuel Description | Fuel Code | Burn No.[a] | Sample Time | Fuel Weight[b] | $PM_{2.5}$ Mass | MCE[c] | $EF_{\sum BrC}$[d] | $EF_{\sum Sugar}$ |
|---|---|---|---|---|---|---|---|---|
| | | | *min* | *g* | *µg* | | *g kg$^{-1}$* | *g kg$^{-1}$* |
| Chaparral (chamise) - Canopy | C-C | 32 | 14 | 3007 | 552 | 0.9539 | 0.11 | 0.18 |
| Chaparral (manzanita) - Canopy | M-C1 | 28 | 19 | 6010 | 755 | 0.9631 | 0.16 | 0.43 |
| Chaparral (manzanita) - Canopy | M-C2 | 33 | 18 | 4493 | 591 | 0.9622 | 0.19 | 0.45 |
| Douglas fir (mixed) | DF | 11 | 22 | 3248 | 626 | 0.9481 | 0.40 | 1.28 |
| Douglas fir - Canopy | DF-C | 64 | 13 | 3148 | 921 | 0.9255 | 0.44 | 1.24 |
| Douglas fir - Litter | DF-L | 22 | 26 | 289 | 152 | 0.9454 | 0.87 | 4.37 |
| Douglas fir - Rotten log | DF-RL | 31 | 32 | 527 | 1558 | 0.7805 | 13.68 | 59.47 |
| Engelmann spruce (mixed) | EP | 8 | 30 | 2299 | 388 | 0.9200 | 0.30 | 1.44 |
| Engelmann spruce - Duff | EP-D | 12 | 48 | 708 | 1718 | 0.8681 | 6.74 | 13.86 |
| Engelmann spruce - Canopy | EP-C | 17 | 10 | 874 | 397 | 0.8903 | 0.93 | 2.33 |
| Lodgepole pine (mixed) | LP | 63 | 26 | 2976 | 960 | 0.9364 | 0.41 | 1.92 |
| Lodgepole pine - Canopy | LP-C | 40 | 13 | 1500 | 855 | 0.9240 | 1.04 | 3.34 |
| Lodgepole pine - Litter | LP-L | 41 | 11 | 355 | 106 | 0.9377 | 0.35 | 2.49 |
| Ponderosa pine (mixed) | PP | 37 | 18 | 3249 | 926 | 0.9396 | 0.34 | 1.49 |
| Ponderosa pine - Rotten Log | PP-RL | 13 | 28 | 708 | 791 | 0.9569 | 3.93 | 10.80 |
| Ponderosa pine - Canopy | PP-C | 39 | 20 | 1627 | 730 | 0.9041 | 0.99 | 3.44 |
| Ponderosa pine - Litter | PP-L | 16 | 26 | 4900 | 887 | 0.9544 | 0.12 | 0.60 |
| Subalpine fir (mixed) | SF | 47 | 22 | 2315 | 749 | 0.9323 | 0.52 | 1.69 |
| Subalpine fir - Canopy | SF-C | 15 | 16 | 833 | 564 | 0.8856 | 1.46 | 2.95 |
| Subalpine fir - Duff | SF-D | 56 | 27 | 261 | 566 | 0.8863 | 1.23 | 4.47 |

[a] "Burn No." is the number of the burn performed at FIREX 2016 (from No. 1-107).
[b] "Fuel Weight" is the dry weight of the fuel burned throughout the burn.
[c] "MCE" is the modified combustion efficiency of the burn, calculated by Selimovic et al..[239]
[d] "$EF_{\sum BrC}$" is the emission factor calculated for the summed mass of the 37 BrC constituents.

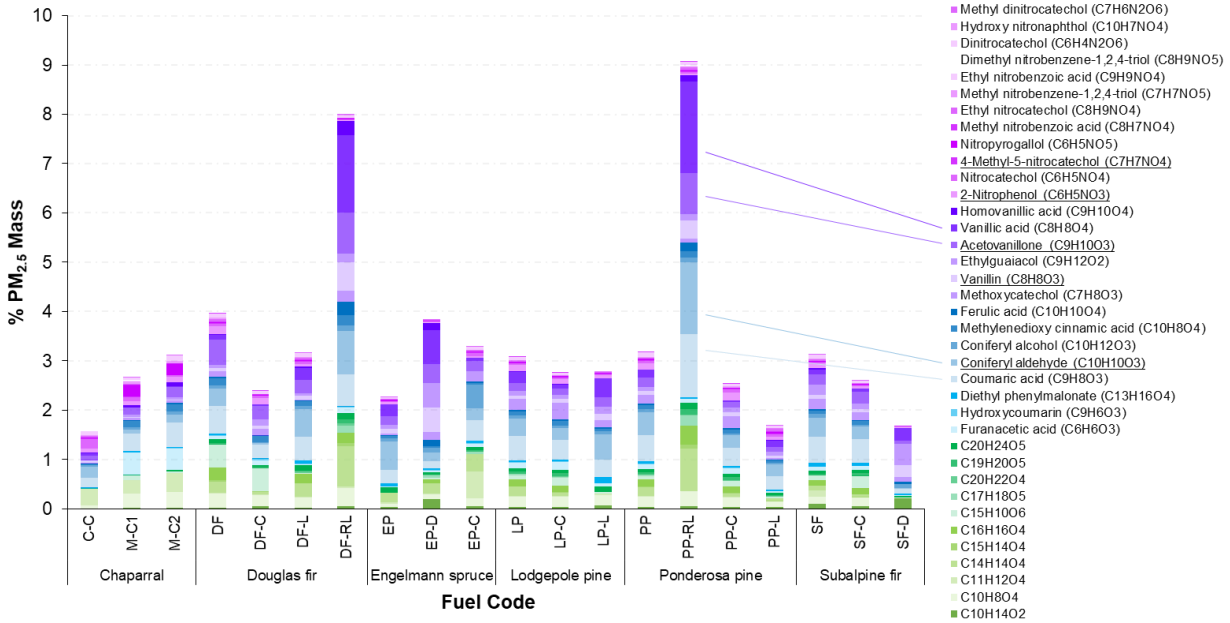


**Figure 4.1.** 37 particulate BrC constituents quantified as % $PM_{2.5}$ mass using UPLC/DAD-ESI-HR-QTOFMS, with tentatively suggested formulas listed in the legend. 5 of them were identified and quantified using authentic standards that underlined in the legend. 26 of them were suggested with compound names, quantified with surrogate standards and categorized into four groups: nitro-aromatics (pink), guaiacol-derivatives (purple), styrene-derivatives (blue), and others (light blue). The fuel code and description are listed in Table 4.1.

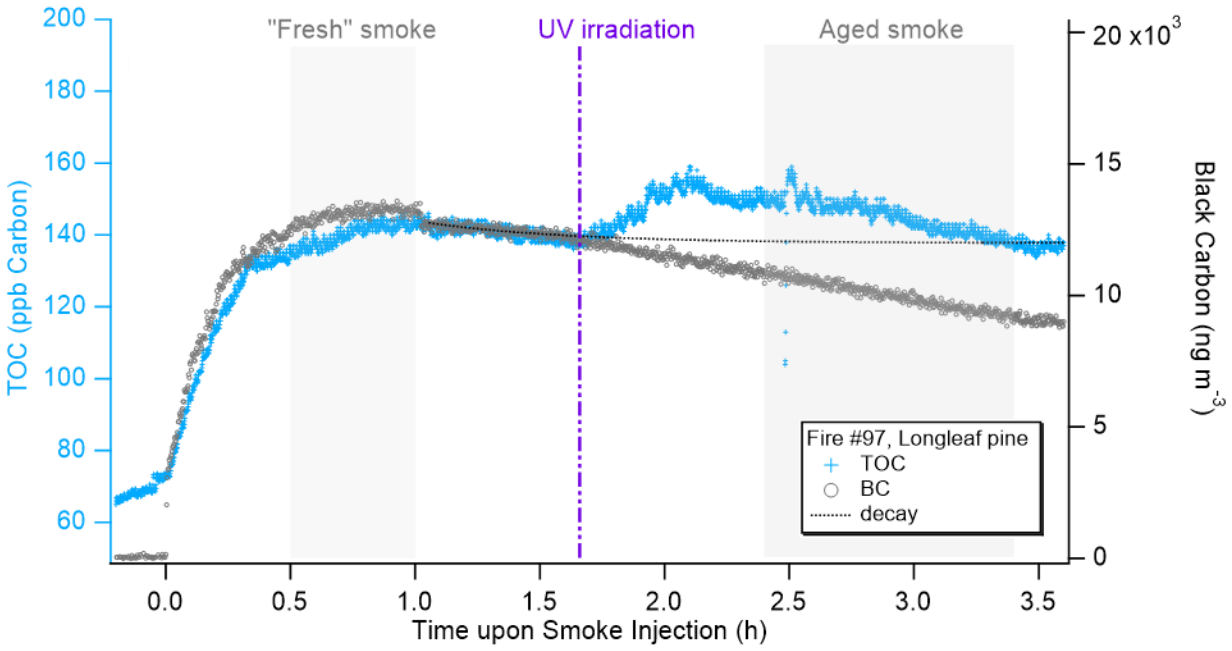


**Figure 4.2.** Time profile of the smog chamber experiment from Longleaf pine (Fire #97). Water-soluble particulate organic carbon was monitored by PILS-TOC in real-time over the course of experiment and plotted as the light blue markers to the left y-axis. Black carbon (BC) was monitored by a micro-aethalometer (AethLabs) and plotted as the light gray circles to the right y-axis. The dashed curve from ~1.0 h indicates the decay rate of particles, determined by the micro-aethalometer during the ~40-min "wall-loss decay" period. Two sets of filter samples were collected for the "fresh" and "aged" smoke. The vertical dashed purple line at ~1.65 h indicates when the UV lamps were turned on.

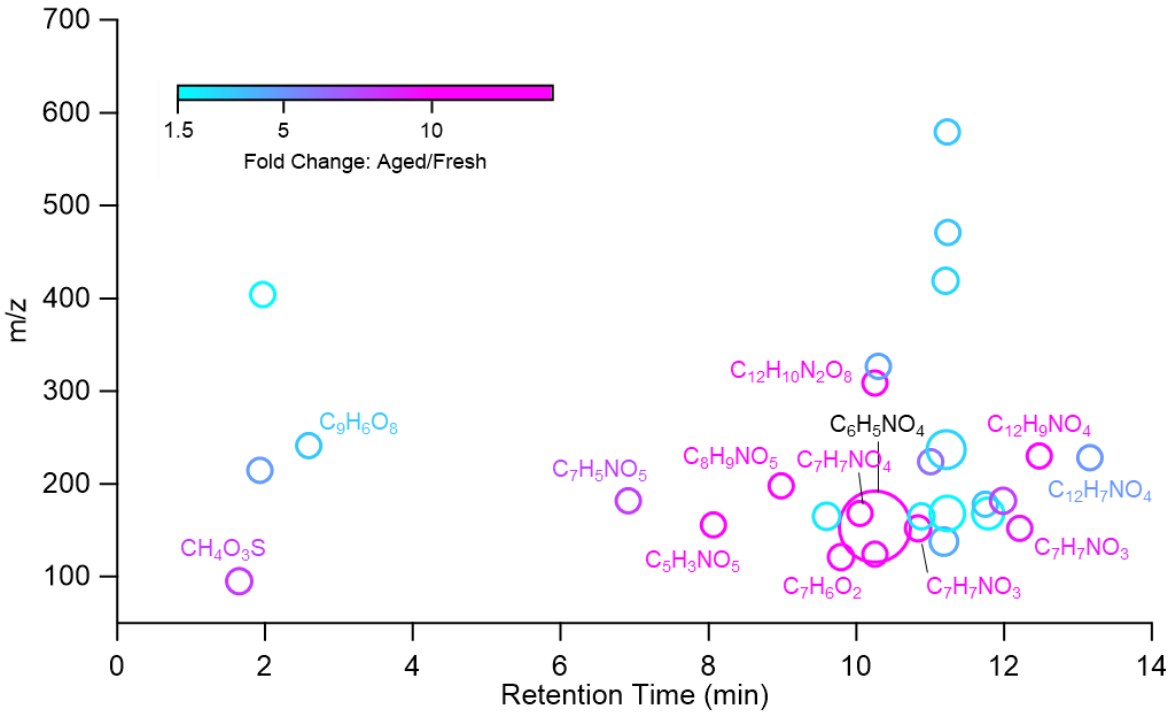


**Figure 4.3.** BrC formed (or enhanced by > 50%) during photooxidation of primary combustion emissions. Each circle represents a feature (ion) detected by UPLC/ESI-HR-QTOFMS in the aged emissions over the "fresh" smoke. Size of the circle (area) is proportional to the ion intensity (integrated peak area, or "abundance" in Table C3). Color of the circles reflect the fold change of the ion response from the aged sample over that from the "fresh" sample, ranging from 1.5 (light blue) to 10 and greater (pink). Selected elemental formulas are labeled next to the circle with the same color, except that the largest circle of ion intensity (C6H5NO4) is highlieghted in black.

# CHAPTER 5: CONCLUSIONS AND FUTURE WORK

In summary, source-specific atmospheric aerosols, such as marine and continental BVOC-derived SOA as well as primary and aged biomass burning aerosol, were analyzed using a suite of established and developed mass spectrometric techniques and methods. Particle-phase constituents from the specific sources above were characterized at the molecular level using UPLC/ESI-HR-QTOFMS and GC/EI-MS with authentic or surrogate standards.

In Chapter 2, we considered marine aerosol samples that originated over the open ocean where terrestrial emissions were largely excluded. Chemical results obtained from this unique aerosol filter archive provided important quantitative background levels of marine biogenic SOA over the 25-year period from 1991-2015. Although isoprene, monoterpenes, and chlorophyll-*a* were not as abundant at Cape Grim as other coastal and oceanic sites, oxidation of isoprene and monoterpenes still yielded measurable seasonal and temporal trends of iSOA and mSOA. Moreover, in the southern mid latitudes (30°S-60°S) where the sampling site is located, iSOA and mSOA were one to two orders of magnitude lower than those in the other oceanic regions and did not contribute substantial mass to the total OA mass (0.26±0.24%, up to 0.71%) measured at this site. Our observations suggested that secondary OA sources other than isoprene and monoterpenes exist in the remote marine atmosphere to explain the uncharacterized OA mass fraction. For example, the summed mass concentrations of oxalic acid and MSA were ~ 28 times higher than the summed concentrations of iSOA and mSOA. As a result, the sum of iSOA, mSOA, oxalic acid, and MSA mass concentrations contributed up to 19.0% of the total OA mass. Our results provide observations and motivation for future laboratory, field, and modelling studies to assess the

potential of the marine sources leading to biogenic SOA and OA formation over the open oceans. However, more work is needed to chemically characterize other OA constituents (e.g., saccharides and fatty acids) that additionally contribute to marine aerosol in order to reveal their sources. In particular, more information is required to fully understand the OA constituents associated with phytoplankton blooms in order to more clearly identify the processes that generate OA such as bubble bursting processes and SOA precursors likely derived from the sea surface microlayer. As discussed in Chapter 2, preliminary findings obtained from the UPLC/ESI-HR-QTOFMS method operated in both negative and positive ion modes revealed the presence of nitrogen (N)-containing organic species. Tentatively identified N-containing species (as well as CHO and CHOS compounds) may also contribute to the uncharacterized OA mass that remains from this study. In the future, the observed N-containing, CHO, and CHOS compounds can be confirmed and quantified with appropriate standards to fully identify their structures as well as to accurately quantify their mass concentrations. Correlations of their concentrations (or relative abundances) can be examined with the measured iSOA and mSOA tracers, as well as with the reported marine bioactivity indicators, to investigate their sources.

As demonstrated in Chapter 3, with authentic 2-methyltetrol and methyltetrol sulfate standards synthesized in-house, we developed a versatile HILIC/ESI-HR-QTOFMS method that can efficiently resolve and measure the major IEPOX-derived and several other water-soluble SOA constituents with enhanced separation, sensitivity, and accuracy. For instance, 2-methyltetrols, which have been mostly measured by GC/EI-MS with prior derivatization in past studies,[22,129,157] were simultaneously resolved along with 4-6 diastereomers of methyltetrol sulfate, allowing efficient quantification of both major classes of SOA constituents by a single non-thermal analytical method. We also demonstrated that conventional GC/EI-MS analyses might largely

overestimate some of the IEPOX-derived SOA tracers, resulting from the thermal decomposition or reaction from derivatization during analysis. Lastly, $C_5$-alkene triols and 3-methyltetrahydrofuran-3,4-diols are found to be potential GC/EI-MS artifacts formed from thermal degradation of 2-methyltetrol sulfates and 3-methyletrol sulfates, respectively, and are not detected with HILIC/ESI-HR-QTOFMS. Therefore, future work should reconsider the proposed formation mechanism of the related IEPOX-derived SOA products and re-examine the traditional analytical methods for carefully measuring these compounds. In addition, since the improved resolution of separation clearly reveals isomeric patterns specific to methyltetrol sulfates from acid-catalyzed multiphase chemistry of β- and δ-IEPOX, the following steps are proposed to further investigate the formation mechanism of the 2-methyletrol sulfates at the isomeric level:

(1) use H- or $C^{13}$-NMR to confirm the proposed structure of the 2-methyletrol sulfate diastereomers collected after separation on the HILIC column;

(2) re-generate IEPOX-derived SOA in smog chamber via acid-catalyzed reactive uptake of *cis*-β-IEPOX (instead of *trans*-β-IEPOX). The hypothesis is that the predominant isomeric peak at *m/z* 215 observed would elute at 4.2 min, as opposed to the one at 5.6 min from *trans*-β-IEPOX as shown in Figure 3.2;

(3) once the structures of the separated 2-methyletrol sulfate diastereomers are confirmed, investigate the effect of acidity on competition of the substitution reaction mechanisms ($S_N1$ vs. $S_N2$) by varying the acidity of seed aerosol (e.g, with reduced amount of $H_2SO_4$ but fixed $SO_4^{2-}$ concentration in seed aerosol). The hypothesis is that the relative abundance of the isomeric peak at 5.6 min mentioned above would reduce with decreased acidity of seed particles.

Current atmospheric models explicitly simulate SOA from the acid-catalyzed multiphase chemistry of IEPOX (i.e., the formation of 2-methyltetrols and methyltetrol sulfates), but have not

included the full pathways distinguishing between $S_N1$ and $S_N2$.[140,220–222] Therefore, accurate quantification of the 2-methyltetrols and methyltetrol sulfates with clear relative abundance of diastereomeric products will increase confidence in evaluation of model predictions, which will in turn lead to improved modeling of IEPOX-derived SOA. With the help of the expected outcomes from above, improvement in quantification of organosulfates will additionally provide much needed data for establishing carbon and sulfur mass closure in IEPOX-derived SOA measured or predicted during future lab and field studies.

From a public health point-of-view, the characterization of the atmospheric OA constituents highlights the need for hazard identification of these emerging but less well characterized compounds from the isoprene-abundant regions with anthropogenic emissions, or even in the background of natural marine and terrestrial environments, especially since isoprene has been classified as "possibly carcinogenic to humans (group 2B)" by the International Agency for Research on Cancer (IARC, http://monographs.iarc.fr/ENG/classification/crthall.php.) in 2008 and as "reasonably anticipated to be a human carcinogen" by the National Toxicity Program (NTP, http://ntp.niehs.nih.gov/ntp/roc/eleventh/profiles/s099isop.pdf.) in 2005. Moreover, since burning of biomass fuels (e.g., wildfire) is one of the most important sources of gaseous and particulate air pollutants on global and regional scales, many of its emissions constituents, such as PAHs, have been subject to major concern in all environmental compartments due to their mutagenic and carcinogenic properties.[112,251] Thus, characterizing hazardous components of these environmental pollutants is required to protect public health, especially for the susceptible US and global populations under the influence of wildfires or other sources of intensive biomass burning emissions.

**APPENDIX A: SUPPLEMENTARY INFORMATION FOR "CHEMICAL CHARACTERIZATION OF ISOPRENE- AND MONOTERPENE-DERIVED SECONDARY ORGANIC AEROSOL TRACERS IN REMOTE MARINE AEROSOLS OVER A QUARTER CENTURY"**

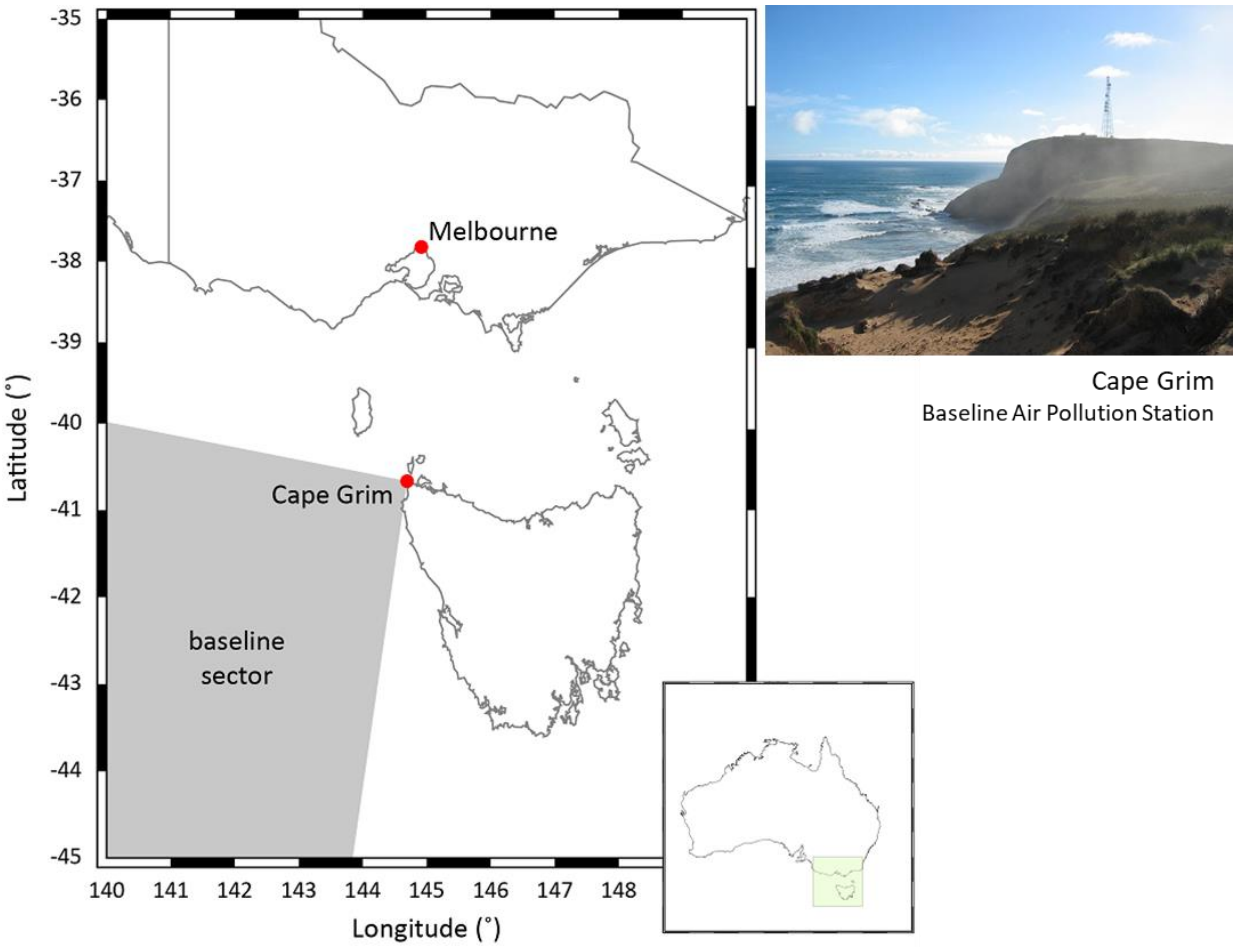


**Figure A1.** Location of Cape Grim site and "baseline" sector of wind direction. The Cape Grim Baseline Air Pollution Station is located at the top of 94-m cliffs on the western side of the north-west tip of Tasmania, Australia (40°40'56" S, 144°41'18" E).

**1. Baseline Conditions and Supporting Data in Baseline Reports**

Details of baseline conditions (i.e., Baseline Event Switch 2 and 3) can be found in Keywood, M.D (2007). Aerosol composition at Cape Grim: an evaluation of the $PM_{10}$ sampling program and baseline event switches. Baseline Atmospheric Program Australia 2005-2006 (page 31-35). Melbourne: Australian Bureau of Meteorology and CSIRO Marine and Atmospheric Research at http://www.cmar.csiro.au/e-print/open/baseline_2005-2006.pdf.

The air mass origin maps (by U.K. Met Office) of selected events and complete baseline definitions built up from five different criteria including wind speed, wind direction, radon concentrations, condensation nuclei (CN) counts, and standard deviation of ozone, are shown by Molloy, S. B. and Galbally, E. in Analysis and identification of a suitable baseline definition for tropospheric ozone at Cape Grim, Tasmania, page 7-16 in the 2009-2010 Baseline Report at http://www.bom.gov.au/inside/cgbaps/baseline/Baseline_2009-2010.pdf.

The angular radon distribution and back trajectory data from 2009-2010 by Zahorowski et al. can be found from page 33-38 in the same Baseline Report above.

Annual or biennial Cape Grim Baseline Reports from more years since 1976 are available at http://www.bom.gov.au/inside/cgbaps/baseline.shtml.

**Table A1**. Concentrations of individual isoprene- and monoterpene-derived SOA tracers, levoglucosan, oxalic acid, methanesulfonic acid (MSA), and calculated chlorophyll-*a* (Chl-*a*) in aerosol samples collected from austral winter and summer seasons from 1991-2015.

| Year-Season | 2-MG[a] | Me.Thr.[b] | Me.Ery.[c] | Terebic Acid | Terpenylic Acid | Pinic Acid | MBTCA[d] | DTAA[e] | Levoglucosan | Oxalic Acid | MSA[f] | Cal. Chl-*a*[g] |
|---|---|---|---|---|---|---|---|---|---|---|---|---|
| yy(s/w) | ng/m$^3$ | ng/m$^3$ | ng/m$^3$ | ng/m$^3$ | ng/m$^3$ | ng/m$^3$ | ng/m$^3$ | ng/m$^3$ | ng/m$^3$ | ng/m$^3$ | ng/m$^3$ | ng/m$^3$ |
| 91s | 0.201 | 0.227 | 0.507 | 0.066 | 0.075 | 0.006 | bdl[h] | 0.059 | 0.241 | n/a[i] | 115.89 | n/a |
| 91w | bdl | bdl | 0.090 | 0.023 | 0.043 | 0.004 | bdl | 0.038 | 0.176 | n/a | 4.49 | n/a |
| 92s | 0.225 | 0.645 | 1.559 | 0.080 | 0.118 | 0.003 | 0.082 | 0.117 | 0.377 | n/a | 126.84 | n/a |
| 92w | 0.115 | 0.075 | 0.199 | 0.014 | 0.036 | 0.011 | 0.015 | 0.055 | 0.630 | n/a | 5.85 | n/a |
| 93s | 0.545 | 0.995 | 2.485 | 0.140 | 0.204 | 0.041 | 0.067 | 0.164 | 0.732 | n/a | 101.67 | n/a |
| 93w | 0.099 | 0.096 | 0.226 | 0.011 | 0.049 | 0.035 | 0.005 | 0.157 | 0.524 | n/a | 3.51 | n/a |
| 94s | 0.216 | 0.605 | 1.208 | 0.116 | 0.161 | 0.048 | 0.020 | 0.361 | 0.348 | n/a | 84.05 | n/a |
| 94w | 0.148 | 0.246 | 0.572 | 0.023 | 0.086 | 0.026 | 0.004 | 0.168 | 0.360 | n/a | 4.56 | n/a |
| 96s | 0.307 | 0.544 | 1.445 | 0.166 | 0.185 | 0.010 | 0.059 | 0.200 | 0.370 | 18.58 | 134.22 | n/a |
| 96w | 0.108 | 0.155 | 0.306 | 0.025 | 0.111 | 0.014 | 0.001 | 0.070 | 1.367 | 12.52 | 6.73 | n/a |
| 97s | 0.328 | 0.262 | 0.975 | 0.102 | 0.223 | 0.038 | 0.040 | 0.086 | 0.180 | 31.47 | 129.97 | n/a |
| 97w | 0.285 | 0.672 | 1.535 | 0.034 | 0.058 | 0.006 | 0.035 | 0.037 | 1.297 | 8.46 | 2.25 | n/a |
| 98s | 0.721 | 1.815 | 4.212 | 0.323 | 0.234 | 0.018 | 0.146 | 0.281 | 0.628 | 37.01 | 99.86 | n/a |
| 98w | 0.237 | 0.258 | 0.629 | 0.045 | 0.091 | 0.013 | 0.070 | 0.080 | 1.183 | 11.44 | 3.18 | n/a |
| 99s | 0.386 | 0.459 | 1.184 | 0.258 | 0.129 | 0.047 | bdl | 0.150 | 0.346 | 15.66 | 76.80 | n/a |
| 99w | 0.176 | 0.350 | 0.861 | 0.031 | 0.041 | 0.012 | 0.026 | 0.021 | 0.316 | 7.14 | 3.09 | n/a |
| 04w | 0.067 | 0.066 | 0.229 | 0.025 | 0.040 | 0.018 | 0.039 | 0.043 | 0.178 | 4.24 | 6.01 | 156.93 |
| 07s | 0.229 | 0.720 | 1.792 | 0.181 | 0.137 | 0.007 | 0.086 | 0.357 | 0.276 | 21.20 | 100.44 | 179.59 |
| 07w | 0.071 | 0.044 | 0.143 | 0.024 | 0.030 | 0.008 | bdl | 0.030 | 0.379 | 5.93 | 2.55 | 82.45 |
| 08s | 0.349 | 1.364 | 3.272 | 0.123 | 0.078 | 0.014 | 0.054 | 0.017 | 0.105 | 15.94 | 65.15 | 160.97 |
| 08w | 0.025 | 0.020 | 0.053 | 0.014 | 0.015 | 0.007 | bdl | 0.014 | 0.110 | 12.87 | 1.78 | 86.42 |
| 09w | 0.057 | 0.042 | 0.103 | 0.007 | 0.007 | 0.005 | bdl | 0.008 | 0.563 | 7.10 | 2.94 | 75.33 |
| 11s | 0.144 | 0.412 | 0.929 | 0.124 | 0.074 | 0.013 | 0.023 | 0.167 | 0.099 | 8.89 | 83.46 | 147.98 |
| 11w | 0.037 | 0.064 | 0.154 | 0.019 | 0.017 | 0.005 | 0.003 | 0.024 | 0.082 | 1.23 | 0.61 | 99.68 |
| 12s | 0.138 | 1.191 | 2.915 | 0.136 | 0.061 | 0.012 | 0.037 | 0.111 | 0.049 | 5.65 | 96.85 | 156.35 |
| 12w | 0.021 | 0.012 | 0.050 | 0.022 | 0.011 | 0.006 | bdl | 0.010 | 0.116 | 1.21 | 0.84 | 82.13 |
| 14s | 0.209 | 0.583 | 1.536 | 0.103 | 0.054 | 0.008 | 0.090 | 0.234 | 1.806 | 20.17 | 113.24 | 170.75 |
| 14w | 0.097 | 0.273 | 0.578 | 0.032 | 0.014 | 0.005 | 0.063 | 0.014 | 0.281 | 12.72 | 3.76 | 99.35 |
| 15s | 0.166 | 0.460 | 1.249 | 0.156 | 0.067 | 0.008 | 0.035 | 0.176 | 0.131 | 13.35 | 90.38 | 136.23 |

[a] 2-MG stands for 2-methylglyceric acid.

[b] Me.Thr. stands for 2-methylthreitol.

[c] Me.Ery. stands for 2-methylerythritol.

[d] MBTCA is 3-methyl-1,2,3-butanetricarboxylic acid.

[e] DTAA is diaterpenylic acid acetate.

[f] MSA stands for methanesulfonic acid.

[g] Calculated chlorophyll-*a* is retrieved from satellite data. See main text Section 3.4 and SI Section 7.1 for details.

[h] "bdl" indicates below detection limit.

[i] "n/a" indicates data unavailable in these years.

**2. Mass of Collected $PM_{10}$**

Gravimetric mass measurements were performed on the high-volume filters using a Sartorius Master Pro LA130S-F balance at relative humidity of approximately 50%. The resolution of the balance was 0.0001 g. Each 25 cm × 20 cm filter was weighed before and after sampling until three weights within 0.0010 g.

**3. Details for Ion Chromatography (IC) Analysis**

Anion and cation concentrations were determined with a Dionex ICS-3000 reagent free ion chromatograph. Anions were separated using a Dionex AS17c analytical column (2 × 250 mm), an AERS-500 suppressor and a gradient eluent of 0.75 mM to 35 mM potassium hydroxide. Cations were separated using a Dionex CS12a column (2 x 250 mm), a CERS-500 suppressor and an isocratic eluent of 20 mM methanesulfonic acid.

Seven calibration standards covering the sample concentration range are included in each analysis run for each analyte and a check standard is analyzed in each analysis run after the 7 calibration standards and then after every 20 samples.

The ion balance (IB) gives an indication of the aerosol chemistry data quality in that the total cation equivalents (positive charged ions) should equal the total anion equivalents (negative charged ions). The Global Atmospheric Watch Program (GAW) which is part of the World Meteorological Organization (WMO) gives the IB equation and criteria for assessing valid data results in its technical report 160, “Manual for the GAW Precipitation Chemistry Programme”. Any samples that fail the IB criteria are re-analyzed.

The blank concentration is subtracted from each measurement. The blanks are also used to calculate the method detection limit (MDL). We followed the Standards Australia procedures which are those of the International Standard ISO 6879 Air quality – Performance characteristics and related concepts for air quality monitoring methods. Section 5.2.7 of the Standard states that

a zero sample has a 5 % probability of causing a measured concentration above the detection limit, so that:

$$MDL = t_{0.95} \times s_{c(0)}$$

where:

$S_{c(0)}$ is the standard deviation of the blanks, and $t_{0.95}$ is value of the 1-tailed t distribution for $P<0.05$ (i.e. the 95 % confidence limit).

**4. Organic Carbon, Elemental Carbon, and Total Carbon Estimation**

The organic carbon (OC), apparent elemental carbon ($EC_a$), and total carbon (TC) contents of the quartz filter samples were measured by the thermal-optical transmission (TOT) technique (Birch and Cary, 1996), using the procedure described in Schmid et al. (2001). This involved stepwise combustion of the aerosol carbon to form carbon dioxide ($CO_2$), which was then reduced to methane ($CH_4$) and detected by a flame ionization detector (FID). The effects of charring during pyrolysis of organic compounds in the early stages of the combustion (artifact $EC_a$) were corrected for by simultaneously monitoring light transmission through the filter and defining $EC_a$ as the only carbon that evolved after the light transmittance through the sample had reached its original level. The uncertainty of the TC measurement was ±0.25 μg $cm^{-2}$. The average concentration of TC for the 32 valid Hi-Vol samples from 2002-2003 was 2.6 μg $cm^{-2}$ (ranging between 0.5 and 11. 6 μg $cm^{-2}$). The limit of detection was 0.4 μg $cm^{-2}$ (determined from the standard deviation of 10 field sample blanks multiplied by the appropriate t value according to ISO, 1994).

The organic matter (OM) in sample was estimated using the following equation:

$$OM = 1.8 \times OC + EC_a$$

Then the ratios of OM/$PM_{10}$ were calculated and averaged to be 4.09% for summer (mid-December to mid-February) and 2.38% for winter (mid-June to mid-August), which were used to convert $PM_{10}$ to OA mass when evaluating measured iSOA and mSOA as a fraction of OA from 2004-2015.

**Table A2.** Summed iSOA (∑iSOA), summed mSOA (∑mSOA), oxalic acid, and MSA estimated as a fraction of organic aerosol mass from 2004-2015.

| | **∑iSOA** | **∑mSOA** | **$PM_{10}$** | **iSOA** | **mSOA** | **[iSOA+mSOA]** | **[iSOA+mSOA+ Oxalic acid+MSA]** |
|---|---|---|---|---|---|---|---|
| | $ng/m^3$ | $ng/m^3$ | $\mu g/m^3$ | to OA | to OA | to OA | to OA |
| **Summer** | | | | | | | |
| 2007 | 2.60 | 0.77 | 16.1 | 0.394% | 0.117% | 0.511% | 18.955% |
| 2008 | 4.73 | 0.29 | 18.9 | 0.612% | 0.037% | 0.649% | 11.145% |
| 2011 | 1.48 | 0.40 | 19.8 | 0.183% | 0.049% | 0.232% | 11.613% |
| 2012 | 4.24 | 0.36 | 15.9 | 0.652% | 0.055% | 0.707% | 16.454% |
| 2014 | 2.33 | 0.49 | 18.1 | 0.315% | 0.066% | 0.381% | 18.416% |
| 2015 | 1.87 | 0.44 | 19.6 | 0.233% | 0.055% | 0.288% | 13.209% |
| *Average* | *2.88* | *0.46* | *18.1* | *0.398%* | *0.063%* | *0.462%* | 14.767% |
| **Winter** | | | | | | | |
| 2004 | 0.36 | 0.16 | 18.2 | 0.084% | 0.038% | 0.122% | 2.493% |
| 2007 | 0.24 | 0.09 | 15.0 | 0.068% | 0.026% | 0.094% | 2.466% |
| 2008 | 0.09 | 0.05 | 17.8 | 0.022% | 0.012% | 0.034% | 3.492% |
| 2009 | 0.20 | 0.03 | 24.3 | 0.035% | 0.005% | 0.040% | 1.775% |
| 2011 | 0.26 | 0.07 | 22.1 | 0.049% | 0.013% | 0.062% | 0.412% |
| 2012 | 0.08 | 0.05 | 19.6 | 0.018% | 0.010% | 0.028% | 0.467% |
| 2014 | 0.95 | 0.13 | 16.5 | 0.241% | 0.033% | 0.274% | 4.461% |
| *Average* | *0.31* | *0.08* | *19.1* | *0.074%* | *0.019%* | *0.093%* | 2.101% |

**5. Surface Ozone at Cape Grim**

Ozone measurements were made at 10 m above the laboratory roof through the main station stainless steel inlet, using the absolute ozone monitor designated as TECO-2 (Model 49, Thermo Instruments, USA) for the whole period, and a newer ozone monitor (Model 49C, Thermo Instruments, USA) designated TECO-3. The absolute accuracy of the ozone monitor was checked regularly against a Thermoelectron Model 49PS ozone calibrator. Automatic calibrations were performed approximately every two weeks.

The provisional surface ozone monthly mean concentrations for all conditions for January 1990 to December 2015 are presented in the figure below.

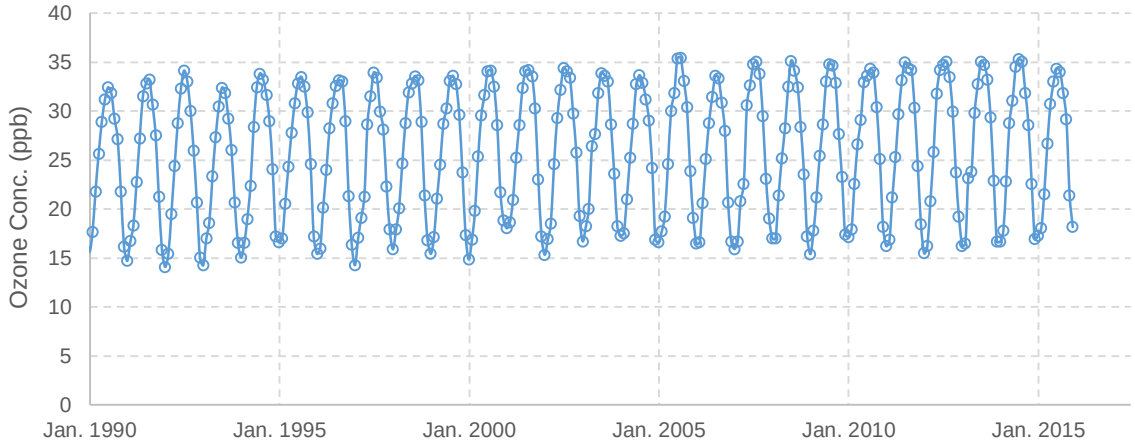


**Figure A2.** Monthly average surface ozone concentrations (nmol/mol, or ppb) at Cape Grim from January 1990 to December 2015.

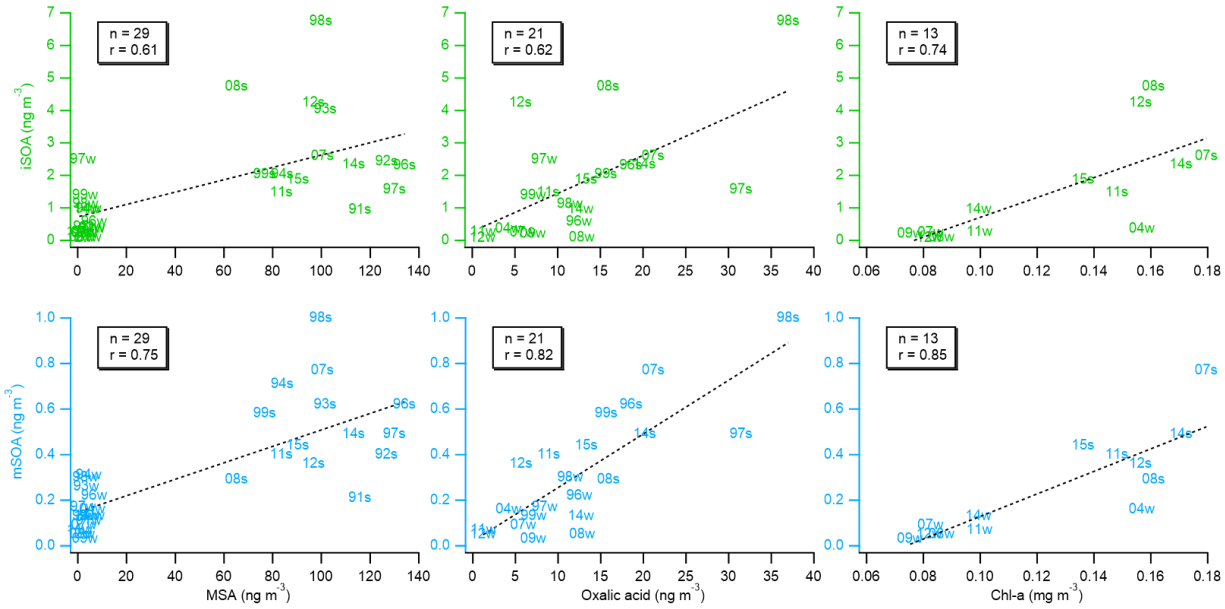


**Figure A3.** Correlations of the summed concentration of the three isoprene-derived SOA tracers (iSOA, green) or the five monoterpene-derived SOA tracers (mSOA, blue) with MSA/Oxalic acid/Chl-*a* (from left to right). Years and austral seasons (n=13-29) with available data are labeled in each sub-panel.

## 6. Chlorophyll-*a* (Chl-*a*) Data Usage and Description

6.1 Satellite measurement by remote sensing

Global Chl-*a* concentrations were derived from ocean color every day with a spatial resolution of 1-km, measured by the Moderate Resolution Imaging Spectroradiometer (MODIS) instrument aboard NASA's Terra and Aqua satellites over the entire planet. The MODIS instrument offers an estimate of the near-surface concentration of chlorophyll calculated using an empirical relationship derived from *in situ* measurements of chlorophyll and remote sensing reflectances in the blue-to-green region of the visible spectrum. Since the values retrieved from the formatted files were scaled and resampled for visualization purposes by NASA Earth Observation (NEO) and not suggested for rigorous scientific examination, we only adapted them for trend detection and simply correlation. See https://neo.sci.gsfc.nasa.gov/view.php?datasetId=MY1DMM_CHLORA for more information for the related websites, description, algorithm, and data file formats.

Total monthly Chl-*a* contents in this study were averaged and integrated from the oceanic region over [30-60°S, 90-150°E]. This region is determined based on previous back trajectory studies for suitable timescale of SOA formation and transport (approximately 4 days for correspoding air parcels to reach Cape Grim, roughly one unit of Rn's half-life = 3.84 days, reported in 2009-2010 Baseline Report, Page 33-38). On the temporal scale, the selected months also cover the same filter sampling period as precise as possible.

It is worth mentioning that the values of high-resolution Chl-*a* concentrations retrieved online in the .csv files have been scaled and resampled, and thus are basically used to examine their seasonal and temporal variation rather than accuracy.

6.2 *In situ* measurements

Chl-*a* concentration was measured in the local seawater samples obtained approximately 9 km offshore from Couta Rocks, 50 km south of Cape Grim, in the selected years from 1995-2007. One-liter ocean water samples were filtered onto 42-mm diameter glass fibre filters followed by extraction with methanol, and then determined by a published acidification method (Holm-Hansen and Riemann, 1978) using a digital fluorometer (Turner Instrument, 10AU).

When both types of Chl-*a* data were available during 2003-2006, we compare the *in situ* measurements at the offshore site made from the sea surface (depth = 0 m, data retrieved from Baseline Reports 2003-2004 (page 81-86) and 2005-2006 (page 80-84), by Cainey et al. at http://www.bom.gov.au/inside/cgbaps/baseline.shtml), and the satellite measurements at the same location and time period (Hi-Res of 0.1×0.1 degree, 8-day average), as shown in Figure A4. Although the location and time coverage between the two types of measurements were not exactly the same, the comparison reveals similar trends of Chl-*a* concentrations over the years. Therefore, it would be reliable to correlate the whole-time satellite measured Chl-*a* with the iSOA concentrations at Cape Grim.

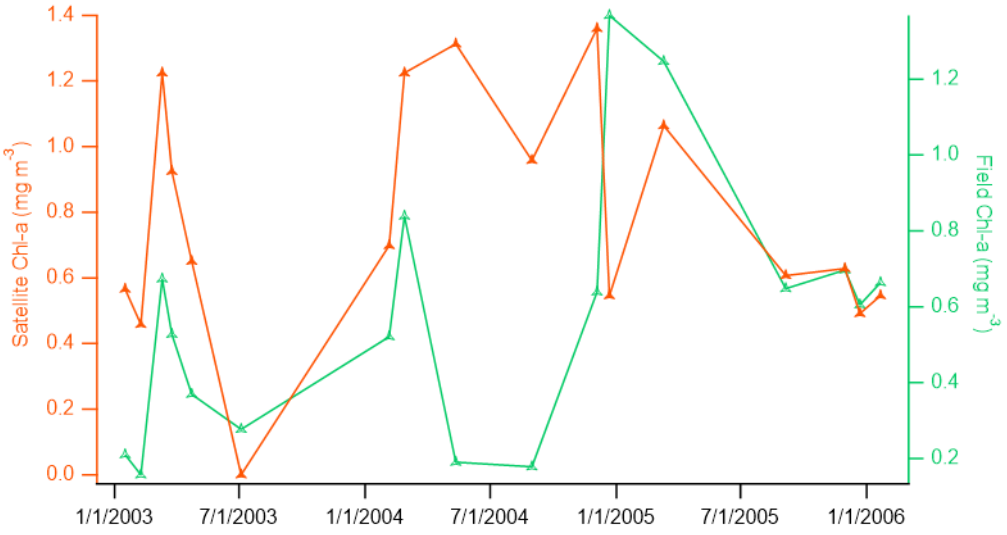


**Figure A4.** Comparison of satellite and *in situ* measurements of Chl-*a* during 2003-2006.

**Table A3.** List of molecular formulas of N-containing and other species tentatively identified by UPLC/ESI-HR-QTOFMS operated in negative (-) and positive (+) ion modes.

| ESI (-) | | | | ESI (+) |
|---|---|---|---|---|
| *CHNO3* | *CHNO4* | *Other N-Containing* | *CHO(S)* | *N-Containing* |
| C7H13NO3 | C9H17NO4 | C5H6N4O5 | C4H6O4 | C4H6N2 |
| C8H15NO3 | C10H19NO4 | C7H5NO3S2 | C5H8O4 | C7H11N7O |
| C9H17NO3 | C11H21NO4 | C7H15NO5S | C6H10O4 | C8H19N |
| C10H19NO3 | C12H23NO4 | C11H12N4O2 | C7H10O4 | C9H17NO2 |
| C11H21NO3 | C13H25NO4 | C8H17NO5S | C8H6O4 | C9H17NO3 |
| C12H23NO3 | | C9H19NO5S | C8H12O4 | C11H19N7O |
| C13H25NO3 | | C12H23NO5 | C8H14O4 | C12H23N7O |
| C14H21NO3 | | C10H21NO5S | C9H18O3 | C13H25NO2 |
| C14H27NO3 | | C11H23NO5S | C8H10O3S | C13H25NO3 |
| C15H29NO3 | | C19H9ClN4O | C8H12O5 | C14H16N6O2 |
| | | C17H32N2O5 | C9H16O4 | C18H28N6O6 |
| | | C17H30N2O3 | C10H18O4 | C27H41N |
| | | C18H34N2O5 | C11H20O4 | |
| | | C19H34N2O5 | C12H20O4 | |
| | | C19H36N2O5 | C12H20O5 | |
| | | C20H38N2O5 | C9H18O6S | |
| | | C20H36N2O3 | C13H22O5 | |
| | | C16H4N2O7S2 | C18H30S2 | |
| | | C21H40N2O5 | C17H26O5 | |
| | | C16H28N2O10 | C17H28O5 | |
| | | C12H6N4O11S | C20H14O9 | |
| | | C14H2N4O12S | | |
| | | C15H6N4O7S3 | | |
| | | C12H6N4O12S2 | | |
| | | C18H4N4O10S2 | | |
| | | C14H4N4O15S | | |

**Reference of Appendix A:**

Annual or biennial Cape Grim Baseline Reports from since 1976: http://www.bom.gov.au/inside/cgbaps/baseline.shtml.

Birch, M. E. and Cary, R. A. Elemental Carbon-Based Method for Monitoring Occupational Exposures to Particulate Diesel Exhaust, *Aerosol Science and Technology*. **1996**, 25 (3), 221-241.

Schmid, H.; Laskus, L.; Abraham, H. J.; Baltensperger, U.; Lavanchy, V.; Bizjak, M.; Burba, P.; Cachier, H.; Crow, D.; Chow, J.; Even, T. G. A.; Brink, H. M.; Giesen, K-P.; Hitzenberger, R.; Hueglin, C.; Maenhaut, W.; Pio, C.; Carvalho, A.; Putaud, J-P.; Toom-Sauntry, D.; Puxbaum, H. Results of the "carbon conference" international aerosol carbon round robin test stage I, *Atmospheric Environment*, **2001**, 35 (12), 2111-2121.

Holm-Hansenm, O. and Riemann, B. Chlorophyll-*a* Determination: Improvements in Methodology, *Oikos*. **1978**, 30 (3), 438-447.

**APPENDIX B: SUPPLEMENTARY INFORMATION FOR "DEVELOPMENT OF A HYDROPHILIC INTERACTION LIQUID CHROMATOGRAPHY METHOD FOR THE CHEMICAL CHARACTERIZATION OF ISOPRENE EPOXYDIOL-DERIVED SECONDARY ORGANIC AEROSOL"**

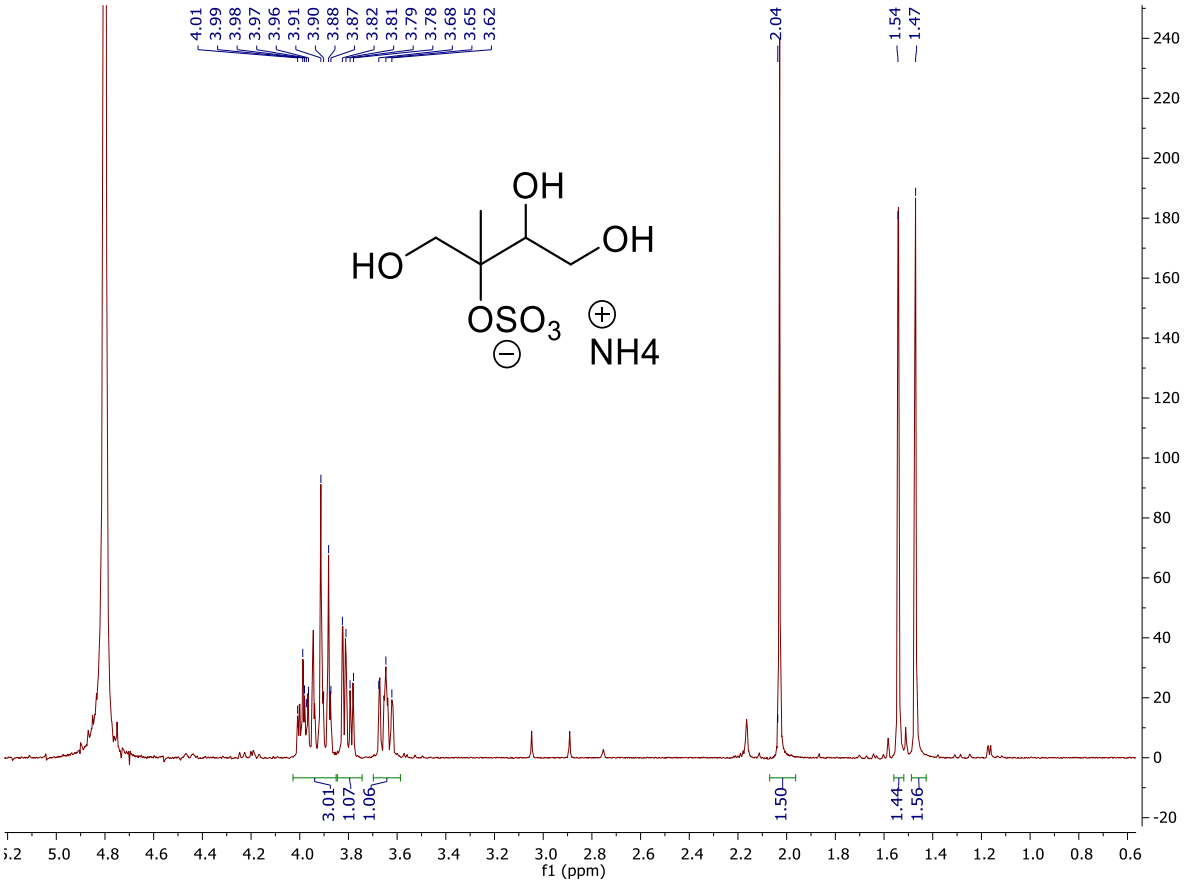


**Figure B1.** Structure and $^{1}H$ NMR ($D_2O$, 400 MHz) of 2-methytetrol sulfate diastereomer standard (ammonium 1, 3, 4-trihydroxy-2-methylbutan-2-yl sulfate; optical configurations indicated below in Figure B2).

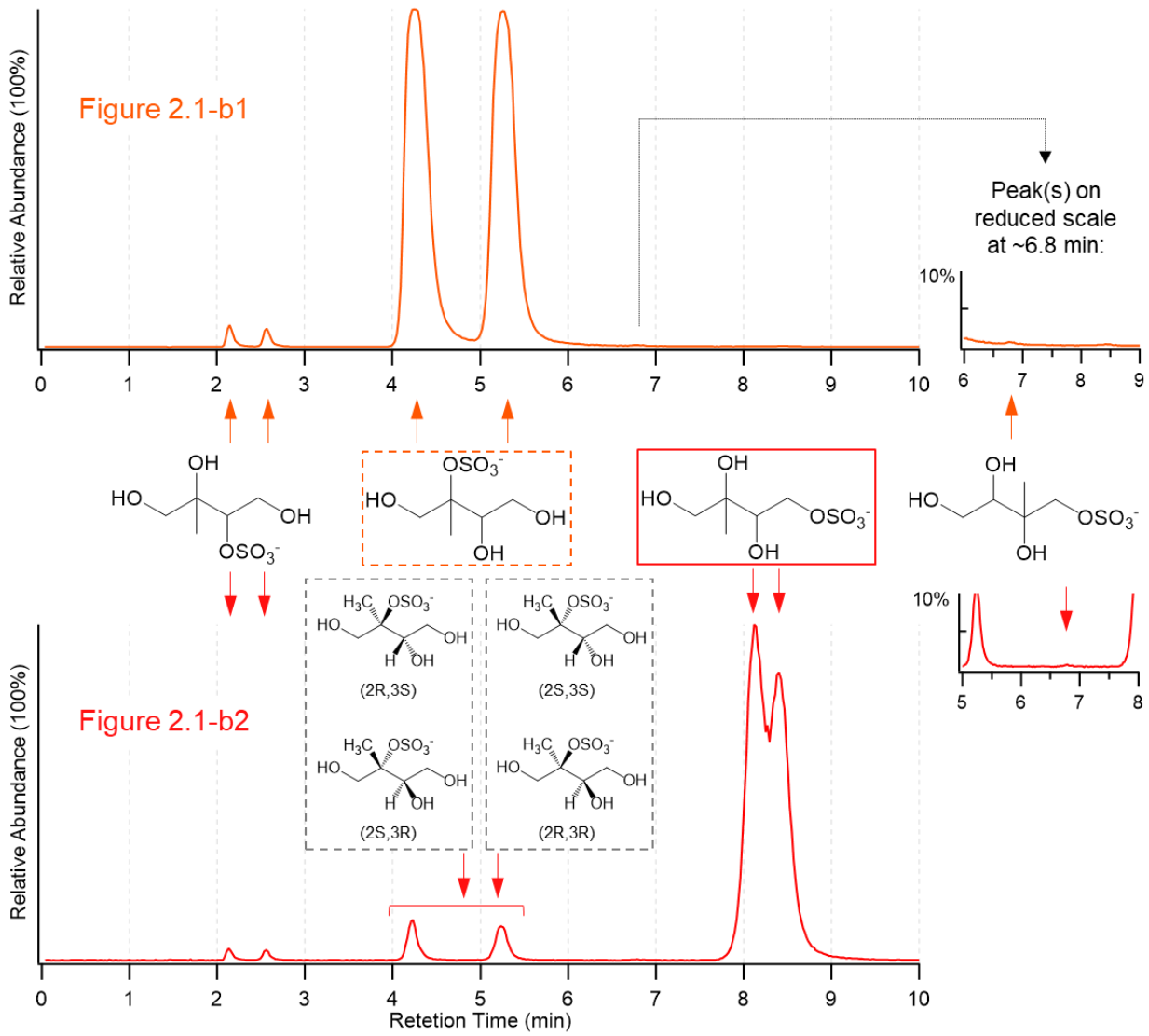


**Figure B2.** The EICs in Figure 2.1 (b1-b2) are reproduced here for the 2- and 3-methyltetrol sulfate standards. The tertiary methyltetrol sulfate esters with correct optical configurations at the asymmetric centers are enclosed in dashed grey boxes. The top row of structures shows all possible the structural isomers without optical configurations indicated. From left to right: 1,3,4-trihydroxy-3-methylbutan-2-yl sulfate, 1,3,4-trihydroxy-2-methylbutan-2-yl sulfate (2-methyltetrol sulfate, in dashed orange box), 2,3,4-trihydroxy-3-methylbutyl sulfate (3-methyltetrol sulfate in solid red box), and 2,3,4-trihydroxy-2-methylbutyl sulfate. In the insets at the right side of the figure, EICs at a reduced scale (10%) indicate a trace peak(s) at ~6.8 min, which may represent the primary sulfate ester derived from δ-IEPOX (2,3,4-trihydroxy-2-methylbutyl sulfate).

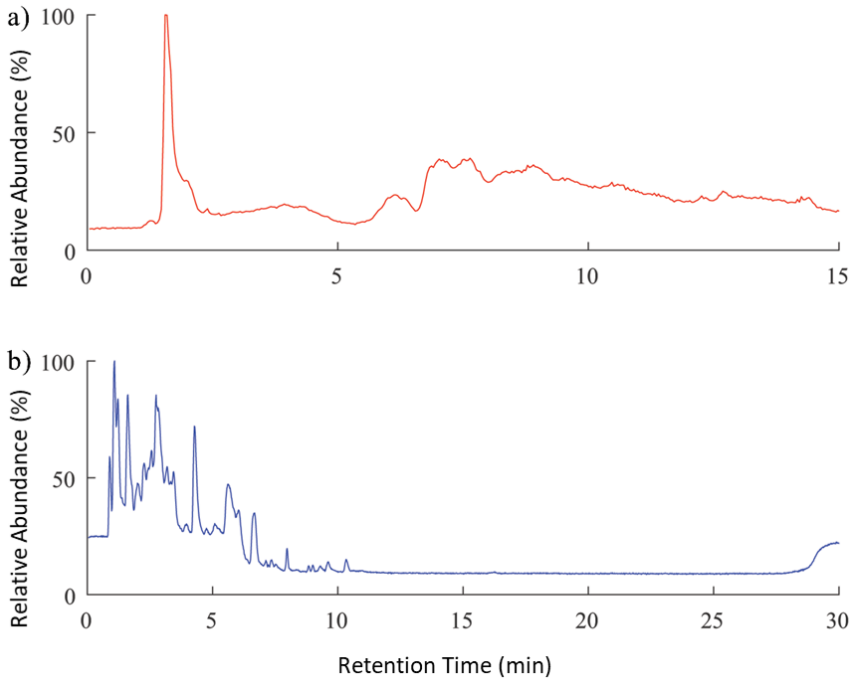


**Figure B3.** Total ion chromatograms (TICs) of a laboratory-generated β-IEPOX-derived SOA sample separated on **a)** RPLC $C_{18}$ column, and **b)** HILIC BEH amide column.

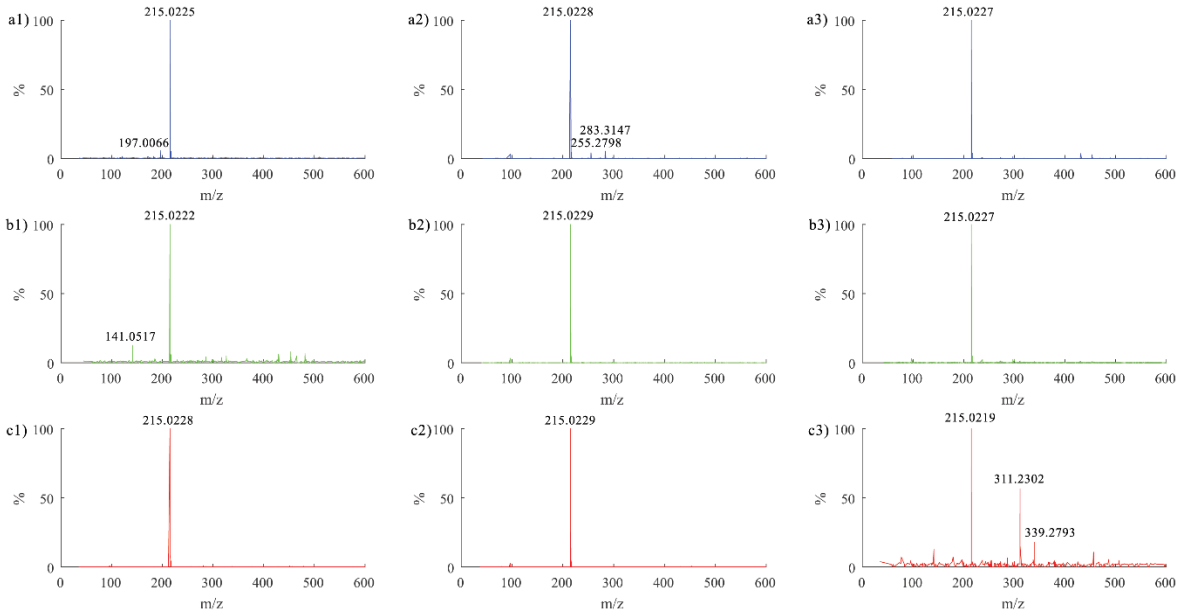


**Figure B4.** Mass spectra from HILIC/ESI-HR-QTOFMS of the chromatographic peak of *m/z* 215.023 from **a)** 10 μg $mL^{-1}$ standard of 3-methyltetrol sulfate, **b)** laboratory-generated δ-IEPOX SOA, and **c)** $PM_{2.5}$ sample collected at Look Rock during 2013 SOAS campaign, at RT at: 1) 2.2 min; 2) 4.5 min; and 3) 9.6 min. Note that the chromatographic peak in "c3" has significantly smaller response rate compared to the other chromatographic peaks.

## 1. Aerosol Volume Measurement, Mass Calculation, and Mass Closure for Laboratory-Generated SOA

Chamber aerosol number distributions, which were subsequently converted to total aerosol surface area and volume concentrations, were measured by a scanning electrical mobility system (SEMS v5.0, Brechtel Manufacturing Inc. – BMI) containing a differential mobility analyzer (DMA, BMI) coupled to a mixing condensation particle counter (MCPC Model 1710, BMI). The SEMS system has an internal Nafion dryer connected inline between its inlet and neutralizer. Total aerosol mass concentration was calculated using the total volume concentration multiplied by the density of 1.42 g $mL^{-1}$ of the particles formed after reaction (for the seed aerosol of acidified ammonium sulfate, a density of 1.77 g $mL^{-1}$ was used). The densities used above were reported by Riva et al. based on single-particle characterizations from experiments conducted with *trans*-β-IEPOX and acidified ammonium sulfate aerosols under similar conditions.[1] However, the volume growth was found to be lower for δ-IEPOX-derived SOA, which means the resulting density was higher than 1.42 g $mL^{-1}$. Therefore, assuming the widely reported organic density of 1.2 g $mL^{-1}$ and volume additivity, the resulting density for total aerosol has been corrected to 1.55 g $mL^{-1}$, which was used to calculate the mass of total aerosols generated from δ-IEPOX and acidified ammonium sulfate. It is also reasonable to assume that sulfates, either in inorganic or organic forms, remained in the aerosol phase and the change in ammonium equilibrium between the gas and aerosol phase after IEPOX uptake was small as indicated by Aerosol Chemical Speciation Monitor (ACSM, Aerodyne Research Inc.) measurements. Therefore, the calculated aerosol mass concentration includes both the inorganic sulfate group and the sulfate groups that are covalently bonded to the organic residue. The averaged aerosol masses during the PILS collection periods for the two chamber experiments are shown in Table B1 below.

**Table B1.** Experimental Conditions and Calculated Aerosol Mass for Laboratory-Generated IEPOX SOA

| IEPOX Isomer | Seed Aerosols | Aerosol Mass ($\mu g\ m^{-3}$) | Temp (°C) | RH (%) |
|---|---|---|---|---|
| *trans*-β-IEPOX | $(NH_4)_2SO_4 + H_2SO_4$ | 188.51 | 21-23 | 50-50 |
| δ-IEPOX | $(NH_4)_2SO_4 + H_2SO_4$ | 150.13 | 21-23 | 50-55 |

Figure B5 shows the aerosol volume concentration and the seed volume decay during the experiments. For the laboratory-generated SOA from *trans*-β-IEPOX (top), the PILS sample selected was collected near the end of the experiment at time 3:27 with 2-methyltetrols measured to be ~64 $\mu g\ m^{-3}$ and methyltetrol sulfates measured to be ~110 $\mu g\ m^{-3}$. At the same time, the SEMS-MCPC system measured 133 $\mu m^3\ cm^{-3}$ total particle volume concentration, which was converted to a total mass concentration of 189 $\mu g\ m^{-3}$ (density = 1.42 $g\ mL^{-1}$); and 42 $\mu m^3\ cm^{-3}$ seed particle volume concentration (assuming first-order decay rate), which was converted to a total seed mass concentration of 75 $\mu g\ m^{-3}$ (density = 1.77 $g\ mL^{-1}$). Thus, the two quantified IEPOX SOA components accounted for ~92% of the total aerosol mass, which suggests that the inorganic sulfate in the seed aerosol might be substantially converted into organosulfates. This was supported by measurements using ion chromatography for the PILS samples collected during the course of the experiment. These details are being expanded upon in another manuscript just submitted. A similar mass-closure situation was observed for the laboratory-generated SOA from δ-IEPOX (Figure B5, bottom).

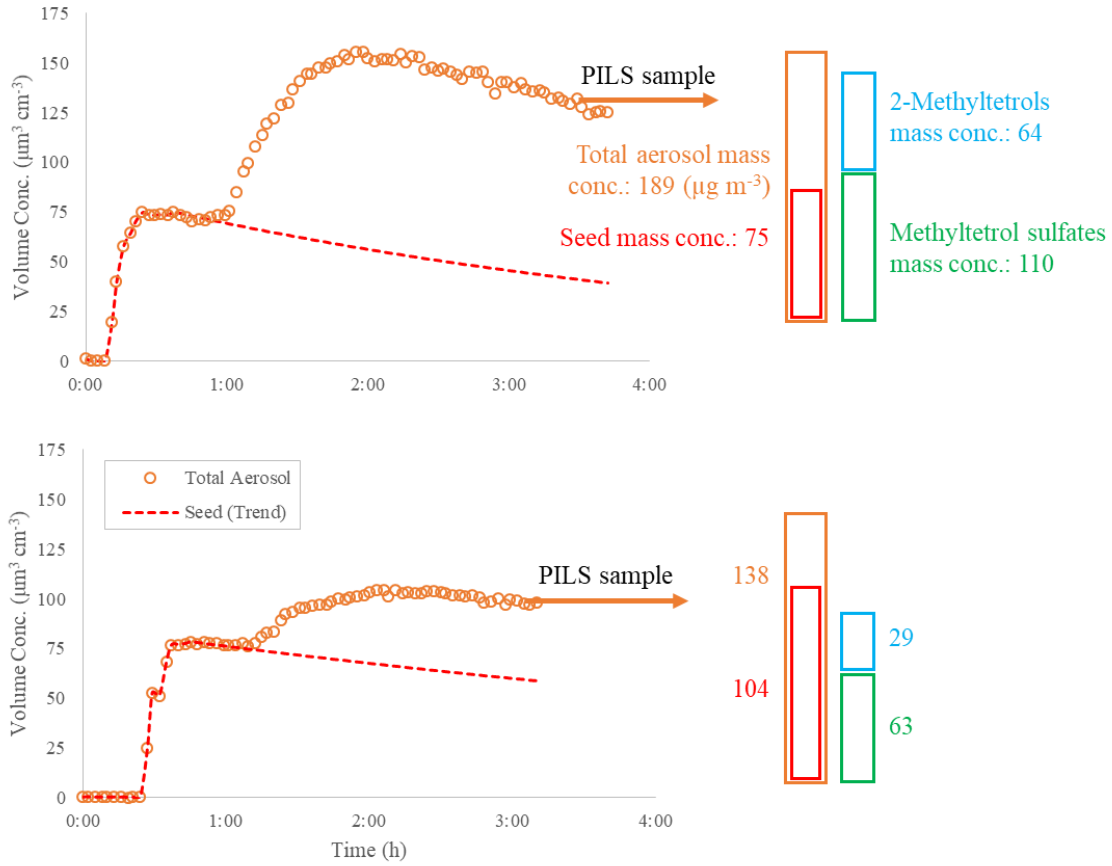


**Figure B5.** Time profile of total aerosol volume concentration and aerosol mass breakdown for the experiments from (top) *trans*-β-IEPOX; and (bottom) δ-IEPOX. Ammonium bisulfate particles were injected into the chamber to reach ~ 75 $\mu m^3\ cm^{-3}$. After seed injection, the chamber was left static for at least 30 min to ensure that the seed aerosol was stable and uniformly mixed. Then, 30 mg of *trans*-β- or δ-IEPOX was injected into the chamber. PILS collection was performed at the end of each experiment, as indicated by the arrow. The bars on the right side show the mass concentrations of the total particles, the initial seed particles measured by the SEMS. 2-Methyltetrols and methyltetrol sulfates concentrations were measured by the HILIC/ESI-HR-QTOFMS protocol and indicated by the blue and green bars as well.

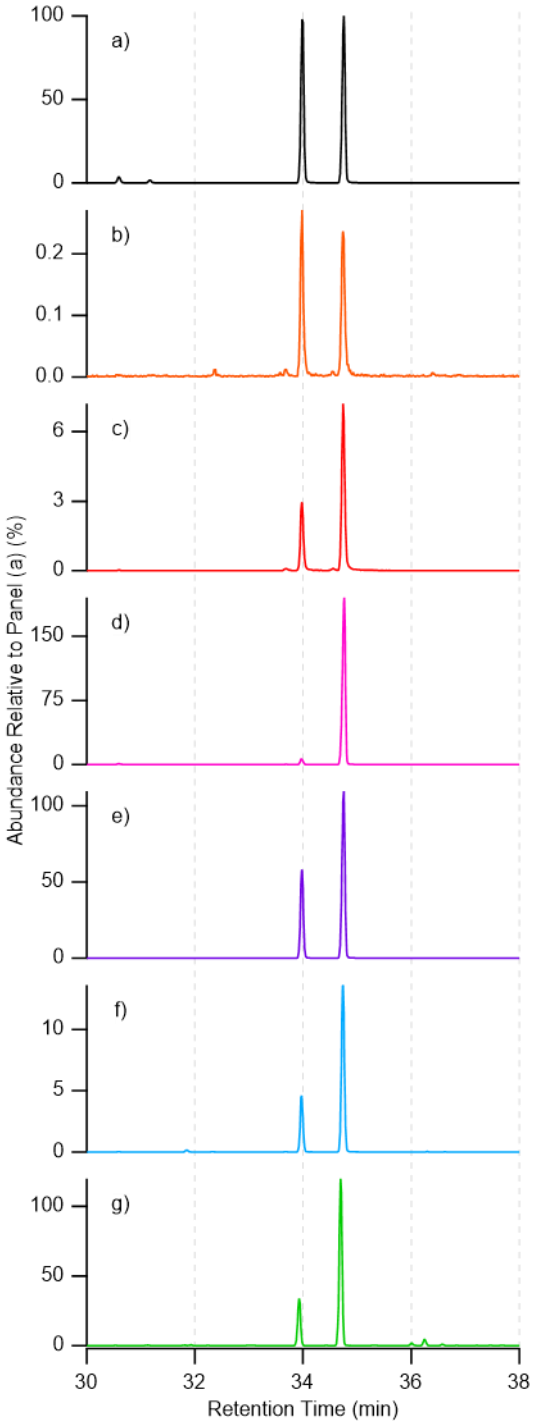


**Figure B6.** GC/EI-MS EICs of *m/z* 219 corresponding to 2-methyltetrols (RT = 34.0, 34.8 min) from: **a)** 50 µg $mL^{-1}$ standard of 2-methyltetrol; **b)** 50 µg $mL^{-1}$ standard of 2-methyltetrol sulfate; **c)** 50 µg $mL^{-1}$ standard of 3-methyltetrol sulfate; **d)** laboratory-generated β-IEPOX SOA; **e)** laboratory-generated δ-IEPOX SOA; **f)** $PM_{2.5}$ sample at Look Rock during 2013 SOAS campaign; **g)** $PM_{2.5}$ sample at Manaus in Nov. 2016. Note that the y-axis scale was adjusted to the highest peak in each panel, with the labelled abundance in percentage relative to that in Panel (a).

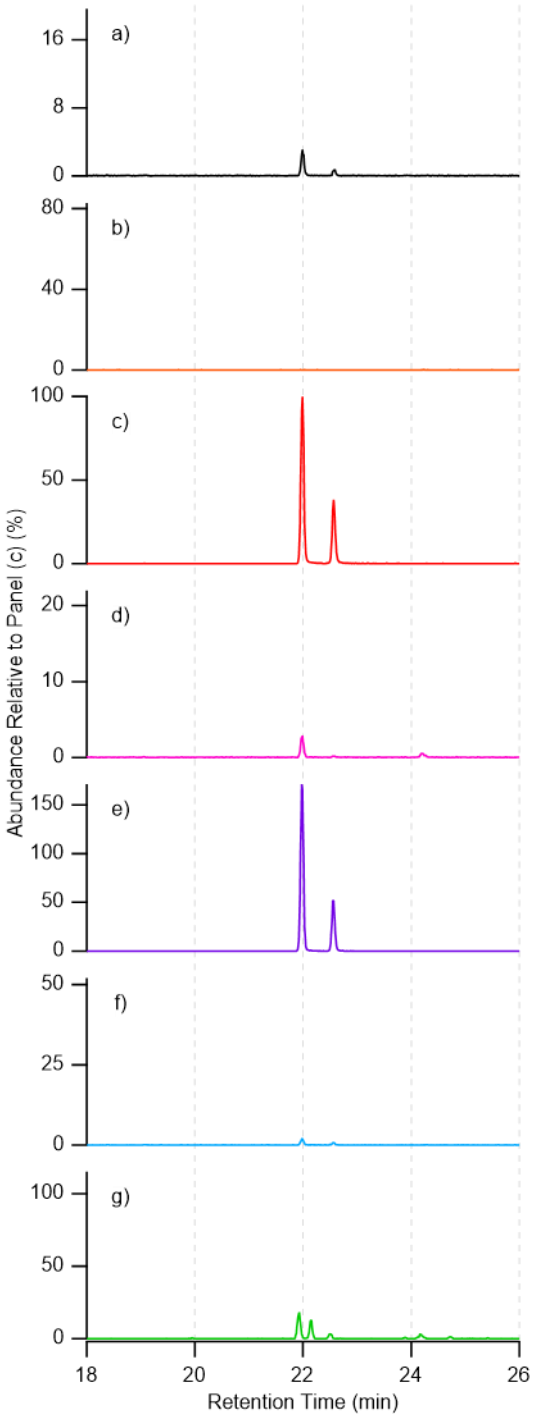


**Figure B7.** GC/EI-MS EICs of *m/z* 262 corresponding to 3-MeTHF-3,4-diols (RT = 22.0, 22.6 min) from: **a)** 50 µg $mL^{-1}$ standard of 2-methyltetrol; **b)** 50 µg $mL^{-1}$ standard of 2-methyltetrol sulfate; **c)** 50 µg $mL^{-1}$ standard of 3-methyltetrol sulfate; **d)** laboratory-generated β-IEPOX SOA; **e)** laboratory-generated δ-IEPOX SOA; **f)** $PM_{2.5}$ sample at Look Rock during 2013 SOAS campaign; **g)** $PM_{2.5}$ sample at Manaus in Nov. 2016. Note that the y-axis scale was adjusted to the highest peak in each panel, with the labelled abundance in percentage relative to that in Panel (c).

**2. Estimation of $C_5$-Alkene Triols, 2-Methyltetrols, and 3-MeTHF-3,4-diols Potentially Resulting from Thermal Degradation of Methyltetrol Sulfates**

As shown in Figure 3.5, a large amount of $C_5$-alkene triols was observed from the 2-methyltetrol sulfate standard using GC/EI-MS, while 2-methyltetrols (Figure B6) and 3-MeTHF-3,4-diols (Figure B7) were observed from the 3-methyltetrol sulfate standard. By running both methyltetrol sulfate standards from 0.25-50 μg $mL^{-1}$, we established a semi-quantitative relationship between the response of $C_5$-alkene triols (as well as 2-methyltetrols and 3-MeTHF-3,4-diols) produced and the concentrations of 2- (or 3-) methyltetrol sulfate standards prepared. For example, the response factor of $C_5$-alkene triols was determined to be 15301 peak area (in EIC of *m/z* 231 at 26.9, 27.9, and 28.3 min, see Figure 3.5) per 1 μg $mL^{-1}$ of 2-methyltetrol sulfate standard. In Table S2, 2-methyltetrol sulfate from the laboratory-generated SOA from β-IEPOX was measured using HILIC/ESI-HR-QTOFMS to be 1.773 μg $mL^{-1}$ in the 150 μL of solution after reconstitution. The solvent of reconstitution was 95:5 ACN/water for HILIC/ESI-HR-QTOFMS or 2:1 BSTFA (N,O-bis (trimethylsilyl) trifluoroacetamide + trimethylchlorosilane, 99:1, Supelco) /pyridine for GC/EI-MS. After correction for the 200-fold dilution, 2-methyltetrol sulfate was determined to be 355 μg $mL^{-1}$ as listed in the table. In another aliquot of the same filter extract, the response of $C_5$-alkene triols was back-calculated as a result of 1183 μg $mL^{-1}$ 2-methyltetrol sulfate, according to the semi-quantitative relationship described above, assuming the same yield of $C_5$-alkene triols from the 2-methyltetrol sulfate standard, since the standards and samples were analyzed in one GC/EI-MS sequence.

By doing this, as shown in Table B2, we attribute 30.0% (355 μg $mL^{-1}$/1183 μg $mL^{-1}$ = 30.0%), 42.8%, and 14.7% of the $C_5$-alkene triols to the potential thermal degradation of 2-

methyltetrol sulfate from the laboratory-generated SOA from β-IEPOX, the Look Rock, and the Manaus samples, respectively.

**Table B2.** Estimation of $C_5$-Alkene Triols due to Thermal Degradation of 2-Methyltetrol Sulfate

| | **2-Methyltetrol sulfate measured** | **$C_5$-Alkene triols attributed to 2-methyltetrol sulfate** | |
|---|---|---|---|
| | μg $mL^{-1}$ | μg $mL^{-1}$ | % |
| Lab. SOA from β-IEPOX | 355 [a] | 1183 | 30.0% |
| Look Rock, TN, USA | 58 | 136 | 42.8% |
| Manaus, Brazil | 175 | 1185 | 14.7% |

[a] The concentrations are converted to those in the 150-μL solution after reconstitution for the dried filter extract.

Similarly, the response factors of 2-methyltetrols and 3-MeTHF-3,4-diols were determined to be 5659 and 2169 peak area per 1 μg $mL^{-1}$ of 3-methyltetrol sulfate standard, respectively. Thus, as shown in Table B3, thermal degradation of 3-methyltetrol sulfate might result in 11.1% and over 100% (112.3%) of the 2-methyltetrols and 3-MeTHF-3,4-diols observed in the laboratory-generated SOA from δ-IEPOX.

**Table B3.** Estimation of 2-Methyltetrols and 3-MeTHF-3,4-diols due to Thermal Degradation of 3-Methyltetrol Sulfate

| | **3-Methyltetrol sulfate measured** | **2-Methyltetrols attributed to 3-methyltetrol sulfate** | | **3-MeTHF-3,4-diols attributed to 3-methyltetrol sulfate** | |
|---|---|---|---|---|---|
| | μg $mL^{-1}$ | μg $mL^{-1}$ | % | μg $mL^{-1}$ | % |
| Lab. SOA from δ-IEPOX | 361 [a] | 3247 | 11.1% | 322 | 112.3% |

[a] The concentrations are converted to those in the 150-μL solution after reconstitution for the dried filter extracts.

**3. Analytical Uncertainty**

The overall analytical uncertainty, $\%e_T$, in our quantification was calculated using the equation below[2].

$$\%e_T = \sqrt{\%e_1^2 + \%e_2^2 + \cdots + \%e_n^2}$$

When most the (n) relative errors reasonably applied, $\%e_T$ = ±17.2%. The relative errors are estimated for:

1. Purity of standards and potential degradation over time - ~5%, estimated by the internal standard from $^1$H NMR and repeated measurements for the same stock standard;
2. Air sampling rate of the filter and PILS samplers - ~0.7%, estimated by repeated measurements for the same condition;
3. Water flow rate of PILS wash flow - ~6%, estimated by repeated measurements for the same condition;
4. Extraction efficiency (filter) - ~1%, the recovery rate of filter extraction using a larger piece of quartz filter (4 cm × 5 cm, rather than the 47-mm diameter) was determined to be 76.2 ± 0.8 % (for the methyltetrol sulfate standards), but we didn't correct for recovery;
5. Collection efficiency (PILS) - ~2%, reported by BMI and examined by comparing the PILS-IC and SEMS-MCPC measurements;
6. Dilution of samples (when needed) - ~1% estimated by the errors caused by transferring liquids;
7. SEMS-MCPC measurement - ~5%;
8. Density of IEPOX-SOA particles: ~1%;
9. Q-TOF detection - 2%, estimated by relative standard deviation from repeated injections;
10. GC/EI-MS - 2%, estimated by relative standard deviation from repeated injections;
11. Data processing - ~15%, this varies by manual integration of chromatographic peak area, selection of linear range of calibration curve, selection of standard for quantification.

## Reference

(1) Riva, M.; Bell, D. M.; Hansen, A.-M.; Drozd, G. T.; Zhang, Z.; Gold, A.; Imre, D.; Surratt, J. D.; Glasius, M.; Zelenyuk, A. Effect of Organic Coatings, Humidity and Aerosol Acidity on Multiphase Chemistry of Isoprene Epoxydiols. *Environ. Sci. Technol.*, 2016, 5580–8, 50 (11).

(2) A. P. S. Hettiyadura, T. Jayarathne, K. Baumann, A. H. Goldstein, J. A. de Gouw, A. Koss, F. N. Keutsch, K. Skog, and E. A. Stone, Qualitative and quantitative analysis of atmospheric organosulfates in Centreville, Alabama, *Atmos. Chem. Phys*., 2017, 17, 1343–1359.

# APPENDIX C: SUPPLEMENTARY INFORMATION FOR "CHEMICAL COMPOSITION OF BROWN CARBON AEROSOL FROM PRIMARY AND PHOTOCHEMICALLY-AGED LABORATORY-SIMULATED WESTERN US WILDFIRE EMISSIONS"

**Table C1.** List of prepared authentic standards for UPLC/(DAD)-ESI-HR-QTOFMS and GC/EI-MS.

| #[a] | Prepared Standard | Molecular Formula | Manufacturer | Purity | RT | Exact Mass | Measured Mass | Diff.[b] | Major Fragments | Linear Range | $R^2$ | Res. Factor[c] |
|---|---|---|---|---|---|---|---|---|---|---|---|---|
| | | | | ≥ | min | m/z | m/z | ppm | m/z | μg $mL^{-1}$ | | |
| 1 | 2-Nitrophenol | C6H5NO3 | Sigma-Aldrich | 98% | 10.96, 11.7 | 138.0197 | 138.0200 | 2.2 | 108, 46, 92 | 0.0125-62.5 | 1.0000 | 1.3E+05 |
| 2 | Vanillin | C8H8O3 | Sigma-Aldrich | 99% | 9.93 | 151.0401 | 151.0403 | 1.3 | 136, 92, 108 | 0.01-10 | 1.0000 | 1.2E+06 |
| 3 | 4-Nitro-o-cresol | C7H7NO3 | TCI America | 98% | 11.85 | 152.0353 | 152.0352 | -0.7 | 122, 46, 106 | 0.0025-1 | 0.9855 | 6.7E+06 |
| 4 | Acetovanillone | C9H10O3 | Sigma-Aldrich | 98% | 10.36 | 165.0557 | 165.0558 | 0.6 | 150, 122 | 0.1-100 | 0.9641 | 5.0E+05 |
| 5 | 4-Methyl-5-nitrocatechol | C7H6NO4 | Toronto Research Chem. | 95% | 9.3 | 168.0297 | 168.0305 | 4.8 | 137, 138, 109, 66, 46 | 0.0025-1 | 0.9946 | 1.7E+07 |
| 6 | Coniferyl aldehyde | C10H9O3 | Sigma-Aldrich | 98% | 9.18 | 177.0552 | 177.0559 | 4.0 | 162, 134 | 0.0025-10 | 0.9995 | 1.1E+06 |
| 7 | 4-Nitro-1-naphthol | C10H7NO3 | TCI America | 98% | 12.8 | 188.0353 | 188.0354 | 0.5 | 158, 142, 46 | 0.01-25 | 0.9813 | 7.4E+06 |
| 8 | Sinapic acid | C11H12O5 | Sigma-Aldrich | 98% | 10.44 | 223.0612 | 223.0608 | -1.8 | 193, 149, 121, 164, 93, 163 | 0.01-12.5 | 0.9982 | 6.7E+05 |
| i.s. | Camphor-10-sulfonic acid | C10H16O4S | Sigma-Aldrich | 98% | 10.52 | 231.0697 | 231.0705 | 3.5 | - | 0.1-100 | 0.9882 | 6.4E+06 |
| i.s. GC | Ketopinic acid | C10H14O3 | Sigma-Aldrich | 99% | 11.23 | 181.0870 | 181.0870 | 0.0 | - | 0.0125-12.5 | 0.9937 | 7.7E+05 |
| GC | Levoglucosan | C6H10O5 | Sigma-Aldrich | 99% | 36.6 | - | - | - | 219 | 1-500 | 0.9989 | 2.2E+04 |
| GC | Mannosan | C6H10O5 | Sigma-Aldrich | 98% | 35.6 | - | - | - | 219 | 2.5-500 | 0.9975 | 1.9E+04 |

[a] As denoted, camphor-10-sulfonic acid and ketopinic acid were prepared as internal standards (i.s.) for UPLC/(DAD)-ESI-HR-QTOFMS, ketopinic acid was also prepared as an internal standard for GC/EI-MS (GC). Levoglucosan and mannosan were used as external standards for GC/EI-MS.

[b] "Diff." is the mass difference between the exact mass and measured mass.

[c] "Res. Factor" is the response factor of each standard determined with UPLC/(DAD)-ESI-HR-QTOFMS (or GC/EI-MS for levoglucosan and mannosan), defined as integrated peak area (on extracted ion chromatogram) per unit concentration of standard.

**Table C2.** List of all seven smog chamber experiments for photochemical aging of primary biomass burning emissions.

| Fire # | Fuel Description | Net WSOC Growth (ppb C) | Time Profile Shown in | Identified BBOA Shown in |
|---|---|---|---|---|
| 97 | Longleaf pine | ~35 | Figure 4.2 | Figure 4.3, Table C2 |
| 83 | Engelmann spruce | ~25 | Figure C8-A | Figure C10-A |
| 91 | Chaparral (manzanita) - canopy | ~25 | Figure C8-B | Figure C10-B |
| 99 | Cow dung, Montana | ~25 | Figure C8-C | Figure C10-C |
| 87 | Lodgepole pine - canopy | ~0 | Figure C8-D | Figure C10-D |
| 101 | Ponderosa pine - rotten log | ~10 | Figure C8-E | Figure C10-E |
| 105 | Ponderosa pine - rotten log | ~5 | Figure C8-F | Figure C10-F |

**Table C3.** List of 29 BBOA species formed or enhanced during photooxidation from the smog chamber experiment (Fire #97, Longleaf pine). The suggest formulas of nitro-aromatics (with number of N from 1-3, DBE from 5-10) are highlighted in bold.

| m/z | RT | Fold Change | Abundance (Aged) | Suggested Formula | DBE | Mass Diff. (ppm) | Tentatively Identified as |
|---|---|---|---|---|---|---|---|
| 152.0354 | 10.84 | 42.90 | 2.3E+05 | **C7H7NO3** | 5 | -0.4 | Methylnitrophenol |
| 121.0296 | 9.79 | 29.68 | 4.0E+05 | C7H6O2 | 5 | 1.01 | Benzoic acid |
| 309.0368 | 10.25 | 17.94 | 1.4E+05 | **C12H10N2O8** | 9 | -2.88 | - |
| 168.0304 | 10.05 | 13.83 | 1.5E+05 | **C7H7NO4** | 5 | -2.2 | Methyl nitrocatechol |
| 198.0408 | 8.98 | 12.46 | 1.3E+05 | **C8H9NO5** | 5 | -4.37 | Dimethylnitrobenzenetriol |
| 154.0144 | 10.25 | 11.33 | 1.1E+07 | **C6H5NO4** | 5 | -2.05 | Nitrocatechol |
| 155.9935 | 8.07 | 11.18 | 1.5E+05 | **C5H3NO5** | 5 | -8.8 | 5-Nitrofuroic acid |
| 230.0463 | 12.48 | 9.93 | 1.3E+05 | **C12H9NO4** | 9 | -0.35 | - |
| 124.0163 | 10.25 | 9.68 | 1.3E+05 | **C4H3N3O2** | 5 | -10.82 | - |
| 152.0355 | 12.21 | 9.20 | 1.9E+05 | **C7H7NO3** | 5 | -0.01 | Methylnitrophenol |
| 94.98114 | 1.65 | 8.12 | 2.6E+05 | CH4O3S | 0 | -1.45 | Methanesulfonic acid |
| 182.0096 | 6.92 | 7.96 | 8.6E+04 | **C7H5NO5** | 6 | -12.67 | Hydroxynitrobenzoic acid |
| 182.0099 | 11.99 | 7.96 | 4.1E+05 | **C7H5NO5** | 6 | -2.54 | Hydroxynitrobenzoic acid |
| 224.0564 | 11.01 | 6.24 | 7.0E+04 | **C10H11NO5** | 6 | 0.08 | - |
| 228.0309 | 13.16 | 4.96 | 6.7E+04 | **C12H7NO4** | 10 | -2.31 | - |
| 214.8801 | 1.93 | 4.75 | 4.4E+04 | - | - | - | - |
| 326.9693 | 10.30 | 4.50 | 3.0E+04 | - | - | - | - |
| 138.0208 | 11.18 | 4.30 | 8.4E+05 | **C6H5NO3** | 5 | -2.48 | 2-Nitrophenol |
| 178.0151 | 11.75 | 3.39 | 3.6E+04 | **C8H5NO4** | 7 | -0.63 | - |
| 471.1319 | 11.24 | 3.36 | 1.2E+05 | C24H24O10 | 13 | 0.19 | - |
| 241.0023 | 2.59 | 3.35 | 1.1E+05 | C9H6O8 | 7 | -10.72 | - |
| 579.1934 | 11.23 | 3.34 | 1.1E+05 | - | - | - | - |
| 237.0767 | 11.22 | 2.87 | 3.4E+06 | C12H14O5 | 6 | -0.65 | Trimethoxycinnamic acid |
| 419.1564 | 11.21 | 2.85 | 2.2E+05 | C18H28O11 | 5 | -1.54 | - |
| 165.0192 | 10.88 | 2.24 | 3.5E+05 | C8H6O4 | 6 | 2.33 | Benzenedioic acid |
| 165.0192 | 9.60 | 2.18 | 7.5E+05 | C8H6O4 | 6 | 1.72 | Benzenedioic acid |
| 168.0302 | 11.78 | 1.77 | 1.8E+06 | **C7H7NO4** | 5 | -0.4 | Methyl nitrocatechol |
| 168.0302 | 11.23 | 1.76 | 2.4E+06 | **C7H7NO4** | 5 | -0.42 | Methyl nitrocatechol |
| 404.1044 | 1.97 | 1.65 | 9.4E+04 | C12H23NO14 | 2 | -0.72 | - |

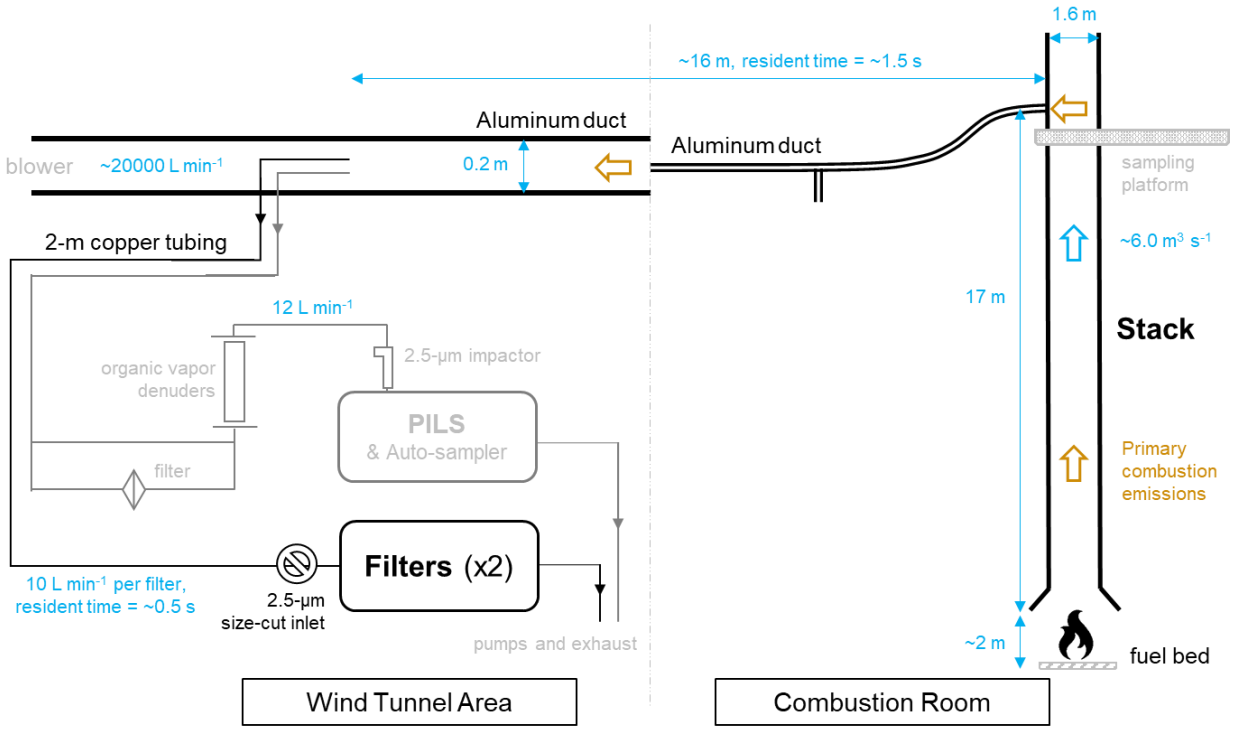


**Figure C1.** Sample collection and primary emission delivery from "Stack Burns". The sample flow direction is indicated by the brown arrows. Air flow rates, dimensions, and resident times are denoted in light blue texts.

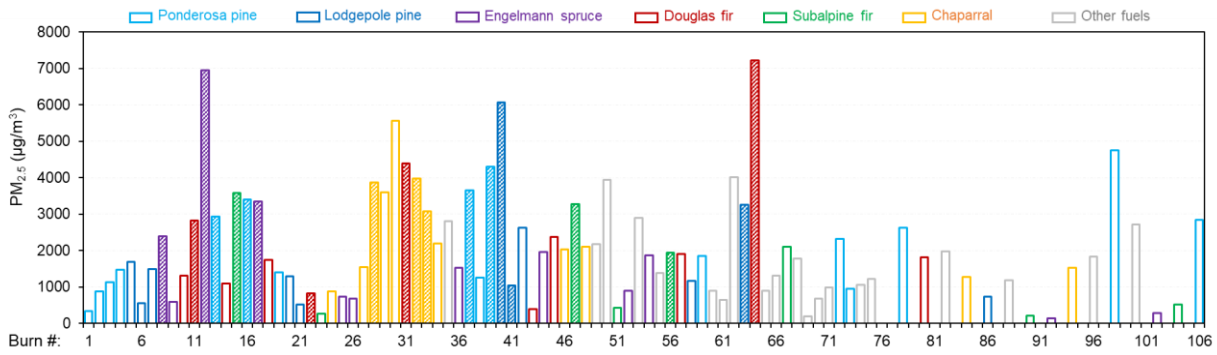


**Figure C2.** $PM_{2.5}$ concentrations from the 75 "Stack Burns" and 15 "Room Burns". $PM_{2.5}$ mass concentration (µg $m^{-3}$, on the y-axis) was determined by weighing the filters using a sensitive electronic balance and then divided by the total sampled air volume. The six most commonly burned fuels are marked in colors as indicated in the legend on top. The 20 selected burns primary emissions are highlighted with patterned fill.

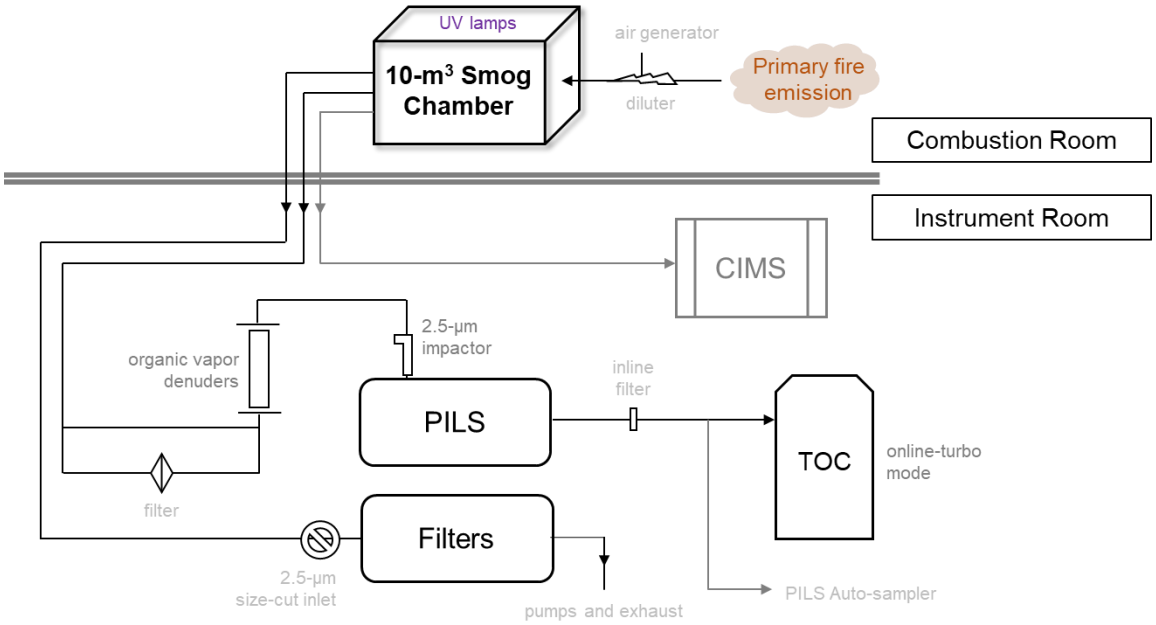


**Figure C3.** Instrumentation for photochemical aging of primary combustion emissions.

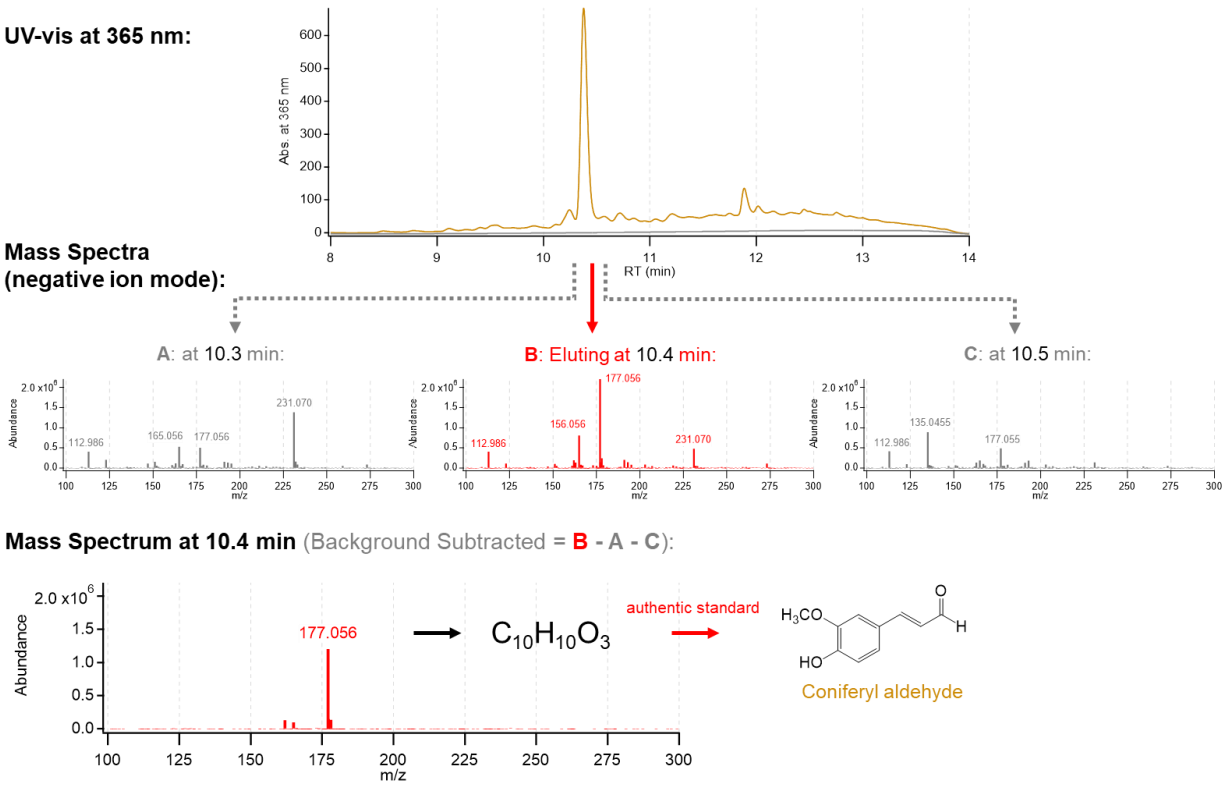


**Figure C4.** Coniferyl aldehyde as an example of BrC identified using UPLC/ESI-(DAD)-HR-QTOFMS with detected light absorption at 365 nm from the rotten log of Douglas fir (DF-RL). The general processes include peak detection aligned on UV-vis and ion chromatograms, background subtraction of mass spectra, and formula assignment and BrC identification assisted with accurate *m/z*, MS/MS fragments, relative abundance of isotopic peaks, possible numbers of elements and DBE, hydrophilicity (or water-solubility) indicated by retention time (RT), and previous literature.

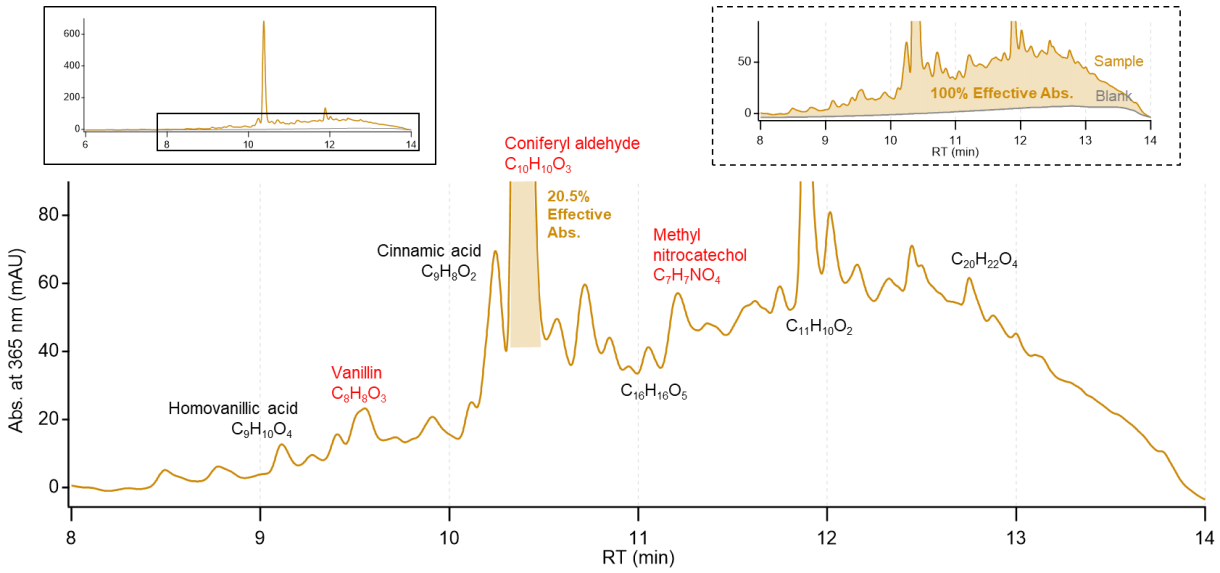


**Figure C5.** Molecular BrC identified on UV-vis (365 nm) chromatogram and contribution of coniferyl aldehyde to total effective absorbance from the rotten log of Douglas fir (DF-RL). Three BrC identified using authentic standards are highlighted in red texts. The full UV-vis chromatogram was shown in the upper left insert. The total effective absorbance determined by UPLC/DAD was defined as the absorbance from the filter sample minus that from the field blank filter, as demonstrated in the upper right insert.

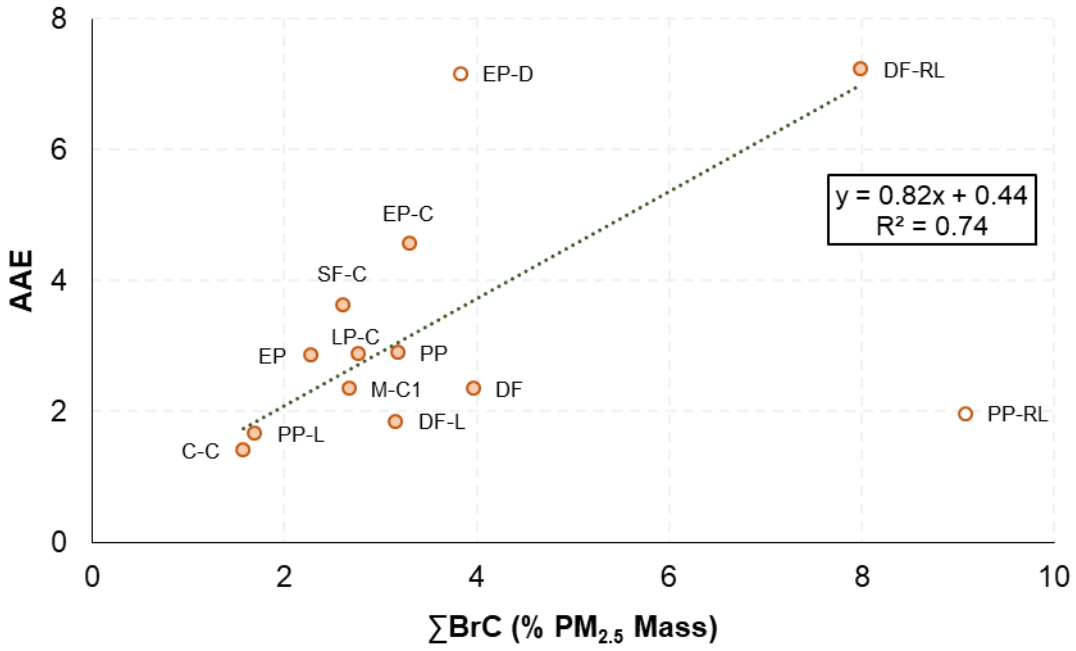


**Figure C6.** Correlation of the summed BrC (∑BrC) with Ångström absorption exponents (AAE) from 11 out of the 20 selected "Stack Burns". AAE from the "Stack Burns" before #31 was obtained from Selimovic et al.[239] and after #32 from Li et al.,[240] if available. Note that there are two outliers (EP-D and PP-RL) excluded from the correlation.

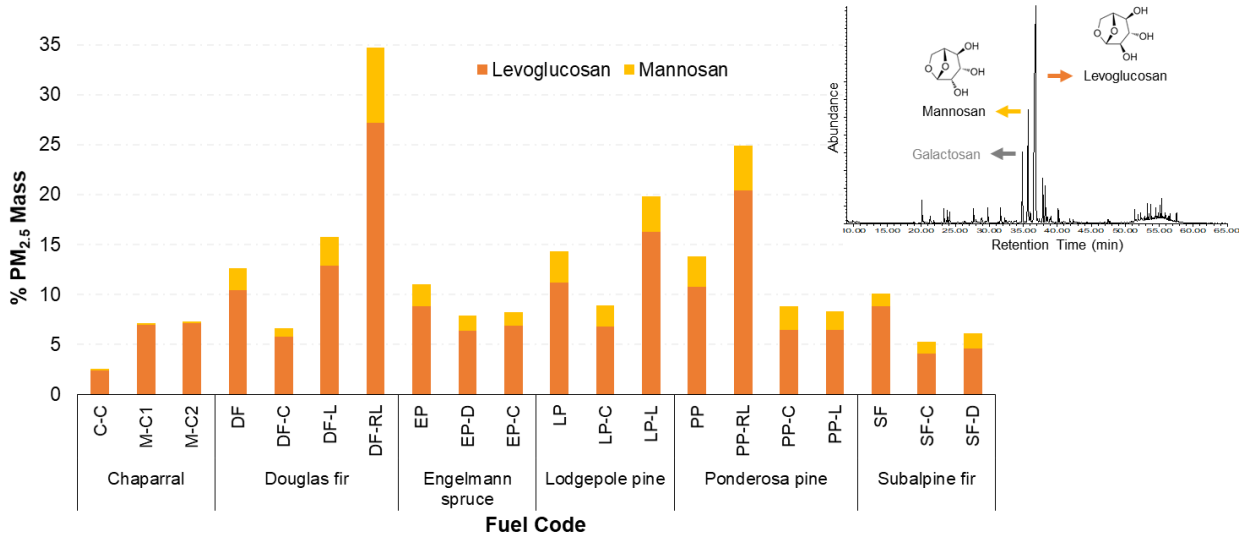


**Figure C7.** Levoglucosan and mannosan quantified as % of collected $PM_{2.5}$ mass by GC/EI-MS using authentic standards. Insert: a GC/EI-MS total ion chromatogram (TIC) from the rotten log of Douglas fir (DF-RL) shows the 1st, 2nd, and 3rd largest peaks on the TIC being levoglucosan, mannosan, and galactosan ($C_6H_{10}O_5$).

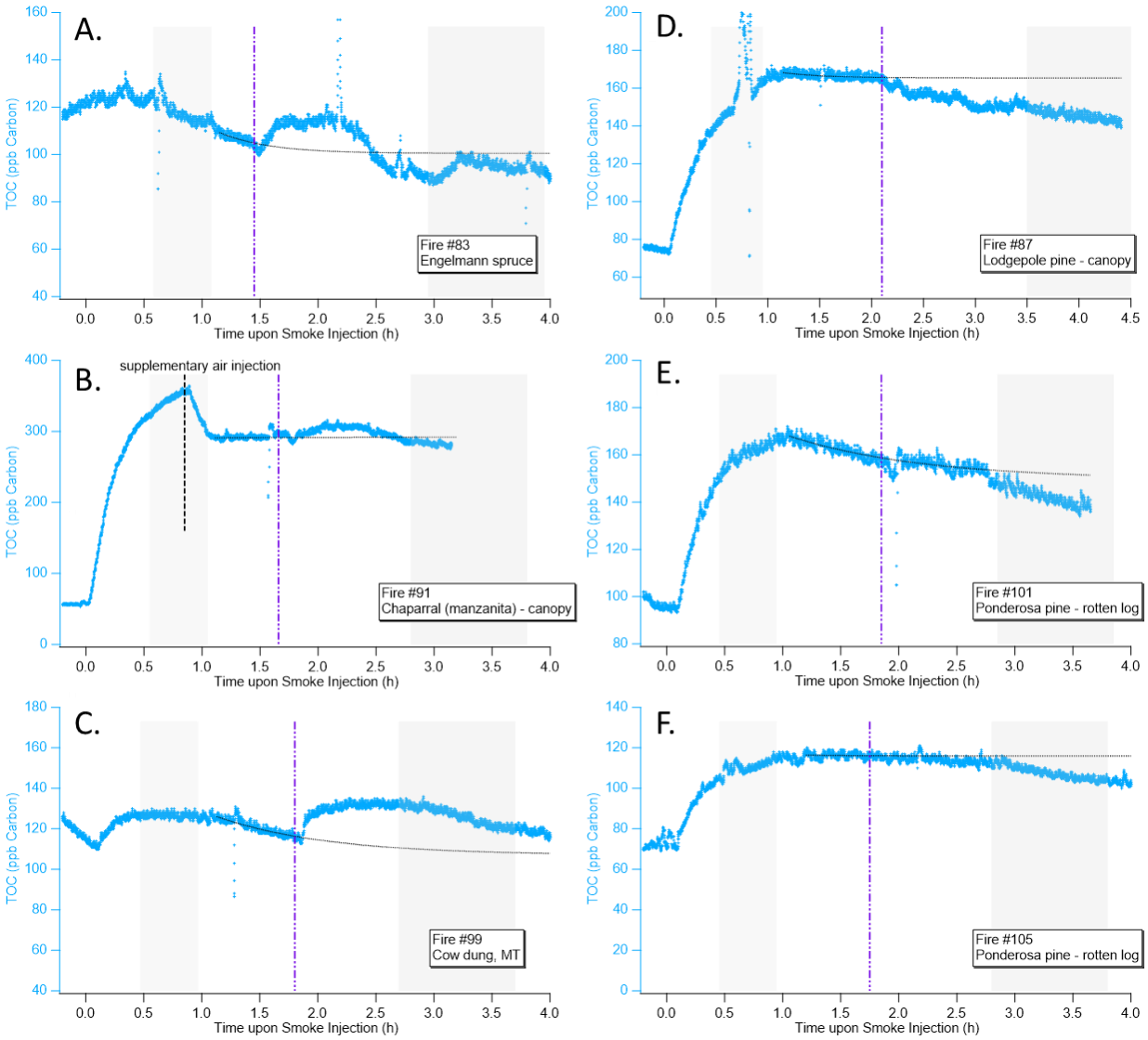


**Figure C8.** Time profile of six smog chamber experiments, with the fire # and fuel type shown in the text box in each panel (A.-F.).Water-soluble particulate organic carbon was monitored by PILS-TOC in real-time over the course of experiment and plotted as the light blue markers to the left y-axis. The dashed curve from ~1.0 h indicates the decay rate of particles. The vertical pruple dashed line indicates when the UV lamps were turned on. Two sets of filter samples were collected for the "fresh" and "aged" smoke.

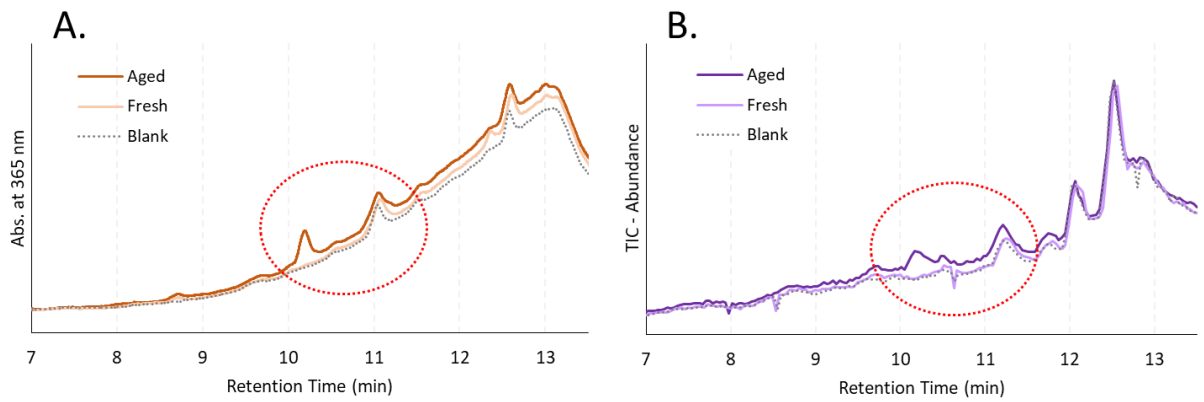


**Figure C9.** (A.) UV-vis absorbance at 365 nm from UPLC/DAD and (B.) total ion chromatogram (TIC, from UPLC/ESI-HR-QTOFMS) from $PM_{2.5}$ collected "fresh" and photochemically-aged emissions from the combustion of Longleaf pine. The red dash-lined circles highlight the elevated signals in both chromatograms from 10.1-11.2 min, likely caused by BrC formed or enhanced through photooxidation of the "fresh" emissions.

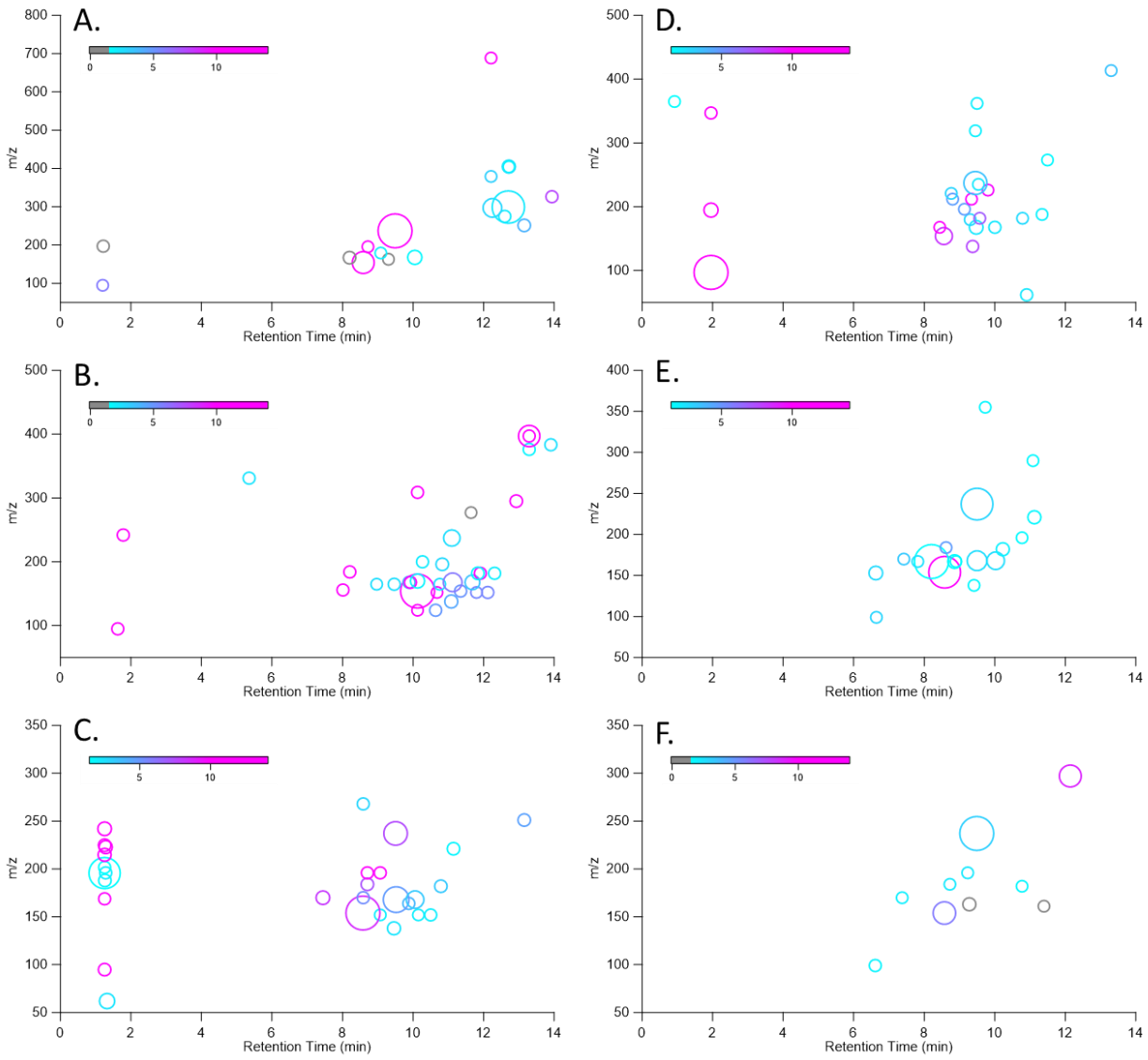


**Figure C10.** BBOA constituents formed/enhanced (or reduced) during photochemistry from the six additional smog chamber experiments. The panel code (A.-F.) is corresponding to the same experiment (from Fire #83, 91, 99, 87, 101, 105, respectively) in Table C3 and Figure C8. Size of the circle (area) is proportional to the ion intensity (integrated peak area). Color of the circles reflect the fold change of the ion response from the aged sample over that from the "fresh" sample, ranging from 1.5 (light blue) to 10 and greater (pink). In the panels A., B., and F., BBOA constituents reduced (by at least 30%, or fold change < 0.7) were indicated by the grey circles.

## REFERENCES


(1) Pöschl, U. Atmospheric Aerosols: Composition, Transformation, Climate and Health Effects. *Angew. Chemie Int. Ed.* **2005**, *44* (46), 7520–7540.

(2) Jacobson, M. Z. Strong Radiative Heating Due to the Mixing State of Black Carbon in Atmospheric Aerosols. *Nature* **2001**, *409* (6821), 695–697.

(3) Charlson, R. J.; Schwartz, S. E.; Hales, J. M.; Cess, R. D.; Coakley, J. A.; Hansen, J. E.; Hofmann, D. J. Climate Forcing by Anthropogenic Aerosols. *Science* **1992**, *255* (5043), 423–430.

(4) Dockery, D. W.; Pope, C. A.; Xu, X.; Spengler, J. D.; Ware, J. H.; Fay, M. E.; Ferris, B. G.; Speizer, F. E. An Association between Air Pollution and Mortality in Six U.S. Cities. *N. Engl. J. Med.* **1993**, *329* (24), 1753–1759.

(5) Pope, C. A.; Burnett, R. T.; Thurston, G. D.; Thun, M. J.; Calle, E. E.; Krewski, D.; Godleski, J. J. Cardiovascular Mortality and Long-Term Exposure to Particulate Air Pollution. *Circulation* **2004**, *109* (1), 71–77.

(6) Katsouyanni, K.; Touloumi, G.; Samoli, E.; Gryparis, A.; Le Tertre, A.; Monopolis, Y.; Rossi, G.; Zmirou, D.; Ballester, F.; Boumghar, A.; et al. Confounding and Effect Modification in the Short-Term Effects of Ambient Particles on Total Mortality: Results from 29 European Cities within the APHEA2 Project. *Epidemiology* **2001**, *12* (5), 521–531.

(7) Gauderman, W. J.; Vora, H.; McConnell, R.; Berhane, K.; Gilliland, F.; Thomas, D.; Lurmann, F.; Avol, E.; Kunzli, N.; Jerrett, M.; et al. Effect of Exposure to Traffic on Lung Development from 10 to 18 Years of Age: A Cohort Study. *Lancet* **2007**, *369* (9561), 571–577.

(8) Jimenez, J. L.; Canagaratna, M. R.; Donahue, N. M.; Prevot, A. S. H.; Zhang, Q.; Kroll, J. H.; DeCarlo, P. F.; Allan, J. D.; Coe, H.; Ng, N. L.; et al. Evolution of Organic Aerosols in the Atmosphere. *Science* **2009**, *326* (5959), 1525–1529.

(9) Seinfeld, J. H.; Pankow, J. F. Organic Atmospheric Particulate Material. *Annu. Rev. Phys. Chem.* **2003**, *54* (1), 121–140.

(10) Andreae, M. O.; Crutzen, P. J. Atmospheric Aerosols: Biogeochemical Sources and Role in Atmospheric Chemistry. *Science* **1997**, *276* (5315), 1052–1058.

(11) Kanakidou, M.; Seinfeld, J. H.; Pandis, S. N.; Barnes, I.; Dentener, F. J.; Facchini, M. C.; van Dingenen, R.; Ervens, B.; Nenes, A.; Nielsen, C. J.; et al. Organic Aerosol and Global Climate Modelling: A Review. *Atmos. Chem. Phys. Discuss.* **2004**, *4* (5), 5855–6024.

(12) Kroll, J. H.; Seinfeld, J. H. Chemistry of Secondary Organic Aerosol: Formation and Evolution of Low-Volatility Organics in the Atmosphere. *Atmos. Environ.* **2008**, *42* (16), 3593–3624.

(13) Turpin, B. J.; Huntzicker, J. J. Identification of Secondary Organic Aerosol Episodes and Quantitation of Primary and Secondary Organic Aerosol Concentrations during SCAQS. *Atmos. Environ.* **1995**, *29* (23), 3527–3544.

(14) Sullivan, A. P.; Peltier, R. E.; Brock, C. A.; de Gouw, J. A.; Holloway, J. S.; Warneke, C.; Wollny, A. G.; Weber, R. J. Airborne Measurements of Carbonaceous Aerosol Soluble in Water over Northeastern United States: Method Development and an Investigation into Water-Soluble Organic Carbon Sources. *J. Geophys. Res. Atmos.* **2006**, *111* (D23), n/a-n/a.

(15) Zhang, Q.; Jimenez, J. L.; Canagaratna, M. R.; Allan, J. D.; Coe, H.; Ulbrich, I.; Alfarra, M. R.; Takami, A.; Middlebrook, A. M.; Sun, Y. L.; et al. Ubiquity and Dominance of Oxygenated Species in Organic Aerosols in Anthropogenically-Influenced Northern Hemisphere Midlatitudes. *Geophys. Res. Lett.* **2007**, *34* (13), n/a-n/a.

(16) Zhang, Q.; Worsnop, D. R.; Canagaratna, M. R.; Jimenez, J. L. Hydrocarbon-like and Oxygenated Organic Aerosols in Pittsburgh: Insights into Sources and Processes of Organic Aerosols. *Atmos. Chem. Phys.* **2005**, *5* (12), 3289–3311.

(17) Baltensperger, U.; Kalberer, M.; Dommen, J.; Paulsen, D.; Alfarra, M. R.; Coe, H.; Fisseha, R.; Gascho, A.; Gysel, M.; Nyeki, S.; et al. Secondary Organic Aerosols from Anthropogenic and Biogenic Precursors. *Faraday Discuss.* **2005**, *130*, 265.

(18) Hallquist, M.; Wenger, J. C.; Baltensperger, U.; Rudich, Y.; Simpson, D.; Claeys, M.; Dommen, J.; Donahue, N. M.; George, C.; Goldstein, A. H.; et al. The Formation, Properties and Impact of Secondary Organic Aerosol: Current and Emerging Issues. *Atmos. Chem. Phys.* **2009**, *9* (14), 5155–5236.

(19) Claeys, M. Formation of Secondary Organic Aerosols Through Photooxidation of Isoprene. *Science* **2004**, *303* (5661), 1173–1176.

(20) Kroll, J. H.; Ng, N. L.; Murphy, S. M.; Flagan, R. C.; Seinfeld, J. H. Secondary Organic Aerosol Formation from Isoprene Photooxidation. *Environ. Sci. Technol.* **2006**, *40* (6), 1869–1877.

(21) Kleindienst, T. E.; Edney, E. O.; Lewandowski, M.; Offenberg, J. H.; Jaoui, M. Secondary Organic Carbon and Aerosol Yields from the Irradiations of Isoprene and α-Pinene in the Presence of NO x and SO 2. *Environ. Sci. Technol.* **2006**, *40* (12), 3807–3812.

(22) Edney, E. O.; Kleindienst, T. E.; Jaoui, M.; Lewandowski, M.; Offenberg, J. H.; Wang, W.; Claeys, M. Formation of 2-Methyl Tetrols and 2-Methylglyceric Acid in Secondary Organic Aerosol from Laboratory Irradiated Isoprene/NOX/SO2/Air Mixtures and Their Detection in Ambient PM2.5 Samples Collected in the Eastern United States. *Atmos. Environ.* **2005**, *39* (29), 5281–5289.

(23) Larsen, B. R.; Di Bella, D.; Glasius, M.; Winterhalter, R.; Jensen, N. R.; Hjorth, J. Gas-Phase OH Oxidation of Monoterpenes: Gaseous and Particulate Products. *J. Atmos. Chem.* **2001**, *38* (3), 231–276.

(24) Jaoui, M.; Kamens, R. M. Gaseous and Particulate Oxidation Products Analysis of a Mixture of α-Pinene + β-Pinene/O3/Air in the Absence of Light and α-Pinene + β-Pinene/NOx/Air in the Presence of Natural Sunlight. *J. Atmos. Chem.* **2003**, *44* (3), 259–297.

(25) Guenther, A.; Karl, T.; Harley, P.; Wiedinmyer, C.; Palmer, P. I.; Geron, C. Estimates of Global Terrestrial Isoprene Emissions Using MEGAN (Model of Emissions of Gases and Aerosols from Nature). *Atmos. Chem. Phys.* **2006**, *6* (11), 3181–3210.

(26) Budisulistiorini, S. H.; Canagaratna, M. R.; Croteau, P. L.; Marth, W. J.; Baumann, K.; Edgerton, E. S.; Shaw, S. L.; Knipping, E. M.; Worsnop, D. R.; Jayne, J. T.; et al. Real-Time Continuous Characterization of Secondary Organic Aerosol Derived from Isoprene Epoxydiols in Downtown Atlanta, Georgia, Using the Aerodyne Aerosol Chemical Speciation Monitor. *Environ. Sci. Technol.* **2013**, *47* (11), 5686–5694.

(27) Chameides, W.; Lindsay, R.; Richardson, J.; Kiang, C. The Role of Biogenic Hydrocarbons in Urban Photochemical Smog: Atlanta as a Case Study. *Science* **1988**, *241* (4872), 1473–1475.

(28) Surratt, J. D.; Murphy, S. M.; Kroll, J. H.; Ng, N. L.; Hildebrandt, L.; Sorooshian, A.; Szmigielski, R.; Vermeylen, R.; Maenhaut, W.; Claeys, M.; et al. Chemical Composition of Secondary Organic Aerosol Formed from the Photooxidation of Isoprene. *J. Phys. Chem. A* **2006**, *110* (31), 9665–9690.

(29) Lin, Y.-H.; Zhang, Z.; Docherty, K. S.; Zhang, H.; Budisulistiorini, S. H.; Rubitschun, C. L.; Shaw, S. L.; Knipping, E. M.; Edgerton, E. S.; Kleindienst, T. E.; et al. Isoprene Epoxydiols as Precursors to Secondary Organic Aerosol Formation: Acid-Catalyzed Reactive Uptake Studies with Authentic Compounds. *Environ. Sci. Technol.* **2012**, *46* (1), 250–258.

(30) Lin, Y.-H.; Zhang, H.; Pye, H. O. T.; Zhang, Z.; Marth, W. J.; Park, S.; Arashiro, M.; Cui, T.; Budisulistiorini, S. H.; Sexton, K. G.; et al. Epoxide as a Precursor to Secondary Organic Aerosol Formation from Isoprene Photooxidation in the Presence of Nitrogen Oxides. *Proc. Natl. Acad. Sci.* **2013**, *110* (17), 6718–6723.

(31) Budisulistiorini, S. H.; Li, X.; Bairai, S. T.; Renfro, J.; Liu, Y.; Liu, Y. J.; McKinney, K. A.; Martin, S. T.; McNeill, V. F.; Pye, H. O. T.; et al. Examining the Effects of Anthropogenic Emissions on Isoprene-Derived Secondary Organic Aerosol Formation during the 2013 Southern Oxidant and Aerosol Study (SOAS) at the Look Rock, Tennessee Ground Site. *Atmos. Chem. Phys.* **2015**, *15* (15), 8871–8888.

(32) Budisulistiorini, S. H.; Baumann, K.; Edgerton, E. S.; Bairai, S. T.; Mueller, S.; Shaw, S. L.; Knipping, E. M.; Gold, A.; Surratt, J. D. Seasonal Characterization of Submicron Aerosol Chemical Composition and Organic Aerosol Sources in the Southeastern United States: Atlanta, Georgia,and Look Rock, Tennessee. *Atmos. Chem. Phys.* **2016**, *16* (8), 5171–5189.

(33) Rattanavaraha, W.; Chu, K.; Budisulistiorini, S. H.; Riva, M.; Lin, Y.-H.; Edgerton, E. S.; Baumann, K.; Shaw, S. L.; Guo, H.; King, L.; et al. Assessing the Impact of Anthropogenic Pollution on Isoprene-Derived Secondary Organic Aerosol Formation in PM2.5 Collected from the Birmingham, Alabama, Ground Site during the 2013 Southern Oxidant and Aerosol Study. *Atmos. Chem. Phys.* **2016**, *16* (8), 4897–4914.

(34) Paulot, F.; Crounse, J. D.; Kjaergaard, H. G.; Kurten, A.; St. Clair, J. M.; Seinfeld, J. H.; Wennberg, P. O. Unexpected Epoxide Formation in the Gas-Phase Photooxidation of Isoprene. *Science* **2009**, *325* (5941), 730–733.

(35) Bates, K. H.; Crounse, J. D.; St. Clair, J. M.; Bennett, N. B.; Nguyen, T. B.; Seinfeld, J. H.; Stoltz, B. M.; Wennberg, P. O. Gas Phase Production and Loss of Isoprene Epoxydiols. *J. Phys. Chem. A* **2014**, *118* (7), 1237–1246.

(36) Wang, W.; Kourtchev, I.; Graham, B.; Cafmeyer, J.; Maenhaut, W.; Claeys, M. Characterization of Oxygenated Derivatives of Isoprene Related to 2-Methyltetrols in Amazonian Aerosols Using Trimethylsilylation and Gas Chromatography/Ion Trap Mass Spectrometry. *Rapid Commun. Mass Spectrom.* **2005**, *19* (10), 1343–1351.

(37) Surratt, J. D.; Chan, A. W. H.; Eddingsaas, N. C.; Chan, M.; Loza, C. L.; Kwan, A. J.; Hersey, S. P.; Flagan, R. C.; Wennberg, P. O.; Seinfeld, J. H. Reactive Intermediates Revealed in Secondary Organic Aerosol Formation from Isoprene. *Proc. Natl. Acad. Sci.* **2010**, *107* (15), 6640–6645.

(38) Surratt, J. D.; Lewandowski, M.; Offenberg, J. H.; Jaoui, M.; Kleindienst, T. E.; Edney, E. O.; Seinfeld, J. H. Effect of Acidity on Secondary Organic Aerosol Formation from Isoprene. *Environ. Sci. Technol.* **2007**, *41* (15), 5363–5369.

(39) Surratt, J. D.; Gómez-González, Y.; Chan, A. W. H.; Vermeylen, R.; Shahgholi, M.; Kleindienst, T. E.; Edney, E. O.; Offenberg, J. H.; Lewandowski, M.; Jaoui, M.; et al. Organosulfate Formation in Biogenic Secondary Organic Aerosol. *J. Phys. Chem. A* **2008**, *112* (36), 8345–8378.

(40) Lin, Y.-H.; Budisulistiorini, S. H.; Chu, K.; Siejack, R. A.; Zhang, H.; Riva, M.; Zhang, Z.; Gold, A.; Kautzman, K. E.; Surratt, J. D. Light-Absorbing Oligomer Formation in Secondary Organic Aerosol from Reactive Uptake of Isoprene Epoxydiols. *Environ. Sci. Technol.* **2014**, *48* (20), 12012–12021.

(41) Gaston, C. J.; Riedel, T. P.; Zhang, Z.; Gold, A.; Surratt, J. D.; Thornton, J. A. Reactive Uptake of an Isoprene-Derived Epoxydiol to Submicron Aerosol Particles. *Environ. Sci. Technol.* **2014**, *48* (19), 11178–11186.

(42) Riedel, T. P.; Lin, Y.-H.; Budisulistiorini, S. H.; Gaston, C. J.; Thornton, J. A.; Zhang, Z.; Vizuete, W.; Gold, A.; Surratt, J. D. Heterogeneous Reactions of Isoprene-Derived Epoxides: Reaction Probabilities and Molar Secondary Organic Aerosol Yield Estimates. *Environ. Sci. Technol. Lett.* **2015**, *2* (2), 38–42.

(43) Xu, L.; Guo, H.; Boyd, C. M.; Klein, M.; Bougiatioti, A.; Cerully, K. M.; Hite, J. R.; Isaacman-VanWertz, G.; Kreisberg, N. M.; Knote, C.; et al. Effects of Anthropogenic Emissions on Aerosol Formation from Isoprene and Monoterpenes in the Southeastern United States. *Proc. Natl. Acad. Sci.* **2015**, *112* (1), 37–42.

(44) Guenther, A.; Hewitt, C. N.; Erickson, D.; Fall, R.; Geron, C.; Graedel, T.; Harley, P.; Klinger, L.; Lerdau, M.; Mckay, W. A.; et al. A Global-Model of Natural Volatile Organic-Compound Emissions. *J. Geophys. Res.* **1995**, *100* (D5), 8873–8892.

(45) Warneke, C.; de Gouw, J. A.; Goldan, P. D.; Kuster, W. C.; Williams, E. J.; Lerner, B. M.; Jakoubek, R.; Brown, S. S.; Stark, H.; Aldener, M.; et al. Comparison of Daytime and Nighttime Oxidation of Biogenic and Anthropogenic VOCs along the New England Coast in Summer during New England Air Quality Study 2002. *J. Geophys. Res.* **2004**, *109* (D10), D10309.

(46) Hallquist, M.; Wenger, J. C.; Baltensperger, U.; Rudich, Y.; Simpson, D.; Claeys, M.; Dommen, J.; Donahue, N. M.; George, C.; Goldstein, A. H.; et al. The Formation, Properties and Impact of Secondary Organic Aerosol: Current and Emerging Issues. *Atmos. Chem. Phys.* **2009**, *9* (14), 5155–5236.

(47) Camredon, M.; Hamilton, J. F.; Alam, M. S.; Wyche, K. P.; Carr, T.; White, I. R.; Monks, P. S.; Rickard, A. R.; Bloss, W. J. Distribution of Gaseous and Particulate Organic Composition during Dark Α-Pinene Ozonolysis. *Atmos. Chem. Phys.* **2010**, *10* (6), 2893–2917.

(48) Perraud, V.; Bruns, E. A.; Ezell, M. J.; Johnson, S. N.; Greaves, J.; Finlayson-Pitts, B. J. Identification of Organic Nitrates in the NO 3 Radical Initiated Oxidation of α-Pinene by Atmospheric Pressure Chemical Ionization Mass Spectrometry. *Environ. Sci. Technol.* **2010**, *44* (15), 5887–5893.

(49) Yu, J. Z.; Iii, D. R. C.; Griffin, R. J.; Flagan, R. C.; Seinfeld, J. H.; Cocker, D. R.; Griffin, R. J.; Flagan, R. C.; Seinfeld, J. H. Gas-Phase Ozone Oxidation of Monoterpenes: Gaseous and Particulate Products. *J. Atmos. Chem.* **1999**, *34* (2), 207–258.

(50) Odum, J. R.; Hoffmann, T.; Bowman, F.; Collins, D.; Flagan, R. C.; Seinfeld, J. H. Gas/Particle Partitioning and Secondary Organic Aerosol Yields. *Environ. Sci. Technol.* **1996**, *30* (8), 2580–2585.

(51) Donahue, N. M.; Robinson, A. L.; Stanier, C. O.; Pandis, S. N. Coupled Partitioning, Dilution, and Chemical Aging of Semivolatile Organics. *Environ. Sci. Technol.* **2006**, *40* (8), 2635–2643.

(52) Hoffmann, T.; Odum, J. R.; Bowman, F.; Collins, D.; Klockow, D.; Flagan, R. C.; Seinfeld, J. H. Formation of Organic Aerosols from the Oxidation of Biogenic Hydrocarbons. *J Atmos Chem* **1997**, *26* (2), 189–222.

(53) Szmigielski, R.; Surratt, J. D.; Gómez-González, Y.; Van der Veken, P.; Kourtchev, I.; Vermeylen, R.; Blockhuys, F.; Jaoui, M.; Kleindienst, T. E.; Lewandowski, M.; et al. 3-Methyl-1,2,3-Butanetricarboxylic Acid: An Atmospheric Tracer for Terpene Secondary Organic Aerosol. *Geophys. Res. Lett.* **2007**, *34* (24), L24811.

(54) Müller, L.; Reinnig, M.-C.; Hayen, H.; Hoffmann, T. Characterization of Oligomeric Compounds in Secondary Organic Aerosol Using Liquid Chromatography Coupled to Electrospray Ionization Fourier Transform Ion Cyclotron Resonance Mass Spectrometry. *Rapid Commun. Mass Spectrom.* **2009**, *23* (7), 971–979.

(55) Iinuma, Y.; Böge, O.; Kahnt, A.; Herrmann, H. Laboratory Chamber Studies on the Formation of Organosulfates from Reactive Uptake of Monoterpene Oxides. *Phys. Chem. Chem. Phys.* **2009**, *11* (36), 7985.

(56) Gao, S.; Ng, N. L.; Keywood, M.; Varutbangkul, V.; Bahreini, R.; Nenes, A.; He, J.; Yoo, K. Y.; Beauchamp, J. L.; Hodyss, R. P.; et al. Particle Phase Acidity and Oligomer Formation in Secondary Organic Aerosol. *Environ. Sci. Technol.* **2004**, *38* (24), 6582–6589.

(57) Kalberer, M.; Paulsen, D.; Sax, M.; Steinbacher, M.; Dommen, J.; Prevot, A. S. H.; Fisseha, R.; Weingartner, E.; Frankevich, V.; Zenobi, R.; et al. Identification of Polymers as Major Components of Atmospheric Organic Aerosols. *Science* **2004**, *303* (5664), 1659–1662.

(58) Tolocka, M. P.; Jang, M.; Ginter, J. M.; Cox, F. J.; Kamens, R. M.; Johnston, M. V. Formation of Oligomers in Secondary Organic Aerosol. *Environ. Sci. Technol.* **2004**, *38* (5), 1428–1434.

(59) Müller, L.; Reinnig, M.-C.; Naumann, K. H.; Saathoff, H.; Mentel, T. F.; Donahue, N. M.; Hoffmann, T. Formation of 3-Methyl-1,2,3-Butanetricarboxylic Acid via Gas Phase Oxidation of Pinonic Acid – a Mass Spectrometric Study of SOA Aging. *Atmos. Chem. Phys.* **2012**, *12* (3), 1483–1496.

(60) Yasmeen, F.; Vermeylen, R.; Szmigielski, R.; Iinuma, Y.; Böge, O.; Herrmann, H.; Maenhaut, W.; Claeys, M. Terpenylic Acid and Related Compounds: Precursors for Dimers in Secondary Organic Aerosol from the Ozonolysis of α-and β-Pinene. *Atmos. Chem. Phys.* **2010**, *10* (19), 9383–9392.

(61) Fitzgerald, J. W. Marine Aerosols: A Review. *Atmos. Environ. Part A. Gen. Top.* **1991**, *25* (3–4), 533–545.

(62) Meskhidze, N.; McClain, C. R.; Petters, M. D.; Vignati, E.; Stetzer, O.; Osburn, C.; Kieber, D. J. Marine Aerosol-Cloud-Climate Interaction. *Adv. Meteorol.* **2010**, *2010*, 1–2.

(63) Charlson, R. J.; Lovelock, J. E.; Andreae, M. O.; Warren, S. G. Oceanic Phytoplankton, Atmospheric Sulphur, Cloud Albedo and Climate. *Nature* **1987**, *326* (16), 655–661.

(64) O'Dowd, C. D.; Facchini, M. C.; Cavalli, F.; Ceburnis, D.; Mircea, M.; Decesari, S.; Fuzzi, S.; Yoon, Y. J.; Putaud, J.-P. Biogenically Driven Organic Contribution to Marine Aerosol. *Nature* **2004**, *431* (7009), 676–680.

(65) Rinaldi, M.; Decesari, S.; Finessi, E.; Giulianelli, L.; Carbone, C.; Fuzzi, S.; O'Dowd, C. D.; Ceburnis, D.; Facchini, M. C. Primary and Secondary Organic Marine Aerosol and Oceanic Biological Activity: Recent Results and New Perspectives for Future Studies. *Adv. Meteorol.* **2010**, *2010* (Article ID 310682), 1–10.

(66) Ayers, G. P.; Gras, J. L. Seasonal Relationship between Cloud Condensation Nuclei and Aerosol Methanesulphonate in Marine Air. *Nature* **1991**, *353* (6347), 834–835.

(67) McCoy, D. T.; Burrows, S. M.; Wood, R.; Grosvenor, D. P.; Elliott, S. M.; Ma, P.-L.; Rasch, P. J.; Hartmann, D. L. Natural Aerosols Explain Seasonal and Spatial Patterns of Southern Ocean Cloud Albedo. *Sci. Adv.* **2015**, *1* (6), e1500157.

(68) Quinn, P. K.; Bates, T. S. The Case against Climate Regulation via Oceanic Phytoplankton Sulphur Emissions. *Nature* **2011**, *480* (7375), 51–56.

(69) Quinn, P. K.; Collins, D. B.; Grassian, V. H.; Prather, K. A.; Bates, T. S. Chemistry and Related Properties of Freshly Emitted Sea Spray Aerosol. *Chem. Rev.* **2015**, *115* (10), 4383–4399.

(70) Ziemann, P. J.; Atkinson, R. Kinetics, Products, and Mechanisms of Secondary Organic Aerosol Formation. *Chem. Soc. Rev.* **2012**, *41* (19), 6582.

(71) Bonsang, B.; Polle, C.; Lambert, G. Evidence for Marine Production of Isoprene. *Geophys. Res. Lett.* **1992**, *19* (11), 1129–1132.

(72) Yassaa, N.; Peeken, I.; Zllner, E.; Bluhm, K.; Arnold, S.; Spracklen, D.; Williams, J. Evidence for Marine Production of Monoterpenes. *Environ. Chem.* **2008**, *5* (6), 391–401.

(73) Shaw, S. L.; Gantt, B.; Meskhidze, N. Production and Emissions of Marine Isoprene and Monoterpenes: A Review. *Adv. Meteorol.* **2010**, *2010* (1), 1–24.

(74) Booge, D.; Marandino, C. A.; Schlundt, C.; Palmer, P. I.; Schlundt, M.; Atlas, E. L.; Bracher, A.; Saltzman, E. S.; Wallace, D. W. R. Can Simple Models Predict Large-Scale Surface Ocean Isoprene Concentrations? *Atmos. Chem. Phys.* **2016**, *16* (18), 11807–11821.

(75) Broadgate, W. J.; Malin, G.; Küpper, F. C.; Thompson, A.; Liss, P. S. Isoprene and Other Non-Methane Hydrocarbons from Seaweeds: A Source of Reactive Hydrocarbons to the Atmosphere. *Mar. Chem.* **2004**, *88* (1–2), 61–73.

(76) Shaw, S. L.; Chisholm, S. W.; Prinn, R. G. Isoprene Production by Prochlorococcus, a Marine Cyanobacterium, and Other Phytoplankton. *Mar. Chem.* **2003**, *80* (4), 227–245.

(77) Foster, P. N.; Prentice, I. C.; Morfopoulos, C.; Siddall, M.; Van Weele, M. Isoprene Emissions Track the Seasonal Cycle of Canopy Temperature, Not Primary Production: Evidence from Remote Sensing. *Biogeosciences* **2014**, *11* (13), 3437–3451.

(78) Liakakou, E.; Vrekoussis, M.; Bonsang, B.; Donousis, C.; Kanakidou, M.; Mihalopoulos, N. Isoprene above the Eastern Mediterranean: Seasonal Variation and Contribution to the Oxidation Capacity of the Atmosphere. *Atmos. Environ.* **2007**, *41* (5), 1002–1010.

(79) Yokouchi, Y.; Li, H.; Machida, T. Isoprene in the Marine Boundary Layer (Southeast Asian Sea, Eastern Indian Ocean , and Southern Ocean ): Comparison with Dimethyl Sulfide and Bromoform. *Geophys. Res. Lett.* **1999**, *104*, 8067–8076.

(80) Hu, Q.-H.; Xie, Z.-Q.; Wang, X.-M.; Kang, H.; He, Q.-F.; Zhang, P. Secondary Organic Aerosols over Oceans via Oxidation of Isoprene and Monoterpenes from Arctic to Antarctic. *Sci. Rep.* **2013**, *3*, 2280.

(81) Luo, G.; Yu, F. A Numerical Evaluation of Global Oceanic Emissions of Alpha-Pinene and Isoprene. *Atmos. Chem. Phys.* **2010**, *10* (4), 2007–2015.

(82) Hackenberg, S. C.; Andrews, S. J.; Airs, R. L.; Arnold, S. R.; Bouman, H. A.; Cummings, D.; Lewis, A. C.; Minaeian, J. K.; Reifel, K. M.; Small, A.; et al. Basin-Scale Observations of Monoterpenes in the Arctic and Atlantic Oceans. *Environ. Sci. Technol.* **2017**, *51* (18), 10449–10458.

(83) Ciuraru, R.; Fine, L.; Pinxteren, M. Van; D'Anna, B.; Herrmann, H.; George, C. Unravelling New Processes at Interfaces: Photochemical Isoprene Production at the Sea Surface. *Environ. Sci. Technol.* **2015**, *49* (22), 13199–13205.

(84) Bernard, F.; Ciuraru, R.; Boréave, A.; George, C. Photosensitized Formation of Secondary Organic Aerosols above the Air/Water Interface. *Environ. Sci. Technol.* **2016**, *50* (16), 8678–8686.

(85) Chakrabarty, R. K.; Moosmüller, H.; Chen, L. W. A.; Lewis, K.; Arnott, W. P.; Mazzoleni, C.; Dubey, M. K.; Wold, C. E.; Hao, W. M.; Kreidenweis, S. M. Brown Carbon in Tar Balls from Smoldering Biomass Combustion. *Atmos. Chem. Phys.* **2010**.

(86) Chen, Y.; Bond, T. C. Light Absorption by Organic Carbon from Wood Combustion. *Atmos. Chem. Phys.* **2010**, *10* (4), 1773–1787.

(87) Lukács, H.; Gelencsér, A.; Hammer, S.; Puxbaum, H.; Pio, C.; Legrand, M.; Kasper-Giebl, A.; Handler, M.; Limbeck, A.; Simpson, D.; et al. Seasonal Trends and Possible Sources of Brown Carbon Based on 2-Year Aerosol Measurements at Six Sites in Europe. *J. Geophys. Res.* **2007**, *112* (D23), D23S18.

(88) Keywood, M.; Kanakidou, M.; Stohl, A.; Dentener, F.; Grassi, G.; Meyer, C. P.; Torseth, K.; Edwards, D.; Thompson, A. M.; Lohmann, U.; et al. Fire in the Air: Biomass Burning Impacts in a Changing Climate. *Crit. Rev. Environ. Sci. Technol.* **2013**, *43* (1), 40–83.

(89) Chen, J.; Li, C.; Ristovski, Z.; Milic, A.; Gu, Y.; Islam, M. S.; Wang, S.; Hao, J.; Zhang, H.; He, C.; et al. A Review of Biomass Burning: Emissions and Impacts on Air Quality, Health and Climate in China. *Sci. Total Environ.* **2017**, *579*, 1000–1034.

(90) Tomaz, S.; Cui, T.; Chen, Y.; Sexton, K. G.; Roberts, J. M.; Warneke, C.; Yokelson, R. J.; Surratt, J. D.; Turpin, B. J. Photochemical Cloud Processing of Primary Wildfire Emissions as a Potential Source of Secondary Organic Aerosol. *Environ. Sci. Technol.* **2018**, *52* (19), 11027–11037.

(91) Akagi, S. K.; Yokelson, R. J.; Wiedinmyer, C.; Alvarado, M. J.; Reid, J. S.; Karl, T.; Crounse, J. D.; Wennberg, P. O. Emission Factors for Open and Domestic Biomass Burning for Use in Atmospheric Models. *Atmos. Chem. Phys.* **2011**, *11* (9), 4039–4072.

(92) Andreae, M. O.; Merlet, P. Emission of Trace Gases and Aerosols from Biomass Burning. *Global Biogeochem. Cycles* **2001**, *15* (4), 955–966.

(93) Stockwell, C. E.; Veres, P. R.; Williams, J.; Yokelson, R. J. Characterization of Biomass Burning Emissions from Cooking Fires, Peat, Crop Residue, and Other Fuels with High-Resolution Proton-Transfer-Reaction Time-of-Flight Mass Spectrometry. *Atmos. Chem. Phys.* **2015**, *15* (2), 845–865.

(94) Yokelson, R. J.; Burling, I. R.; Gilman, J. B.; Warneke, C.; Stockwell, C. E.; de Gouw, J.; Akagi, S. K.; Urbanski, S. P.; Veres, P.; Roberts, J. M.; et al. Coupling Field and Laboratory Measurements to Estimate the Emission Factors of Identified and Unidentified Trace Gases for Prescribed Fires. *Atmos. Chem. Phys.* **2013**, *13* (1), 89–116.

(95) Hatch, L. E.; Luo, W.; Pankow, J. F.; Yokelson, R. J.; Stockwell, C. E.; Barsanti, K. C. Identification and Quantification of Gaseous Organic Compounds Emitted from Biomass Burning Using Two-Dimensional Gas Chromatography–Time-of-Flight Mass Spectrometry. *Atmos. Chem. Phys.* **2015**, *15* (4), 1865–1899.

(96) Jen, C. N.; Hatch, L. E.; Selimovic, V.; Yokelson, R. J.; Weber, R.; Fernandez, A. E.; Kreisberg, N. M.; Barsanti, K. C.; Goldstein, A. H. Speciated and Total Emission Factors of Particulate Organics from Burning Western US Wildland Fuels and Their Dependence on Combustion Efficiency. *Atmos. Chem. Phys.* **2019**, *19* (2), 1013–1026.

(97) Koss, A. R.; Sekimoto, K.; Gilman, J. B.; Selimovic, V.; Coggon, M. M.; Zarzana, K. J.; Yuan, B.; Lerner, B. M.; Brown, S. S.; Jimenez, J. L.; et al. Non-Methane Organic Gas Emissions from Biomass Burning: Identification, Quantification, and Emission Factors from PTR-ToF during the FIREX 2016 Laboratory Experiment. *Atmos. Chem. Phys.* **2018**, *18* (5), 3299–3319.

(98) Liu, X.; Huey, L. G.; Yokelson, R. J.; Selimovic, V.; Simpson, I. J.; Müller, M.; Jimenez, J. L.; Campuzano-Jost, P.; Beyersdorf, A. J.; Blake, D. R.; et al. Airborne Measurements of Western U.S. Wildfire Emissions: Comparison with Prescribed Burning and Air Quality Implications. *J. Geophys. Res. Atmos.* **2017**, *122* (11), 6108–6129.

(99) Mazzoleni, L. R.; Zielinska, B.; Moosmüller, H. Emissions of Levoglucosan, Methoxy Phenols, and Organic Acids from Prescribed Burns, Laboratory Combustion of Wildland Fuels, and Residential Wood Combustion. *Environ. Sci. Technol.* **2007**, *41* (7), 2115–2122.

(100) Oros, D. R.; Abas, M. R. bin; Omar, N. Y. M. J.; Rahman, N. A.; Simoneit, B. R. T. Identification and Emission Factors of Molecular Tracers in Organic Aerosols from Biomass Burning: Part 3. Grasses. *Appl. Geochemistry* **2006**, *21* (6), 919–940.

(101) Oros, D. R.; Simoneit, B. R. . Identification and Emission Factors of Molecular Tracers in Organic Aerosols from Biomass Burning Part 1. Temperate Climate Conifers. *Appl. Geochemistry* **2001**, *16* (13), 1513–1544.

(102) Oros, D. R.; Simoneit, B. R. . Identification and Emission Factors of Molecular Tracers in Organic Aerosols from Biomass Burning Part 2. Deciduous Trees. *Appl. Geochemistry* **2001**, *16* (13), 1545–1565.

(103) Lin, Y.-H. H.; Budisulistiorini, S. H.; Chu, K.; Siejack, R. A.; Zhang, H.; Riva, M.; Zhang, Z.; Gold, A.; Kautzman, K. E.; Surratt, J. D. Light-Absorbing Oligomer Formation in Secondary Organic Aerosol from Reactive Uptake of Isoprene Epoxydiols. *Environ. Sci. Technol.* **2014**, *48* (20), 12012–12021.

(104) Laskin, A.; Laskin, J.; Nizkorodov, S. A. Chemistry of Atmospheric Brown Carbon. *Chem. Rev.* **2015**, *115* (10), 4335–4382.

(105) Desyaterik, Y.; Sun, Y.; Shen, X.; Lee, T.; Wang, X.; Wang, T.; Collett, J. L. Speciation of "Brown" Carbon in Cloud Water Impacted by Agricultural Biomass Burning in Eastern China. *J. Geophys. Res. Atmos.* **2013**, *118* (13), 7389–7399.

(106) Zhang, X.; Lin, Y.-H.; Surratt, J. D.; Weber, R. J. Sources, Composition and Absorption Ångström Exponent of Light-Absorbing Organic Components in Aerosol Extracts from the Los Angeles Basin. *Environ. Sci. Technol.* **2013**, *47* (8), 3685–3693.

(107) Teich, M.; van Pinxteren, D.; Kecorius, S.; Wang, Z.; Herrmann, H. First Quantification of Imidazoles in Ambient Aerosol Particles: Potential Photosensitizers, Brown Carbon Constituents, and Hazardous Components. *Environ. Sci. Technol.* **2016**, *50* (3), 1166–1173.

(108) Laskin, J.; Laskin, A.; Nizkorodov, S. A.; Roach, P.; Eckert, P.; Gilles, M. K.; Wang, B.; Lee, H. J. (Julie); Hu, Q. Molecular Selectivity of Brown Carbon Chromophores. *Environ. Sci. Technol.* **2014**, *48* (20), 12047–12055.

(109) Xie, M.; Chen, X.; Hays, M. D.; Holder, A. L. Composition and Light Absorption of N-Containing Aromatic Compounds in Organic Aerosols from Laboratory Biomass Burning. *Atmos. Chem. Phys.* **2019**, *19* (5), 2899–2915.

(110) Xie, M.; Chen, X.; Hays, M. D.; Lewandowski, M.; Offenberg, J.; Kleindienst, T. E.; Holder, A. L. Light Absorption of Secondary Organic Aerosol: Composition and Contribution of Nitroaromatic Compounds. *Environ. Sci. Technol.* **2017**, *51* (20), 11607–11616.

(111) Huang, R.-J.; Yang, L.; Cao, J.; Chen, Y.; Chen, Q.; Li, Y.; Duan, J.; Zhu, C.; Dai, W.; Wang, K.; et al. Brown Carbon Aerosol in Urban Xi'an, Northwest China: The Composition and Light Absorption Properties. *Environ. Sci. Technol.* **2018**, *52* (12), 6825–6833.

(112) Samburova, V.; Connolly, J.; Gyawali, M.; Yatavelli, R. L. N.; Watts, A. C.; Chakrabarty, R. K.; Zielinska, B.; Moosmüller, H.; Khlystov, A. Polycyclic Aromatic Hydrocarbons in Biomass-Burning Emissions and Their Contribution to Light Absorption and Aerosol Toxicity. *Sci. Total Environ.* **2016**, *568*, 391–401.

(113) Teich, M.; van Pinxteren, D.; Wang, M.; Kecorius, S.; Wang, Z.; Müller, T.; Močnik, G.; Herrmann, H. Contributions of Nitrated Aromatic Compounds to the Light Absorption of Water-Soluble and Particulate Brown Carbon in Different Atmospheric Environments in Germany and China. *Atmos. Chem. Phys.* **2017**, *17* (3), 1653–1672.

(114) Lin, P.; Aiona, P. K.; Li, Y.; Shiraiwa, M.; Laskin, J.; Nizkorodov, S. A.; Laskin, A. Molecular Characterization of Brown Carbon in Biomass Burning Aerosol Particles. *Environ. Sci. Technol.* **2016**, *50* (21), 11815–11824.

(115) Adler, G.; Flores, J. M.; Abo Riziq, A.; Borrmann, S.; Rudich, Y. Chemical, Physical, and Optical Evolution of Biomass Burning Aerosols: A Case Study. *Atmos. Chem. Phys.* **2011**, *11* (4), 1491–1503.

(116) Forrister, H.; Liu, J.; Scheuer, E.; Dibb, J.; Ziemba, L.; Thornhill, K. L.; Anderson, B.; Diskin, G.; Perring, A. E.; Schwarz, J. P.; et al. Evolution of Brown Carbon in Wildfire Plumes. *Geophys. Res. Lett.* **2015**, *42* (11), 4623–4630.

(117) Lambe, A. T.; Cappa, C. D.; Massoli, P.; Onasch, T. B.; Forestieri, S. D.; Martin, A. T.; Cummings, M. J.; Croasdale, D. R.; Brune, W. H.; Worsnop, D. R.; et al. Relationship between Oxidation Level and Optical Properties of Secondary Organic Aerosol. *Environ. Sci. Technol.* **2013**, *47* (12), 6349–6357.

(118) Liu, J.; Lin, P.; Laskin, A.; Laskin, J.; Kathmann, S. M.; Wise, M.; Caylor, R.; Imholt, F.; Selimovic, V.; Shilling, J. E. Optical Properties and Aging of Light-Absorbing Secondary Organic Aerosol. *Atmos. Chem. Phys.* **2016**, *16* (19), 12815–12827.

(119) Sareen, N.; Moussa, S. G.; McNeill, V. F. Photochemical Aging of Light-Absorbing Secondary Organic Aerosol Material. *J. Phys. Chem. A* **2013**, *117* (14), 2987–2996.

(120) Zhong, M.; Jang, M. Dynamic Light Absorption of Biomass-Burning Organic Carbon Photochemically Aged under Natural Sunlight. *Atmos. Chem. Phys.* **2014**, *14* (3), 1517–1525.

(121) Zhao, R.; Lee, A. K. Y.; Huang, L.; Li, X.; Yang, F.; Abbatt, J. P. D. Photochemical Processing of Aqueous Atmospheric Brown Carbon. *Atmos. Chem. Phys.* **2015**, *15* (11), 6087–6100.

(122) Lee, H. J. (Julie); Aiona, P. K.; Laskin, A.; Laskin, J.; Nizkorodov, S. A. Effect of Solar Radiation on the Optical Properties and Molecular Composition of Laboratory Proxies of Atmospheric Brown Carbon. *Environ. Sci. Technol.* **2014**, *48* (17), 10217–10226.

(123) De Haan, D. O.; Hawkins, L. N.; Kononenko, J. A.; Turley, J. J.; Corrigan, A. L.; Tolbert, M. A.; Jimenez, J. L. Formation of Nitrogen-Containing Oligomers by Methylglyoxal and Amines in Simulated Evaporating Cloud Droplets. *Environ. Sci. Technol.* **2011**, *45* (3), 984–991.

(124) Lee, A. K. Y.; Zhao, R.; Li, R.; Liggio, J.; Li, S.-M.; Abbatt, J. P. D. Formation of Light Absorbing Organo-Nitrogen Species from Evaporation of Droplets Containing Glyoxal and Ammonium Sulfate. *Environ. Sci. Technol.* **2013**, *47* (22), 12819–12826.

(125) Laskin, A.; Laskin, J.; Nizkorodov, S. A. Mass Spectrometric Approaches for Chemical Characterisation of Atmospheric Aerosols: Critical Review of the Most Recent Advances. *Environmental Chemistry*. CSIRO PUBLISHING 2012, pp 163–189.

(126) Laskin, J.; Laskin, A.; Nizkorodov, S. A. Mass Spectrometry Analysis in Atmospheric Chemistry. *Anal. Chem.* **2018**, *90* (1), 166–189.

(127) Pratt, K. A.; Prather, K. A. Mass Spectrometry of Atmospheric Aerosols-Recent Developments and Applications. Part II: On-Line Mass Spectrometry Techniques. *Mass Spectrom. Rev.* **2012**, *31* (1), 17–48.

(128) Pratt, K. A.; Prather, K. A. Mass Spectrometry of Atmospheric Aerosols-Recent Developments and Applications. Part I: Off-Line Mass Spectrometry Techniques. *Mass Spectrom. Rev.* **2012**, *31* (1), 1–16.

(129) Claeys, M.; Graham, B.; Vas, G.; Wang, W.; Vermeylen, R.; Pashynska, V.; Cafmeyer, J.; Guyon, P.; Andreae, M. O.; Artaxo, P.; et al. Formation of Secondary Organic Aerosols Through Photooxidation of Isoprene. *Science* **2004**, *303* (5661), 1173–1176.

(130) Szmigielski, R.; Surratt, J. D.; Gomez-Gonzalez, Y.; van der Veken, P.; Kourtchev, I.; Vermeylen, R.; Blockhuys, F.; Jaoui, M.; Kleindienst, T. E.; Lewandowski, M.; et al. 3-Methyl-1,2,3-Butanetricarboxylic Acid: An Atmospheric Tracer for Terpene Secondary Organic Aerosol. *Geophys. Res. Lett.* **2007**, *34* (24), 2–7.

(131) Lin, Y.-H. Y.; Zhang, H.; Pye, H. H. O. T.; Zhang, Z.; Marth, W. J.; Park, S.; Arashiro, M.; Cui, T.; Budisulistiorini, S. H.; Sexton, K. G.; et al. Epoxide as a Precursor to Secondary Organic Aerosol Formation from Isoprene Photooxidation in the Presence of Nitrogen Oxides. *Proc. Natl. Acad. Sci.* **2013**, *110* (17), 6718–6723.

(132) Iinuma, Y.; Böge, O.; Keywood, M.; Gnauk, T.; Herrmann, H. Diaterebic Acid Acetate and Diaterpenylic Acid Acetate: Atmospheric Tracers for Secondary Organic Aerosol Formation from 1,8-Cineole Oxidation. *Environ. Sci. Technol.* **2009**, *43* (2), 280–285.

(133) Ng, N. L.; Chhabra, P. S.; Chan, A. W. H.; Surratt, J. D.; Kroll, J. H.; Kwan, A. J.; McCabe, D. C.; Wennberg, P. O.; Sorooshian, A.; Murphy, S. M.; et al. Effect of NOx Level on Secondary Organic Aerosol (SOA) Formation from the Photooxidation of Terpenes. *Atmos. Chem. Phys.* **2007**, *7* (19), 5159–5174.

(134) Surratt, J. D.; Gomez-Gonzalez, Y.; Chan, A. W. H.; Vermeylen, R.; Shahgholi, M.; Kleindienst, T. E.; Edney, E. O.; Offenberg, J. H.; Lewandowski, M.; Jaoui, M.; et al. Organosulfate Formation in Biogenic Secondary Organic Aerosol. *J. Phys. Chem. Atmos.* **2008**, *112* (36), 8345–8378.

(135) Kristensen, K.; Cui, T.; Zhang, H.; Gold, A.; Glasius, M.; Surratt, J. D. D. Dimers in α-Pinene Secondary Organic Aerosol: Effect of Hydroxyl Radical, Ozone, Relative Humidity and Aerosol Acidity. *Atmos. Chem. Phys.* **2014**, *14* (8), 4201–4218.

(136) Lin, P.; Fleming, L. T.; Nizkorodov, S. A.; Laskin, J.; Laskin, A. Comprehensive Molecular Characterization of Atmospheric Brown Carbon by High Resolution Mass Spectrometry with Electrospray and Atmospheric Pressure Photoionization. *Anal. Chem.* **2018**, *90* (21), 12493–12502.

(137) Turpin, B. J.; Saxena, P.; Andrews, E. Measuring and Simulating Particulate Organics in the Atmosphere: Problems and Prospects. *Atmos. Environ.* **2000**, *34* (18), 2983–3013.

(138) Schauer, C.; Niessner, R.; Pöschl, U. Polycyclic Aromatic Hydrocarbons in Urban Air Particulate Matter: Decadal and Seasonal Trends, Chemical Degradation, and Sampling Artifacts. *Environ. Sci. Technol.* **2003**, *37* (13), 2861–2868.

(139) Riedel, T. P.; Lin, Y.-H.; Zhang, Z.; Chu, K.; Thornton, J. A.; Vizuete, W.; Gold, A.; Surratt, J. D. Constraining Condensed-Phase Formation Kinetics of Secondary Organic Aerosol Components from Isoprene Epoxydiols. *Atmos. Chem. Phys.* **2016**, *16* (3), 1245–1254.

(140) Budisulistiorini, S. H.; Nenes, A.; Carlton, A. G.; Surratt, J. D.; McNeill, V. F.; Pye, H. O. T. Simulating Aqueous-Phase Isoprene-Epoxydiol (IEPOX) Secondary Organic Aerosol Production During the 2013 Southern Oxidant and Aerosol Study (SOAS). *Environ. Sci. Technol.* **2017**, *51* (9), 5026–5034.

(141) Lopez-Hilfiker, F. D.; Mohr, C.; D'Ambro, E. L.; Lutz, A.; Riedel, T. P.; Gaston, C. J.; Iyer, S.; Zhang, Z.; Gold, A.; Surratt, J. D.; et al. Molecular Composition and Volatility of Organic Aerosol in the Southeastern U.S.: Implications for IEPOX Derived SOA. *Environ. Sci. Technol.* **2016**, *50* (5), 2200–2209.

(142) Isaacman, G.; Kreisberg, N. M.; Yee, L. D.; Worton, D. R.; Chan, A. W. H.; Moss, J. A.; Hering, S. V.; Goldstein, A. H. Online Derivatization for Hourly Measurements of Gas- and Particle-Phase Semi-Volatile Oxygenated Organic Compounds by Thermal Desorption Aerosol Gas Chromatography (SV-TAG). *Atmos. Meas. Tech.* **2014**, *7* (12), 4417–4429.

(143) Isaacman-VanWertz, G.; Yee, L. D.; Kreisberg, N. M.; Wernis, R.; Moss, J. A.; Hering, S. V.; de Sá, S. S.; Martin, S. T.; Alexander, M. L.; Palm, B. B.; et al. Ambient Gas-Particle Partitioning of Tracers for Biogenic Oxidation. *Environ. Sci. Technol.* **2016**, *50* (18), 9952–9962.

(144) Williams, B. J.; Zhang, Y.; Zuo, X.; Martinez, R. E.; Walker, M. J.; Kreisberg, N. M.; Goldstein, A. H.; Docherty, K. S.; Jimenez, J. L. Organic and Inorganic Decomposition Products from the Thermal Desorption of Atmospheric Particles. *Atmos. Meas. Tech.* **2016**, *9* (4), 1569–1586.

(145) Stark, H.; Yatavelli, R. L. N.; Thompson, S. L.; Kang, H.; Krechmer, J. E.; Kimmel, J. R.; Palm, B. B.; Hu, W.; Hayes, P. L.; Day, D. A.; et al. Impact of Thermal Decomposition on Thermal Desorption Instruments: Advantage of Thermogram Analysis for Quantifying Volatility Distributions of Organic Species. *Environ. Sci. Technol.* **2017**, *51* (15), 8491–8500.

(146) Gómez-González, Y.; Surratt, J. D.; Cuyckens, F.; Szmigielski, R.; Vermeylen, R.; Jaoui, M.; Lewandowski, M.; Offenberg, J. H.; Kleindienst, T. E.; Edney, E. O.; et al. Characterization of Organosulfates from the Photooxidation of Isoprene and Unsaturated Fatty Acids in Ambient Aerosol Using Liquid Chromatography/(−) Electrospray Ionization Mass Spectrometry. *J. Mass Spectrom.* **2008**, *43* (3), 371–382.

(147) Fu, P.; Kawamura, K.; Miura, K. Molecular Characterization of Marine Organic Aerosols Collected during a Round-the-World Cruise. *J. Geophys. Res. Atmos.* **2011**, *116* (13), 1–14.

(148) Pokhrel, A.; Kawamura, K.; Ono, K.; Seki, O.; Fu, P.; Matoba, S.; Shiraiwa, T. Ice Core Records of Monoterpene- and Isoprene-SOA Tracers from Aurora Peak in Alaska since 1660s: Implication for Climate Change Variability in the North Pacific Rim. *Atmos. Environ.* **2016**, *130*, 105–112.

(149) Fu, P.; Kawamura, K.; Seki, O.; Izawa, Y.; Shiraiwa, T.; Ashworth, K. Historical Trends of Biogenic SOA Tracers in an Ice Core from Kamchatka Peninsula. *Environ. Sci. Technol. Lett.* **2016**, *3* (10), 351–358.

(150) Capaldo, K.; Corbett, J. J.; Kasibhatla, P. Effects of Ship Emissions on Sulphur Cycling and Radiative Climate Forcing over the Ocean. *Nature* **1999**, *400* (August), 743–746.

(151) Claeys, M.; Graham, B.; Vas, G.; Wang, W.; Vermeylen, R.; Pashynska, V.; Cafmeyer, J.; Guyon, P.; Andreae, M. O.; Artaxo, P.; et al. Formation of Secondary Organic Aerosols Through Photooxidation of Isoprene. *Science* **2004**, *303* (5661), 1173–1176.

(152) Claeys, M.; Iinuma, Y.; Szmigielski, R.; Surratt, J. D.; Blockhuys, F.; Van Alsenoy, C.; Böge, O.; Sierau, B.; Gómez-González, Y.; Vermeylen, R.; et al. Terpenylic Acid and Related Compounds from the Oxidation of α-Pinene: Implications for New Particle Formation and Growth above Forests. *Environ. Sci. Technol.* **2009**, *43* (18), 6976–6982.

(153) Glasius, M.; Lahaniati, M.; Calogirou, A.; Di Bella, D.; Jensen, N. R.; Hjorth, J.; Kotzias, D.; Larsen, B. R. Carboxylic Acids in Secondary Aerosols from Oxidation of Cyclic Monoterpenes by Ozone. *Environ. Sci. Technol.* **2000**, *34* (6), 1001–1010.

(154) Rinaldi, M.; Decesari, S.; Carbone, C.; Finessi, E.; Fuzzi, S.; Ceburnis, D.; O'Dowd, C. D.; Sciare, J.; Burrows, J. P.; Vrekoussis, M.; et al. Evidence of a Natural Marine Source of Oxalic Acid and a Possible Link to Glyoxal. *J. Geophys. Res. Atmos.* **2011**, *116* (16), 1–12.

(155) Meskhidze, N.; Nenes, A. Phytoplankton and Cloudiness in the Southern Ocean. *Science* **2006**, *314* (5804), 1419–1423.

(156) Crawford, J.; Cohen, D. D.; Stelcer, E.; Atanacio, A. J. Long Term Fine Aerosols at the Cape Grim Global Baseline Station: 1998 to 2016. *Atmos. Environ.* **2017**, *166*, 34–46.

(157) Lin, Y. H.; Zhang, Z.; Docherty, K. S.; Zhang, H.; Budisulistiorini, S. H.; Rubitschun, C. L.; Shaw, S. L.; Knipping, E. M.; Edgerton, E. S.; Kleindienst, T. E.; et al. Isoprene Epoxydiols as Precursors to Secondary Organic Aerosol Formation: Acid-Catalyzed Reactive Uptake Studies with Authentic Compounds. *Environ. Sci. Technol.* **2012**, *46* (1), 250–258.

(158) Surratt, J. D.; Chan, A. W. H.; Eddingsaas, N. C.; Chan, M.; Loza, C. L.; Kwan, A. J.; Hersey, S. P.; Flagan, R. C.; Wennberg, P. O.; Seinfeld, J. H. Reactive Intermediates Revealed in Secondary Organic Aerosol Formation from Isoprene. *Proc. Natl. Acad. Sci.* **2010**, *107* (15), 6640–6645.

(159) Zhang, Z.; Lin, Y. H.; Zhang, H.; Surratt, J. D.; Ball, L. M.; Gold, A. Technical Note: Synthesis of Isoprene Atmospheric Oxidation Products: Isomeric Epoxydiols and the Rearrangement Products Cis-and Trans-3-Methyl-3,4- Dihydroxytetrahydrofuran. *Atmos. Chem. Phys.* **2012**, *12* (18), 8529–8535.

(160) Budisulistiorini, S. H.; Li, X.; Bairai, S. T.; Renfro, J.; Liu, Y.; Liu, Y. J.; McKinney, K. A.; Martin, S. T.; McNeill, V. F.; Pye, H. O. T.; et al. Examining the Effects of Anthropogenic Emissions on Isoprene-Derived Secondary Organic Aerosol Formation during the 2013 Southern Oxidant and Aerosol Study (SOAS) at the Look Rock, Tennessee Ground Site. *Atmos. Chem. Phys.* **2015**, *15* (15), 8871–8888.

(161) Olson, C. N.; Galloway, M. M.; Yu, G.; Hedman, C. J.; Lockett, M. R.; Yoon, T.; Stone, E. A.; Smith, L. M.; Keutsch, F. N. Hydroxycarboxylic Acid-Derived Organosulfates: Synthesis, Stability, and Quantification in Ambient Aerosol. *Environ. Sci. Technol.* **2011**, *45* (15), 6468–6474.

(162) Zhang, H.; Worton, D. R.; Lewandowski, M.; Ortega, J.; Rubitschun, C. L.; Park, J. H.; Kristensen, K.; Campuzano-Jost, P.; Day, D. A.; Jimenez, J. L.; et al. Organosulfates as Tracers for Secondary Organic Aerosol (SOA) Formation from 2-Methyl-3-Buten-2-Ol (MBO) in the Atmosphere. *Environ. Sci. Technol.* **2012**, *46* (17), 9437–9446.

(163) Nguyen, T. B.; Bates, K. H.; Crounse, J. D.; Schwantes, R. H.; Zhang, X.; Kjaergaard, H. G.; Surratt, J. D.; Lin, P.; Laskin, A.; Seinfeld, J. H.; et al. Mechanism of the Hydroxyl Radical Oxidation of Methacryloyl Peroxynitrate (MPAN) and Its Pathway toward Secondary Organic Aerosol Formation in the Atmosphere. *Phys. Chem. Chem. Phys.* **2015**, *17* (27), 17914–17926.

(164) Yasmeen, F.; Szmigielski, R.; Vermeylen, R.; Gõmez-González, Y.; Surratt, J. D.; Chan, A. W. H.; Seinfeld, J. H.; Maenhaut, W.; Claeys, M. Mass Spectrometric Characterization of Isomeric Terpenoic Acids from the Oxidation of α-Pinene, β-Pinene, d-Limonene, and Î"3-Carene in Fine Forest Aerosol. *J. Mass Spectrom.* **2011**, *46* (4), 425–442.

(165) Hu, W.; Palm, B. B.; Day, D. A.; Campuzano-Jost, P.; Krechmer, J. E.; Peng, Z.; De Sa Suzane, S.; Martin, S. T.; Alexander, M. L.; Baumann, K.; et al. Volatility and Lifetime against OH Heterogeneous Reaction of Ambient Isoprene-Epoxydiols-Derived Secondary Organic Aerosol (IEPOX-SOA). *Atmos. Chem. Phys.* **2016**, *16* (18), 11563–11580.

(166) Wang, W.; Kourtchev, I.; Graham, B.; Cafmeyer, J.; Maenhaut, W.; Claeys, M. Characterization of Oxygenated Derivatives of Isoprene Related to 2-Methyltetrols in Amazonian Aerosols Using Trimethylsilylation and Gas Chromatography/Ion Trap Mass Spectrometry. *Rapid Commun. Mass Spectrom.* **2005**, *19* (10), 1343–1351.

(167) Lin, Y. H.; Knipping, E. M.; Edgerton, E. S.; Shaw, S. L.; Surratt, J. D. Investigating the Influences of SO2 and NH3 Levels on Isoprene-Derived Secondary Organic Aerosol Formation Using Conditional Sampling Approaches. *Atmos. Chem. Phys.* **2013**, *13* (16), 8457–8470.

(168) Rattanavaraha, W.; Chu, K.; Budisulistiorini, S. H.; Riva, M.; Lin, Y. H.; Edgerton, E. S.; Baumann, K.; Shaw, S. L.; Guo, H.; King, L.; et al. Assessing the Impact of Anthropogenic Pollution on Isoprene-Derived Secondary Organic Aerosol Formation in PM2.5 Collected from the Birmingham, Alabama, Ground Site during the 2013 Southern Oxidant and Aerosol Study. *Atmos. Chem. Phys.* **2016**, *16* (8), 4897–4914.

(169) Ding, X.; Zheng, M.; Yu, L.; Zhang, X.; Weber, R. J.; Yan, B.; Russell, A. G.; Edgerton, E. S.; Wang, X. Spatial and Seasonal Trends in Biogenic Secondary Organic Aerosol Tracers and Water-Soluble Organic Carbon in the Southeastern United States. *Environ. Sci. Technol.* **2008**, *42* (14), 5171–5176.

(170) Hu, D.; Bian, Q.; Li, T. W. Y.; Lau, A. K. H.; Yu, J. Z. Contributions of Isoprene, Monoterpenes, β-Caryophyllene, and Toluene to Secondary Organic Aerosols in Hong Kong during the Summer of 2006. *J. Geophys. Res. Atmos.* **2008**, *113* (22), 1–14.

(171) Kleindienst, T. E.; Jaoui, M.; Lewandowski, M.; Offenberg, J. H.; Lewis, C. W.; Bhave, P. V.; Edney, E. O. Estimates of the Contributions of Biogenic and Anthropogenic Hydrocarbons to Secondary Organic Aerosol at a Southeastern US Location. *Atmos. Environ.* **2007**, *41* (37), 8288–8300.

(172) Kourtchev, I.; Ruuskanen, T.; Maenhaut, W.; Kulmala, M.; Claeys, M. Observation of 2-Methyltetrols and Related Photo-Oxidation Products of Isoprene in Boreal Forest Aerosols from Hyytiala, Finland. *Atmos. Chem. Phys. Discuss.* **2005**, *5* (3), 2947–2971.

(173) Shen, R. Q.; Ding, X.; He, Q. F.; Cong, Z. Y.; Yu, Q. Q.; Wang, X. M. Seasonal Variation of Secondary Organic Aerosol Tracers in Central Tibetan Plateau. *Atmos. Chem. Phys.* **2015**, *15* (15), 8781–8793.

(174) Xia, X.; Hopke, P. K. Seasonal Variation of 2-Methyltetrols in Ambient Air Samples. *Environ. Sci. Technol.* **2008**, *40* (22), 1–4.

(175) Fu, P.; Kawamura, K.; Chen, J.; Barrie, L. A. Isoprene, Monoterpene, and Sesquiterpene Oxidation Products in the High Arctic Aerosols during Late Winter to Early Summer. *Environ. Sci. Technol.* **2009**, *43* (11), 4022–4028.

(176) Fu, P.; Kawamura, K.; Chen, J.; Charrière, B.; Sempéré, R. Organic Molecular Composition of Marine Aerosols over the Arctic Ocean in Summer: Contributions of Primary Emission and Secondary Aerosol Formation. *Biogeosciences* **2013**, *10* (2), 653–667.

(177) Chavez, F. P.; Strutton, P. G.; Friederich, G. E.; Feely, R. A.; Feldman, G. C.; Foley, D. G.; McPhaden, M. J. Biological and Chemical Response of the Equatorial Pacific Ocean to the 1997-98 El Nino. *Science* **1999**, *286* (5447), 2126–2131.

(178) Cui, T.; Zeng, Z.; dos Santos, E. O.; Zhang, Z.; Chen, Y.; Zhang, Y.; Rose, C. A.; Budisulistiorini, S. H.; Collins, L. B.; Bodnar, W. M.; et al. Development of a Hydrophilic Interaction Liquid Chromatography (HILIC) Method for the Chemical Characterization of Water-Soluble Isoprene Epoxydiol (IEPOX)-Derived Secondary Organic Aerosol. *Environ. Sci. Process. Impacts* **2018**, *20* (11), 1524–1536.

(179) Claeys, M.; Wang, W.; Vermeylen, R.; Kourtchev, I.; Chi, X.; Farhat, Y.; Surratt, J. D.; Gomez-Gonzalez, Y.; Sciare, J.; Maenhaut, W. Chemical Characterisation of Marine Aerosol at Amsterdam Island during the Austral Summer of 2006-2007. *J. Aerosol Sci.* **2010**, *41* (1), 13–22.

(180) Xu, L.; Guo, H.; Boyd, C. M.; Bougiatioti, A.; Cerully, K. M.; Hite, J. R.; Isaacman-vanwertz, G.; Kreisberg, N. M.; Olson, K.; Koss, A.; et al. Effects of Anthropogenic Emissions on Aerosol Formation from Isoprene and Monoterpenes in the Southeastern United States. *Proc. Natl. Acad. Sci.* **2015**, *112* (32), 201512277.

(181) Darer, A. I.; Cole-Filipiak, N. C.; O'Connor, A. E.; Elrod, M. J. Formation and Stability of Atmospherically Relevant Isoprene-Derived Organosulfates and Organonitrates. *Environ. Sci. Technol.* **2011**, *45* (5), 1895–1902.

(182) Paulot, F.; Crounse, J. D.; Kjaergaard, H. G.; Kurten, A.; St. Clair, J. M.; Seinfeld, J. H.; Wennberg, P. O. Unexpected Epoxide Formation in the Gas-Phase Photooxidation of Isoprene. *Science* **2009**, *325* (5941), 730–733.

(183) Nguyen, T. B.; Coggon, M. M.; Bates, K. H.; Zhang, X.; Schwantes, R. H.; Schilling, K. A.; Loza, C. L.; Flagan, R. C.; Wennberg, P. O.; Seinfeld, J. H. Organic Aerosol Formation from the Reactive Uptake of Isoprene Epoxydiols (IEPOX) onto Non-Acidified Inorganic Seeds. *Atmos. Chem. Phys.* **2014**, *14* (7), 3497–3510.

(184) Lim, H.-J.; Carlton, A. G.; Turpin, B. J. Isoprene Forms Secondary Organic Aerosol through Cloud Processing: Model Simulations. *Environ. Sci. Technol.* **2005**, *39* (12), 4441–4446.

(185) Kleindienst, T. E.; Lewandowski, M.; Offenberg, J. H.; Jaoui, M.; Edney, E. O. Ozone-Isoprene Reaction: Re-Examination of the Formation of Secondary Organic Aerosol. *Geophys. Res. Lett.* **2007**, *34* (1), L01805.

(186) Riva, M.; Budisulistiorini, S. H.; Zhang, Z.; Gold, A.; Surratt, J. D. Chemical Characterization of Secondary Organic Aerosol Constituents from Isoprene Ozonolysis in the Presence of Acidic Aerosol. *Atmos. Environ.* **2016**, *130*, 5–13.

(187) Surratt, J. D.; Murphy, S. M.; Kroll, J. H.; Ng, N. L.; Hildebrandt, L.; Sorooshian, A.; Szmigielski, R.; Vermeylen, R.; Maenhaut, W.; Claeys, M.; et al. Chemical Composition of Secondary Organic Aerosol Formed from the Photooxidation of Isoprene. *J. Phys. Chem. A* **2006**, *110* (31), 9665–9690.

(188) Ridley, B. A.; Carroll, M. A.; Gregory, G. L. Measurements of Nitric Oxide in the Boundary Layer and Free Troposphere over the Pacific Ocean. *J. Geophys. Res.* **1987**, *92* (D2), 2025.

(189) Kleindienst, T. E.; Lewandowski, M.; Offenberg, J. H.; Jaoui, M.; Edney, E. O. The Formation of Secondary Organic Aerosol from the Isoprene + OH Reaction in the Absence of NOx. *Atmos. Chem. Phys. Discuss.* **2009**, *9* (2), 10015–10054.

(190) Claeys, M.; Szmigielski, R.; Kourtchev, I.; Van Der Veken, P.; Vermeylen, R.; Maenhaut, W.; Jaoui, M.; Kleindienst, T. E.; Lewandowski, M.; Offenberg, J. H.; et al. Hydroxydicarboxylic Acids: Markers for Secondary Organic Aerosol from the Photooxidation of α-Pinene. *Environ. Sci. Technol.* **2007**, *41* (5), 1628–1634.

(191) Kahnt, A.; Iinuma, Y.; Blockhuys, F.; Mutzel, A.; Vermeylen, R.; Kleindienst, T. E.; Jaoui, M.; Offenberg, J. H.; Lewandowski, M.; B??ge, O.; et al. 2-Hydroxyterpenylic Acid: An Oxygenated Marker Compound for α-Pinene Secondary Organic Aerosol in Ambient Fine Aerosol. *Environ. Sci. Technol.* **2014**, *48* (9), 4901–4908.

(192) Kristensen, K.; Watne, Å. K.; Hammes, J.; Lutz, A.; Petäjä, T.; Hallquist, M.; Bilde, M.; Glasius, M. High-Molecular Weight Dimer Esters Are Major Products in Aerosols from α-Pinene Ozonolysis and the Boreal Forest. *Environ. Sci. Technol. Lett.* **2016**, *3* (8), 280–285.

(193) Zhang, X.; McVay, R. C.; Huang, D. D.; Dalleska, N. F.; Aumont, B.; Flagan, R. C.; Seinfeld, J. H. Formation and Evolution of Molecular Products in α-Pinene Secondary Organic Aerosol. *Proc. Natl. Acad. Sci.* **2015**, *112* (46), 14168–14173.

(194) Gao, Y.; Hall, W. A.; Johnston, M. V. Molecular Composition of Monoterpene Secondary Organic Aerosol at Low Mass Loading. *Environ. Sci. Technol.* **2010**, *44* (20), 7897–7902.

(195) Keller, M. D.; Bellows, W. K.; Guillard, R. R. L. Dimethyl Sulfide Production in Marine Phytoplankton. In *Biogenic Sulfur in the Environment*; 1989; pp 167–182.

(196) Carlton, A. G.; Turpin, B. J.; Altieri, K. E.; Seitzinger, S.; Reff, A.; Lim, H. J.; Ervens, B. Atmospheric Oxalic Acid and SOA Production from Glyoxal: Results of Aqueous Photooxidation Experiments. *Atmos. Environ.* **2007**, *41* (35), 7588–7602.

(197) Altieri, K. E.; Seitzinger, S. P.; Carlton, A. G.; Turpin, B. J.; Klein, G. C.; Marshall, A. G. Oligomers Formed through In-Cloud Methylglyoxal Reactions: Chemical Composition, Properties, and Mechanisms Investigated by Ultra-High Resolution FT-ICR Mass Spectrometry. *Atmos. Environ.* **2008**, *42* (7), 1476–1490.

(198) Carlton, A. G.; Turpin, B. J.; Lim, H.-J.; Altieri, K. E.; Seitzinger, S. Link between Isoprene and Secondary Organic Aerosol (SOA): Pyruvic Acid Oxidation Yields Low Volatility Organic Acids in Clouds. *Geophys. Res. Lett.* **2006**, *33* (6), L06822.

(199) Kawamura, K.; Sakaguchi, F. Molecular Distributions of Water Soluble Dicarboxylic Acids in Marine Aerosols over the Pacific Ocean Including Tropics. *J. Geophys. Res.* **1999**, *104*, 3501–3509.

(200) Wang, H.; Kawamura, K.; Yamazaki, K. Water-Soluble Dicarboxylic Acids, Ketoacids and Dicarbonyls in the Atmospheric Aerosols over the Southern Ocean and Western Pacific Ocean. *J. Atmos. Chem.* **2006**, *53* (1), 43–61.

(201) Bikkina, S.; Kawamura, K.; Miyazaki, Y.; Fu, P. High Abundances of Oxalic, Azelaic, and Glyoxylic Acids and Methylglyoxal in the Open Ocean with High Biological Activity: Implication for Secondary OA Formation from Isoprene. *Geophys. Res. Lett.* **2014**, *41* (10), 3649–3657.

(202) Berresheim, H.; Eisele, F. L.; Tanner, D. J.; McInnes, L. M.; Ramsey-Bell, D. C.; Covert, D. S. Atmospheric Sulfur Chemistry and Cloud Condensation Nuclei (CCN) Concentrations over the Northeastern Pacific Coast. *J. Geophys. Res.* **1993**, *98* (D7), 12701.

(203) Engelhart, G. J.; Moore, R. H.; Nenes, A.; Pandis, S. N. Cloud Condensation Nuclei Activity of Isoprene Secondary Organic Aerosol. *J. Geophys. Res.* **2011**, *116* (D2), D02207.

(204) Pratt, K. A.; Fiddler, M. N.; Shepson, P. B.; Carlton, A. G.; Surratt, J. D. Organosulfates in Cloud Water above the Ozarks' Isoprene Source Region. *Atmos. Environ.* **2013**, *77*, 231–238.

(205) Croft, B.; Martin, R. V.; Leaitch, W. R.; Burkart, J.; Chang, R. Y.-W.; Collins, D. B.; Hayes, P. L.; Hodshire, A. L.; Huang, L.; Kodros, J. K.; et al. Arctic Marine Secondary Organic Aerosol Contributes Significantly to Summertime Particle Size Distributions in the Canadian Arctic Archipelago. *Atmos. Chem. Phys.* **2019**, *19* (5), 2787–2812.

(206) Willis, M. D.; Köllner, F.; Burkart, J.; Bozem, H.; Thomas, J. L.; Schneider, J.; Aliabadi, A. A.; Hoor, P. M.; Schulz, H.; Herber, A. B.; et al. Evidence for Marine Biogenic Influence on Summertime Arctic Aerosol. *Geophys. Res. Lett.* **2017**, *44* (12), 6460–6470.

(207) Mungall, E. L.; Abbatt, J. P. D.; Wentzell, J. J. B.; Lee, A. K. Y.; Thomas, J. L.; Blais, M.; Gosselin, M.; Miller, L. A.; Papakyriakou, T.; Willis, M. D.; et al. Microlayer Source of Oxygenated Volatile Organic Compounds in the Summertime Marine Arctic Boundary Layer. *Proc. Natl. Acad. Sci.* **2017**, *114* (24), 6203–6208.

(208) Wang, Y. H.; Liu, Z. R.; Zhang, J. K.; Hu, B.; Ji, D. S.; Yu, Y. C.; Wang, Y. S. Aerosol Physicochemical Properties and Implications for Visibility during an Intense Haze Episode during Winter in Beijing. *Atmos. Chem. Phys.* **2015**, *15* (6), 3205–3215.

(209) Davidson, C. I.; Phalen, R. F.; Solomon, P. A. Airborne Particulate Matter and Human Health: A Review. *Aerosol Sci. Technol.* **2005**, *39* (8), 737–749.

(210) Jacobson, M. C.; Hansson, H. C.; Noone, K. J.; Charlson, R. J. Organic Atmospheric Aerosols: Review and State of the Science. *Rev. Geophys.* **2000**, *38* (2), 267–294.

(211) Jimenez, J. L.; Canagaratna, M. R.; Donahue, N. M.; Prevot, A. S. H.; Zhang, Q.; Kroll, J. H.; DeCarlo, P. F.; Allan, J. D.; Coe, H.; Ng, N. L.; et al. Evolution of Organic Aerosols in the Atmosphere. *Science* **2009**, *326* (5959), 1525–1529.

(212) Docherty, K. S.; Stone, E. A.; Ulbrich, I. M.; DeCarlo, P. F.; Snyder, D. C.; Schauer, J. J.; Peltier, R. E.; Weber, R. J.; Murphy, S. M.; Seinfeld, J. H.; et al. Apportionment of Primary and Secondary Organic Aerosols in Southern California during the 2005 Study of Organic Aerosols in Riverside (SOAR-1). *Environ. Sci. Technol.* **2008**, *42* (20), 7655–7662.

(213) Alpert, A. J. Hydrophilic-Interaction Chromatography for the Separation of Peptides, Nucleic Acids and Other Polar Compounds. *J. Chromatogr. A* **1990**, *499*, 177–196.

(214) Spolnik, G.; Wach, P.; Rudzinski, K. J.; Skotak, K.; Danikiewicz, W.; Szmigielski, R. Improved UHPLC-MS/MS Methods for Analysis of Isoprene-Derived Organosulfates. *Anal. Chem.* **2018**, *90* (5), 3416–3423.

(215) Hettiyadura, A. P. S.; Stone, E. A.; Kundu, S.; Baker, Z.; Geddes, E.; Richards, K.; Humphry, T. Determination of Atmospheric Organosulfates Using HILIC Chromatography with MS Detection. *Atmos. Meas. Tech.* **2015**, *8* (6), 2347–2358.

(216) Hettiyadura, A. P. S.; Jayarathne, T.; Baumann, K.; Goldstein, A. H.; de Gouw, J. A.; Koss, A.; Keutsch, F. N.; Skog, K.; Stone, E. A. Qualitative and Quantitative Analysis of Atmospheric Organosulfates in Centreville, Alabama. *Atmos. Chem. Phys.* **2017**, *17* (2), 1343–1359.

(217) Jandera, P. Stationary Phases for Hydrophilic Interaction Chromatography, Their Characterization and Implementation into Multidimensional Chromatography Concepts. *J. Sep. Sci.* **2008**, *31* (9), 1421–1437.

(218) Hemström, P.; Irgum, K. Hydrophilic Interaction Chromatography. *J. Sep. Sci.* **2006**, *29* (12), 1784–1821.

(219) Guo, Y.; Gaiki, S. Retention and Selectivity of Stationary Phases for Hydrophilic Interaction Chromatography. *J. Chromatogr. A* **2011**, *1218* (35), 5920–5938.

(220) Pye, H. O. T.; Pinder, R. W.; Piletic, I. R.; Xie, Y.; Capps, S. L.; Lin, Y.-H.; Surratt, J. D.; Zhang, Z.; Gold, A.; Luecken, D. J.; et al. Epoxide Pathways Improve Model Predictions of Isoprene Markers and Reveal Key Role of Acidity in Aerosol Formation. *Environ. Sci. Technol.* **2013**, *47* (19), 11056–11064.

(221) McNeill, V. F. Aqueous Organic Chemistry in the Atmosphere: Sources and Chemical Processing of Organic Aerosols. *Environ. Sci. Technol.* **2015**, *49* (3), 1237–1244.

(222) Marais, E. A.; Jacob, D. J.; Jimenez, J. L.; Campuzano-Jost, P.; Day, D. A.; Hu, W.; Krechmer, J.; Zhu, L.; Kim, P. S.; Miller, C. C.; et al. Aqueous-Phase Mechanism for Secondary Organic Aerosol Formation from Isoprene: Application to the Southeast United States and Co-Benefit of SO2 Emission Controls. *Atmos. Chem. Phys. Discuss.* **2015**, *15* (21), 32005–32047.

(223) Bondy, A. L.; Craig, R. L.; Zhang, Z.; Gold, A.; Surratt, J. D.; Ault, A. P. Isoprene-Derived Organosulfates: Vibrational Mode Analysis by Raman Spectroscopy, Acidity-Dependent Spectral Modes, and Observation in Individual Atmospheric Particles. *J. Phys. Chem. A* **2018**, *122* (1), 303–315.

(224) Zhang, Z.; Lin, Y.-H.; Zhang, H.; Surratt, J. D.; Ball, L. M.; Gold, A. Technical Note: Synthesis of Isoprene Atmospheric Oxidation Products: Isomeric Epoxydiols and the Rearrangement Products Cis-and Trans-3-Methyl-3,4- Dihydroxytetrahydrofuran. *Atmos. Chem. Phys.* **2012**, *12* (18), 8529–8535.

(225) Váradi, A.; Gergely, A.; Béni, S.; Jankovics, P.; Noszál, B.; Hosztafi, S. Sulfate Esters of Morphine Derivatives: Synthesis and Characterization. *Eur. J. Pharm. Sci.* **2011**, *42* (1–2), 65–72.

(226) Zhang, H.; Surratt, J. D.; Lin, Y. H.; Bapat, J.; Kamens, R. M. Effect of Relative Humidity on SOA Formation from Isoprene/NO Photooxidation: Enhancement of 2-Methylglyceric Acid and Its Corresponding Oligoesters under Dry Conditions. *Atmos. Chem. Phys.* **2011**, *11* (13), 6411–6424.

(227) Krechmer, J. E.; Groessl, M.; Zhang, X.; Junninen, H.; Massoli, P.; Lambe, A. T.; Kimmel, J. R.; Cubison, M. J.; Graf, S.; Lin, Y.-H.; et al. Ion Mobility Spectrometry–Mass Spectrometry (IMS–MS) for on- and Offline Analysis of Atmospheric Gas and Aerosol Species. *Atmos. Meas. Tech.* **2016**, *9* (7), 3245–3262.

(228) Nguyen, T. B.; Bates, K. H.; Crounse, J. D.; Schwantes, R. H.; Zhang, X.; Kjaergaard, H. G.; Surratt, J. D.; Lin, P.; Laskin, A.; Seinfeld, J. H.; et al. Mechanism of the Hydroxyl Radical Oxidation of Methacryloyl Peroxynitrate (MPAN) and Its Pathway toward Secondary Organic Aerosol Formation in the Atmosphere. *Phys. Chem. Chem. Phys.* **2015**, *17* (27), 17914–17926.

(229) de Sá, S. S.; Palm, B. B.; Campuzano-Jost, P.; Day, D. A.; Newburn, M. K.; Hu, W.; Isaacman-VanWertz, G.; Yee, L. D.; Thalman, R.; Brito, J.; et al. Influence of Urban Pollution on the Production of Organic Particulate Matter from Isoprene Epoxydiols in Central Amazonia. *Atmos. Chem. Phys.* **2017**, *17* (11), 6611–6629.

(230) Watanabe, A. C.; Stropoli, S. J.; Elrod, M. J. Assessing the Potential Mechanisms of Isomerization Reactions of Isoprene Epoxydiols on Secondary Organic Aerosol. *Environ. Sci. Technol.* **2018**, *52* (15), 8346–8354.

(231) McNeill, V. F.; Woo, J. L.; Kim, D. D.; Schwier, A. N.; Wannell, N. J.; Sumner, A. J.; Barakat, J. M. Aqueous-Phase Secondary Organic Aerosol and Organosulfate Formation in Atmospheric Aerosols: A Modeling Study. *Environ. Sci. Technol.* **2012**, *46* (15), 8075–8081.

(232) Pye, H. O. T.; Luecken, D. J.; Xu, L.; Boyd, C. M.; Ng, N. L.; Baker, K. R.; Ayres, B. R.; Bash, J. O.; Baumann, K.; Carter, W. P. L.; et al. Modeling the Current and Future Roles of Particulate Organic Nitrates in the Southeastern United States. *Environ. Sci. Technol.* **2015**, *49* (24), 14195–14203.

(233) Woo, J. L.; McNeill, V. F. SimpleGAMMA v1.0 – a Reduced Model of Secondary Organic Aerosol Formation in the Aqueous Aerosol Phase (AaSOA). *Geosci. Model Dev.* **2015**, *8* (6), 1821–1829.

(234) Ramanathan, V.; Li, F.; Ramana, M. V.; Praveen, P. S.; Kim, D.; Corrigan, C. E.; Nguyen, H.; Stone, E. A.; Schauer, J. J.; Carmichael, G. R.; et al. Atmospheric Brown Clouds: Hemispherical and Regional Variations in Long-Range Transport, Absorption, and Radiative Forcing. *J. Geophys. Res.* **2007**, *112* (D22), D22S21.

(235) Andreae, M. O.; Gelencsér, A. Black Carbon or Brown Carbon? The Nature of Light-Absorbing Carbonaceous Aerosols. *Atmos. Chem. Phys.* **2006**, *6* (10), 3131–3148.

(236) Bond, T. C.; Bergstrom, R. W. Light Absorption by Carbonaceous Particles: An Investigative Review. *Aerosol Sci. Technol.* **2006**, *40* (1), 27–67.

(237) Feng, Y.; Ramanathan, V.; Kotamarthi, V. R. Brown Carbon: A Significant Atmospheric Absorber of Solar Radiation? *Atmos. Chem. Phys.* **2013**, *13* (17), 8607–8621.

(238) Moise, T.; Flores, J. M.; Rudich, Y. Optical Properties of Secondary Organic Aerosols and Their Changes by Chemical Processes. *Chem. Rev.* **2015**, *115* (10), 4400–4439.

(239) Selimovic, V.; Yokelson, R. J.; Warneke, C.; Roberts, J. M.; de Gouw, J.; Reardon, J.; Griffith, D. W. T. Aerosol Optical Properties and Trace Gas Emissions by PAX and OP-FTIR for Laboratory-Simulated Western US Wildfires during FIREX. *Atmos. Chem. Phys.* **2018**, *18* (4), 2929–2948.

(240) Li, H.; Lamb, K. D.; Schwarz, J. P.; Selimovic, V.; Yokelson, R. J.; McMeeking, G. R.; May, A. A. Inter-Comparison of Black Carbon Measurement Methods for Simulated Open Biomass Burning Emissions. *Atmos. Environ.* **2019**, *206*, 156–169.

(241) Hatch, L. E.; Rivas-Ubach, A.; Jen, C. N.; Lipton, M.; Goldstein, A. H.; Barsanti, K. C. Measurements of I/SVOCs in Biomass-Burning Smoke Using Solid-Phase Extraction Disks and Two-Dimensional Gas Chromatography. *Atmos. Chem. Phys.* **2018**, *18* (24), 17801–17817.

(242) Christian, T. J.; Kleiss, B.; Yokelson, R. J.; Holzinger, R.; Crutzen, P. J.; Hao, W. M.; Shirai, T.; Blake, D. R. Comprehensive Laboratory Measurements of Biomass-Burning Emissions: 2. First Intercomparison of Open-Path FTIR, PTR-MS, and GC-MS/FID/ECD. *J. Geophys. Res.* **2004**, *109* (D2), D02311.

(243) Ng, N. L.; Kroll, J. H.; Chan, a W. H.; Chhabra, P. S.; Flagan, R. C.; Seinfeld, J. H. Secondary Organic Aerosol Formation from M-Xylene, Toluene, and Benzene. *Atmos. Chem. Phys.* **2007**, *7* (14), 3909–3922.

(244) Lin, P.; Laskin, J.; Nizkorodov, S. A.; Laskin, A. Revealing Brown Carbon Chromophores Produced in Reactions of Methylglyoxal with Ammonium Sulfate. *Environ. Sci. Technol.* **2015**, *49* (24), 14257–14266.

(245) Ward, D. E.; Radke, L. F. Emissions Measurements from Vegetation Fires : A Comparative Evaluation of Methods and Results. In *Fire in the Environment: The Ecological, Atmospheric, and Climatic Importance of Vegetation Fires.*; Crutzen, P. J. and Goldammer, J. G., Ed.; John Wiley: New York, 1993; pp 53–76.

(246) Chambers, M. C.; Maclean, B.; Burke, R.; Amodei, D.; Ruderman, D. L.; Neumann, S.; Gatto, L.; Fischer, B.; Pratt, B.; Egertson, J.; et al. A Cross-Platform Toolkit for Mass Spectrometry and Proteomics. *Nat. Biotechnol.* **2012**, *30* (10), 918–920.

(247) Tautenhahn, R.; Patti, G. J.; Rinehart, D.; Siuzdak, G. XCMS Online: A Web-Based Platform to Process Untargeted Metabolomic Data. *Anal. Chem.* **2012**, *84* (11), 5035–5039.

(248) Tian, Z.; Gold, A.; Nakamura, J.; Zhang, Z.; Vila, J.; Singleton, D. R.; Collins, L. B.; Aitken, M. D. Nontarget Analysis Reveals a Bacterial Metabolite of Pyrene Implicated in the Genotoxicity of Contaminated Soil after Bioremediation. *Environ. Sci. Technol.* **2017**, *51* (12), 7091–7100.

(249) Lack, D. A.; Langridge, J. M. On the Attribution of Black and Brown Carbon Light Absorption Using the Ångström Exponent. *Atmos. Chem. Phys.* **2013**, *13* (20), 10535–10543.

(250) Reid, J. S.; Koppmann, R.; Eck, T. F.; Eleuterio, D. P. A Review of Biomass Burning Emissions, Part II: Intensive Physical Properties of Biomass Burning Particles. *Atmos. Chem. Phys. Discuss.* **2004**, *4* (5), 5135–5200.

(251) Lewtas, J. Air Pollution Combustion Emissions: Characterization of Causative Agents and Mechanisms Associated with Cancer, Reproductive, and Cardiovascular Effects. *Mutat. Res. Mutat. Res.* **2007**, *636* (1–3), 95–133.